Granules for Abrasive Cleaning
(using High-Shear Granulation)

VOLUME **II**
(Bibliography and Appendices)

Robert E Maxim
September 2006

PhD *Chemical Engineering*

Sheffield University – Chemical Engineering Dept

SOME PAGES BOUND INTO/CLOSE TO SPINE.

ABSTRACT

PhD Research – Robert Maxim

Designing Granules for Abrasive Cleaning (using High-Shear Granulation)

Abstract:

This work investigates the granulation of fine calcium carbonate powder to form micro-granules (less than 100μm). The influence of formulation and operating conditions on granule properties was investigated. This work analyses experimental data using a database approach to relate granulation conditions to granule properties, to find property-to-property relationships and to investigate the influence on the abrasion of Perspex. It was found that the granulation was undertaken in an unstable regime dictated by the need to produce small granules. As a result, it was not possible to achieve reproducibility in making the granules. For the range of granules produced it was difficult to determine variation in abrasiveness within the experimental errors, a detailed error analysis was carried out. A theoretical relationship between strength and porosity is developed and the factors influencing abrasive wear are investigated.

Two theoretical models are presented: 1) Impact Failure model and 2) Granule Consolidation model. The impact failure model relates dynamic impact strength to static strength, which enables the prediction of a failure distribution curve (how many particles will fail per hundred impacts as a function of velocity). This is done using a "*critical normal impact velocity*" determined from the properties of the granule, properties of the impact surface and experimentally measured granule static strength. The granule consolidation model allows the qualitative prediction of the rate and extent of consolidation from granulation conditions. It models the compaction of a granule by describing the packing of its primary particles within an imaginary internal granule. Sphere packing is discussed with implications for determining the maximum packing of a primary particle size distribution.

15 Bibliography

1 Maxim, R E, Salman, A D, Hounslow, M J and Pickles, M, (2003), Theoretical impact failure distribution of granules, *Advanced Powder Technology* 4, Vol. 14, pp 393-400

2 Tabor, D, (1995), Tribology - the last 25 years A personal view, *Tribology International* 1, Vol. 28, pp 7-10

3 Sochon, R P J, Dorvlo, S K, Rudd, A, Hayati, I, Hounslow, M J and Salman, A D, (2004), Granulation of Zinc Oxide - 4th Year Project Report, *Chemical Engineering Dept. University of Sheffield* Vol. pp

4 Aulton, M E and Banks, M, (1981), Fluidised bed granulation - factors influencing the quality of the product, *International Journal of Pharmaceutical Technology Product Manufacturing* Vol. 2, pp 24-29

5 Sherrington, P and Oliver, R, (1981) Granulation, *Monographs in Powder Science and Technology, G. AS, Heyden & Sons,*

6 Scott, A C, (2000), Direct evidence of heterogeneity during high-shear granulation, *Powder Technology* Vol. 113, pp 205-213

7 Iveson, S M, Litster, J D, Hapgood, K and Ennis, B J, (2001), Nucleation, growth and breakage phenomena in agitated wet granulation processes: a review, *Powder Technology* 117, Vol. pp 3-39

8 Litster, J D, Hapgood, K, Michaels, J N, Sims, A, Roberts, M, Kameneni, S K and Hsu, T, (2001), Liquid distribution in wet granulation: dimensionless spray flux, *Powder Technology* 114, Vol. pp 32-39

9 Rankell, A S, Scott, M W, Lieberman, H A, Chow, F S and Battista, J V, (1964), Continuous production of tablet granulations in fluidized bed II. Operation and performance of equipment, *Journal of Pharmaceutical Science* Vol. 53, pp 320-324

10 Davies, W I and Gloor, W T, (1971), Batch production of pharmaceutical granulations in a fluidized bed: I Effects of process variables on physical properties of final granulation, *Journal of Pharmaceutical Science* Vol. 60, pp 1869-1874

11 Schaefer, T and Worts, O, (1977), Control of fluidised bed granulation: I Effects of spray angle, nozzle height and starting materials on granule size and size distribution, *Arch. Pharm. Chem.* Vol. 5, pp 51-60

12 Mazzone, D N, Tardos, G I and Pfeffer, R, (1987), The behaviour of liquid bridges between two relatively moving particles, *Powder Technology* Vol. 51, pp 71-83

13 Harnby, N, Hawkins, A E and Opalinski, I, (1996), Measurement of the adhesive force between individual particles with moisture present: Part 1. A Review, *Transactions Institute Chemical Engineering* Vol. 74, pp 605-615

14 Iveson, S M, Wauters, P A L, Forrest, S, Litster, J D, Meesters, G M H and Scarlett, B, (2001), Growth Regime map for liquid-bound granules: further development and experimental validation, *Powder Technology* 117, Vol. pp 83-97

15 Mort, P R, (2003), A multi-scale approach to modelling and simulation of particle formation and handling process, *CHoPS 4 - Conveying and Handling of Particulate Solids 4 (Hungary)* Vol. 2, pp

16 Iveson, S M, Litster, J D and Ennis, B J, (1996), Fundamental studies of granule consolidation Part 1: Effects of binder content and binder viscosity, *Powder Technology* 88, Vol. pp 15-20

17 . Meng, H C and Ludema, K C, (1995), Wear Models and predictive equations: their form and content, *Wear* Vol. 181, pp 443-457

18 Williams, J A, (1999), Wear modelling: analytical, computational and mapping: a continuum mechanics approach, *wear* Part 1, Vol. 225-229, pp 1-17

19 Lim, S C and Ashby, M F, (1987), Wear Mechanism maps, *Acta Metallurgica* 35, Vol. pp 1-24

20 Briscoe, B J, Evans, P D, Pelillo, E and Sinha, S K, (1996), Scratching maps for polymers, *Wear* 1-2, Vol. 200, pp 137-147

21 Knight , P C, (2004), Challenges in granulation technology, *Powder Technology* 140, Vol. pp 156-162

22 Salman, A D and Hounslow, M J, (2004), Special Issue: 1st International Workshop on Granulation (Granulation across the length scales: linking microscopic experiments and models to real process operation), *Powder Technology* 3, Vol. 140, pp 155-296

23 Bardin, M, Knight, P C and Seville, J P K, (2004), On control of particle size distribution in granulation using high-shear mixers, *Powder Technology* 140, Vol. pp 169-175

24 Reynolds, G K, Biggs, C A, Salman, A D and Hounslow, M J, (2004), Non-uniformity of binder distribution in high-shear granulation, *Powder Technology* 140, Vol. pp 203-208

25 Fu, J, Cheong, Y S, Reynolds, G K, Adams, M J, Salman, A D and Hounslow, M J, (2004), An experimental study of variability in the properties and quality of wet granules, *Powder Technology* Vol. 140, pp 209-216

26 Litster, J D and Ennis, B J, (2004) The science and engineering of granulation processes, *Particle Technology Series, Kluwer Academic Publishers,*

27 Sloane, N J A, (1984), The packing of spheres, *scientific american* Vol. 250, pp 116-125

28 Tardos, G I, Khan, M I and Mort, P R, (1997), Critical parameters and limiting conditions in binder granulation of fine powders, *Powder Technology* Vol. 94, pp 245-258

29 Ennis, B J, Tardos G I, Pfeffer R, (1991), A micro-level characterization of granulation phenomena, *Powder Technology* Vol. 65, pp 257-272

30 Iveson, S M and Litster, J D, (1998), Fundamental studies of granules consolidation Part 2: Quantifying the effects of particle and binder properties, *Powder Technology* Vol. 99, pp 243-250

31 Lu, B, An Investigation of effects of Process Variables to Porosity and Binder Distribution in Wet Granules,

32 Fu, J, Literature Review, *University of Sheffield* - PhD Thesis,

33 Azadehnia, AH, Literature Review Report: Development of a predictive model for fluidised bed granulation, *University of Sheffield* - PhD Thesis

34 Gabbott, I P, Private Communication, (2005),

35 Salman, A D, Particle Science - Course Notes, 3rd Year MEng. Chemical and Process Engineering with Fuel Technology, *University of Sheffield,* (1999)

36 Weideman, G, Lewis, P and Reid, N, (1990) Structural Materials, *Materials in Action Series, T. O. University, Butterworth-Heinemann Ltd.,*

37 Samimi, A, Hassanpour, A and Ghadiri, M, (2005) Single and Bulk Compressions of Soft Granules: Experimental study and DEM Evaluation, (*University of Leeds*) - thesis

38 Cheong, Y S, (2005) Mechanical characteristics of model binderless granules, *University of Sheffield* PhD thesis

39 Salman, A D, Gorham, D A and Hounslow, M J, (2001), Impact Breakage of fertilizer granules, *7th International symposium on Agglomeration* Vol. Albi 1, pp 451-461

40 Ghadiri, M and Papadopoulos, D G, (1995) FRR 16-06 Impact Attrition of particulate solids, *University of Surrey* - PhD thesis

41 Adams, M J, Briscoe, B J and Biswas, S K, (1996) Solid-Solid Interactions, *Imperial College Press*,

42 Hutchings, I M, (1996) Solid-Solid Interactions, *Imperial College Press*, Deformation and fracture of brittle solids pp 211-224

43 Bowden, F P and Tabor, D, Friction An Introduction to Tribology, *Heinemann*,

44 Hutchings, I M, (1992) Tribology friction and wear of engineering materials, *butterworth-Heinemann*,

45 Hutchings, I M, (1998), Abrasive and erosive wear tests for thin coatings: a unified approach, *Tribology International* 1-3, Vol. 31, pp 5-15

46 Williams, J A, (1994) Engineering Tribology, *Oxford Science Publications*,

47 Johnson, K L, (1985) Contact Mechanics, *Cambridge University Press*,

48 Conrad, H, Keshavan, M K and Sargent, G A, (1979), Hertzian fracture of Pyrex glass under quasi-static loading conditions, *Journal of Materials Science* 14, Vol. pp 1473-1494

49 Laugier, M T, (1984), Hertzian indentation of sintered alumina, *Journal of Materials Science* 19, Vol. pp 254-258

50 Holmberg, K and Matthews, A, (1994) Coatings Tribology: Properties, techniques and application in surface engineering, *Tribology Series, 28, Editor: Dawson D*,

51 Schonert, K, (1979), Aspects of physics of breakage relevant to comminution, *Fourth Tewksbury Symposium* Melbourne, Vol. pp

52 Simons, S, (2003), Predicting granule behaviour through micro-mechanistic investigations, *Granulation across length scales: linking microscopic experiments and models to real process operation, Conf* Sheffield University, Vol. pp

53 Ramkrishna, D, (2000) Population Balances: Theory and applications to particulate systems in Engineering, *Academic Press*,

54 Collocott, T C and Dobson, A B, (1975) Chambers Dictionary of science and technology, *1*, *W&R Chambers Ltd*,

55 Pickles, M, Private Communication, (2001), Dental Hygiene Group Unilever Port Sunlight research laboratories

56 Mondal, D P, Das, S, Jha, A K and Yegneswaran, A H, (1998), Abrasive wear of Al alloy - Al2O3 particle composite: a study on the combined effect of load and size of abrasive, *Wear* 223, Vol. pp 131-138

57 Hamblin, M G and Stachowiak, G W, (1996), Description of abrasive particle shape and its relation to two-body abrasive wear, *Tribology Transactions* 4, Vol. 39, pp 803-810

58 Murugesh, L and Scattergood, R O, (1991), Effect of erodent properties on the erosion of alumina, *Journal of Materials Science* 26, Vol. pp 5456-5466

59 Knight, J C, Page, T F and Hutchings, I M, (1989), The influence of substrate hardness on the response of TiN-coated steels to surface deformation, *Thin Solid Films* 177, Vol. pp 117-132

60 Haan, J J and Steif, P S, (1998), Abrasive wear due to the slow loading of a concentrated suspension, *Wear* 219, Vol. pp 177-183

61 Hutchings, I M, (1992) Tribology friction and wear of engineering materials, *Butterworth-Heinemann*, Chapter 5.8 pp 14-17

62 Bowden, F P and Tabor, D, Friction An Introduction to Tribology, Lubrication - chapter 8

63 Studman, C J and Field, J E, (1984), The influence of brittle particles on the contact between rigid surfaces, *Journal of Physics D: Applied Physics* 17, Vol. pp 1631-1646

64 Su, Y T, Hung, T C and Chang, Y Y, (1998), On machining rate of hydrodynamic polishing process under semi-contact lubricating condition, *Wear* 220, Vol. pp 22-33

65 Dwyer-Joyce, R S, Sayles, R S and Ioannides, E, (1994), An investigation into the mechanisms of closed three-body abrasive wear, *Wear* 175, Vol. pp 133-142

66 Maxim, R E, Salman A D, Hounslow, M J, (2006), Predicting dynamic failure of dense granules from static compression tests, *International Journal of Mineral Processing 79*, pp188-197

67 Han, T, Kalman, H and Levy, A, (2003), Theoretical and experimental study of multi-compression particle breakage, *Advanced Powder Technology* 5, Vol. 14, pp 505-628

68 Pis, J J, Fuertes, A B, Artos, V, Suarez, A and Rubiera, F, (1991), Attrition of coal ash particles in a fluidised bed, *Powder Technology* Vol. 66, pp 41-46

69 Veesler, S and Boistell, R, (1993), Attrition of hydragillite (Al(OH)3): mechanism and quantification of particle fragility by a new attrition index, *Powder Technology* Vol. 76, pp 49-57

70 Montmittonnet, P, Edlinger, M L and Felder, E, (1993), Finite element analysis of elastoplastic indentation: Part II - Application to Hard Coatings, *journal of Tribology* Vol. 115, pp 15-19

71 Doerner, N F and Nix, W D, (1986), A method for interpreting the data from depth-sensing indentation instruments, *J. Mat. Res.*, Vol. 1 (4), pp 601

72 Hutchings, I M, (1992) Tribology friction and wear of engineering materials, *Butterworth-Heinemann*, Chapter 2.5 pp 14-17

73 Hutchings, I M, (1992) Tribology friction and wear of engineering materials, *Butterworth-Heinemann*, Chapter 6.2.1 pp 14-17

74 Gee, M G, (2001), Low load multiple scratch tests of ceramics and hard metals, *Wear* Vol. 250, pp 264-281

75 Dwyer-Joyce, R S, Private Communication, (2002),

76 Pickles, M, Private Communication, (2001),

77 Gauthier, C, Lafaye, S and Schirrer, R, (2001), Elastic recovery of a scratch in a polymeric surface: experiments and analysis, *Tribology International* 7, Vol. 34, pp 469-479

78 Barbezat, G and Nicoll, A R, (1993), Abrasion, erosion and scuffing resistance of carbide and oxide ceramic thermal sprayed coatings for different applications, *Wear* 162-164, Vol. pp 529-537

79 ASTM, (1985), Standard Test Method for measuring abrasion using the dry sand/rubber wheel apparatus, *ASTM standard G65-00e1* Vol. pp

80 Kelly, D A and Hutchings, I M, (2001), A new method for measurement of particle abrasivity, *Wear* 250, Vol. pp 76-80

81 Urban Architecture - Glossary of Terms , Virginia University www.urban.arch.virginia.edu/~km6e/references/glossary/struc-glossary.html

82 Wikberg, M and Alderhorn, G, (1992), Pore size distributions, assessed by mercury penetration of compacts of two lactose granulations with different fragmentation propensities, *International Journal of Pharmaceutics* Vol. 84, pp 191-195

83 Rumpf, H, (1962) AIME, Agglomeration, *Interscience*, The Strength of Granules and Agglomerates pp 379-418

84 Kendall, K, (1987), Relevance of contact mechanics to powders - elasticity, friction and agglomerate strength pp 110-122 *Tribology in Particulate Technology* (eds Briscoe and Adams)

85 Adams, M J, Mullier, M A and Seville, J P K, (1994), Agglomerate strength measurement using uniaxial confined compression test, *Powder Technology* 78, Vol. pp 5-13

86 Shipway, P H and Hutchings, I M, (1993), Fracture of brittle spheres under compression and impact loading 1. Elastic stress distributions, *Philosophical magazine A* 6, Vol. 67, pp 1389-1404

87 Knight, P C, Instone, T, Pearson, J M K and Hounslow, M J, (1998), An investigation into the kinetics of liquid distribution and growth in high shear agglomeration, *Powder Technology* 97, Vol. pp 246-257

88 Van Den Dries, K, De Vegt, O M, Girard, V and Vromans, H, (2003), Granule breakage phenomena in a high shear mixer; influence of process and formulation variables and consequences on granule homogeneity, *Powder Technology* 1-3, Vol. 133, pp 228-236

89 Scott, A C, Heterogeneity in high-shear granulation - *University of Sheffield* PhD Dissertation,

90 Schaefer, T and Mathiesen, C, (1996), Melt pelletization in a high shear mixer IX. Effects of binder particle size, *International Journal of Pharmaceutics* 139, Vol. pp 139-148

91 Watano, S, Numa, T, Miyanami, K and Osako, Y, (2001), A fuzzy control system of high shear granulation using image processing, *Powder Technology* 115, Vol. pp 124-130

92 Holm, P, T, S and Kristensen, H G, (1985), Granulation in high-speed mixers part V. Power consumption and temperature changes during granulation, *Powder Technology* 43, Vol. pp 213-223

93 Ritala, M, Jungerson, O, Holm, P and Kristensen, H G, (1988), *Drug Dev. Ind. Pharm.* Vol. 14, pp 1041

94 Hemati, M, Cherif, R, Saleh, K and Pont, V, (2003), Fluidized bed coating and granulation: influence of process-related variables and physicochemical properties on the growth kinetics., *Powder Technology* 130, Vol. pp 18-34

95 Rambali, B, Baert, L and Massart, D, (2001), Using experimental design to optimize the process parameters in fluidized bed granulation on semi-full scale, *International Journal of Pharmaceutics* 1-2, Vol. 220, pp 149-160

96 Westerhuis, J A, Coenegracht, P M J and Lerk, C F, (1997), Multivariate modelling of the tablet manufacturing process with wet granulation for tablet optimization and in-process control, *International Journal of Pharmaceutics* 156, Vol. pp 109-117

97 Knight, P C, Johansen, A, Kristensen, H G, T, S and Seville, J P K, (2000), An investigation of the effects on agglomeration of changing the speed of a mechanical mixer, *Powder Technology* 3, Vol. 110, pp 204-209

98 Ouchiyama, N and Tanaka, T, (1980), Stochastic model for compaction of pellets in granulation, *Industrial Engineering Chem. Fundam.* Vol. 19, pp 555-560

99 Capes, C E and Danckwerts, P V, (1965), Granule formation by the agglomeration of damp powders: Part 1. The mechanism of granule growth, *Transactions Institute Chemical Engineering* Vol. 43, pp 116-124

100 Maxim, R E, FU, J, Pickles, M, Salman, A D and Hounslow, M J, (2004), Modelling effects of processing parameters on granule porosity in high-shear granulation, *Granular Matter* 2-3, Vol. 6 (CHoPS special Edition), pp 131-135

101 Jaegerskou, A, Holm, P, Schaefer, T and Kristensen, H G, (1984), Granulation in High Speed Mixers, *Pharm. Ind.* 3, Vol. 46, pp 310-314

102 Mathworld,www.mathworld.wolfram.com/spherepacking.html,

103 Edmondson, A C, (1987) A Fuller Explanation The Synergetic Geometry of R. Buckminster Fuller, (e-book)

104 Hales, T C, An Overview of the Kepler Conjecture http://arxiv.org/PS_cache/math/pdf/9811/9811071.pdf,

105 Rogers, C A, (1958), The packing of equal spheres, *Proceedings London Mathematical Society* Vol. 8, pp 609-620

106 Mathworld,http://mathworld.wolfram.com/KissingNumber.html,

107 Robert, C,
http://ourworld.compuserve.com/homepages/robert_conroy/molecula.htm,

110 Referee, Private Communication, (2002), Referees Comments - Article Submitted to Powder Technology

111 Fu, J S, Reynolds, G K, Cheong, Y S, Adams, M J, Salman, A D and Hounslow, M J, (2003), Feasibility of improving granule quality (working title), *Powder Technology* Vol. to be submitted, pp

112 Holm, P, Jungersen, O, Schaefer T and Kristensen, H G, (1983), Granulation in High Speed Mixers part1: Effects of process variables during kneading, *Pharm. Ind.* 45, Vol. pp 806-811

113 Gan, M, Jia, X and Williams, R A, (2003), A new method for predicting packing properties of particles of any shape, *4th international conference for conveying and handling of particulate solids* Vol. pp

114 Puri, V M, (2003), Bulk mechanical properties as influenced by particle shape, moisture and sphagum peat using the cubical triaxial tester, *4th international conference for conveying and handling of particulate solids* Vol. pp

115 Pickles, M, Private Communication, (2003), Dental Hygiene Group Unilever Port Sunlight research laboratories

117 Deacon, J, Descriptive Statistics,
http://helios.bto.ed.ac.uk/bto/statistics/tress3.html University of Edinburgh, Biology Dept.

118 Harris, T, Physics 2110 Course - Experimental Errors,
http://www2.volstate.edu/tfarris/PHYS2110-2120/experimental_error.htm, Volunteer State Community College, Astrology and Physics Dept.

119 Unknown Author, Experimental Errors and Error Analysis
http://documents.wolfram.com/applications/eda/ExperimentalErrorsAndErrorAnalysis.html, Wolfram Research Publications

120 Gamberg, Experimental Error
http://www.bklv.psu.edu/faculty/gamberg/exp_err.doc, Penn State University, Berks Campus

121 Lane, DM, Error Analysis, http://davidmlane.com/hyperstat/A103397.html, HyperStat Online

122 Gabbott, I P, Reynolds, G K, Salman, A D and Hounslow, M J, (2005), Single and Bulk Uniaxial Compression Testing of Granules, *Draft Paper* Vol. pp

123 Fu, JS, Cheong YS, Reynolds, GK, Adams, MJ, Salman, AD, Hounslow, MJ (2005), An experimental study of the variability in the properties and quality of wet granules, *Powder Technology* Vol 140, Issue 3, pp209-216

Appendices list

Summary of Technical Terms

Appendix A	Predicting dynamic failure of dense granules from static compression tests (full version of Maxim [66])
Appendix B	Crushing tests graphs showing qualitative effects of the variables in equations (4), (5) and (6): force, radius and Youngs modulus and k factor. Chart 1 shows total contact area as a function of size and pressure Chart 2 shows the load per particle as a function of particle size Chart 3 shows the effect of particle size on total pressure Chart 4 large to small shows the effect of reduction in size of particles on both the pressure and total contact area Chart 5 Shows he effect of different k values and particles diameter on the contact area
Appendix C	Derivation of analysis of binder content and packing structure.
Appendix D	Abrasion testing report (early copy)
Appendix E	Original drawings for design of abrasion rig
Appendix F	Binder Content Verification
Appendix G	Database – electronic form
Appendix H	Plots from queries from results database
Appendix I	Plots from preliminary testing – Mercury Porosimetry
Appendix J	Experiments Table (from database)
Appendix K	Theoretical impact failure distribution of granules (Maxim [1])
Appendix L	Modelling effects of processing parameters on granule porosity in high-shear granulation (Maxim [100])

Technical Terminology

2-body abrasion

Abrasion involving 2 surfaces, normally abrasive particles are held fixed in the counterbody

3-body abrasion

Abrasion involving a freely moving abrasive that is forced into contact with the abraded surface by the 3rd body

Abrasion

Removal of matter by scratching and grinding

Abrasive

A substance used for the removal of matter by abrasion

Abrasive energy

Energy input during an abrasive process: Applied load x Time x Abrasive speed

Abrasive strength

Resistance of abrasive to failure during abrasion

Abrasivity

Amount of material removed relative to a standard abrasion test (similar to abrasive strength)

Absorption

Penetration (not scratching) of a substance (normally gas or liquid) into the body of another

Adhesion

Intermolecular forces which hold matter together, particularly closely contiguous surfaces of neighbouring media, eg liquid in contact with a solid. Also applies to intimate sticking of metal surfaces due to metal bonds formed as a function of stress, time and temperature.

Adsorption

The taking up of one substance at the surface of another

Agglomerate

(noun) Assemblage of particles rigidly held together, as by partial fusion, e.g. by sintering or by growing together. In the case of granules, held by binder bridges.

(verb) To form an agglomerate

Aggregate

(noun) Assemblage of particles that are loosely held together, e.g. by electrostatic forces (as in clusters of fine primary particles) or by weak / temporary bonds (as in poorly formed granules or powder sticking to a wet surface)

(verb) To form a weak assemblage

Arithmetic Mean

Sum of all values divided by the number of items

Attrition

Wear damage caused by repetition of an action singularly causes relatively little wear

Binder

Substance used to stick primary particle together in a granule (normally liquid during granulation process)

Binder Content

A general term referring to the actual amount of binder within a granule, sieve cut or whole batch, usually quoted as a mass when found experimentally by thermogravimetric analysis (or quoted as a volume if converted using appropriate density)

Binder Ratio

The ratio of the mass of binder added to the mass of primary particle powder within a batch of granules, a sieve fraction or an individual granule quoted as a percentage or fraction of the original mass of primary particles. NOT the percentage of the total mass which is binder.

Bulky

A particle is bulky if its length ≈ Breadth ≈ thickness

Capillary (bonding)

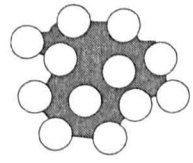

Characteristic Length

The size (l) of particles on a sieve cut (with upper sieve size s_u and lower sieve size s_l) weighted by the mass-based size distribution. Such that:

$$l = \frac{s_l m_l + s_u m_u}{m_l + m_u}$$

Where m_u and m_l are the weighted masses of the mass-based size distribution corresponding to s_u and s_l respectively

Chipping

Removal of small fragments of material from the mother body

Coalesce

Combining of 2 bodies into 1. e.g. 2 wet granules collide and agglomerate to form a single new granule in which the parent granules are indistinguishable.

Coating

Layer of a substance spread over a substrate (either desirable to provide protection or undesirable in the case of a stain)

Compressive Strength

The compressive force per unit area that a body can withstand before failure

Consolidation

Primary particles within a granule packing closer together squeezing out air and binder in the process

Contact Angle

The angle between the liquid and the solid at the solid-liquid-gas interface. It is acute for wetting and obtuse for non-wetting

Counterbody

A second body in abrasion tests that either contains the abrasive within itself or is used to push the abrasive particles into the substrate and coating

Crack

A partial split or break in a substance, a fissure. Energy input generates new surface area (crack)

Critical packing state

Closest packing of solid particles forming a granule

Cutting

Ductile material removal characterised by material flowing up and forming a lip or separated chip in front of the impression site.

Dislocation

A lattice imperfection in a crystal resulting from the absence of an atom or atoms in one or more layers

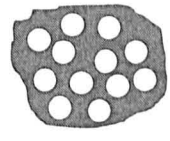

Droplet

Ductile

Capable of being reshaped and moulded whilst retaining strength and freedom from cracks

Elastic

Returning to or capable of returning to an initial form after deformation

Elastic constants

Quantities expressed in MN / m^2 used to describe the behaviour of a material when subjected to stress in one of three modes: longitudinal (Young's modulus) , shear (rigidity modulus) and compression (bulk modulus)

Elongation (shape descriptor)

The ratio of length to breadth

Equivalent Diameter

The diameter of a sphere having the same volume as the particle

Erosion

Wearing away of a surface due to weathering, dissolution, abrasion, corrosion and transportation under the influence of gravity, wind and running water. (Usually applied to land)

Failure Load

Force required to produce failure

Failure Stress

The force per unit area required to produce failure

Flakey

A particle is flakey if length ≈ breadth > thickness

Flakiness (shape descriptor)

The ratio of breadth to thickness

Flaw

An imperfection; can be an air pocket, impurity, foreign body (inclusion) or a dislocation

Formulation parameter

Something that goes into a granulation process, e.g. the ingredients: binder type, particle type and binder : solid ratio

Free Energy

The capacity of a system to perform work, a change in free energy being measured as the maximum work obtainable from a given process

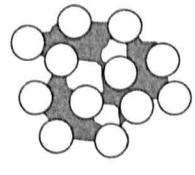

Funicular (bonding)

GSD (Granule Size Distribution)

Granule

An agglomerate made up of primary particles and held together by binder

Granule size distribution (GSD)

A mass based or number based size distribution of a mass of granules, usually referring to the size distribution of all the granules produced in a granulation process

Hardness

Resistance to deformation. It is actually measured by determining the resistance to indentation as in Brinell, Rockwell, Vickers diamond pyramid and scleroscope hardness tests... The values of hardness obtained by the different methods are of some extent related to each other, and to the ultimate tensile stress of non-brittle metals.

Hardness (Mohs)

The resistance which a mineral offers to abrasion (and indentation). The absolute hardness is measured with the aid of a sclerometer. The comparative hardness is expressed in terms of Moh's scale, and is determined by testing against ten standard minerals: (1) talc, (2) gypsum, (3) calcite, (4) fluorite, (5) apatite, (6) orthoclase, (7) quartz, (8) topaz, (9) corundum, (10) diamond. Thus a mineral with 'hardness 5' will scratch or abrade fluorite but will be scratched by orthoclase.

Hardness (Vickers hardness number – H_v)

A 136° diamond pyramid is pushed with constant force into the surface of a specimen for a specified time. At the end of the indentation the diagonal length of the indentation is measured. The hardness is the force divided by the contact surface area of the indentation (kg force mm^{-2})

Inelastic

Relating to permanent deformation (normally of a brittle material)

Inter-particle space

Fraction of granule occupied by binder and air

Limiting interparticle space

The interparticle space at maximum compaction for a given PPSD and binder combination

Mass based size distribution

A size distribution where the mass of particles of a given size is used as the Y-axis (visually this emphasises larger particles)

Median

Middle particle size, 50% of the particles are coarser and 50% are finer

Mode

The particle size corresponding to the maximum frequency on a frequency-particle size plot

Needle-like

A particle is needle-like if length > breadth ≈ thickness

Nucleation

The initial formation of a granule start point from binder (liquid phase) and primary particles (solid phase) in the early stages of granulation

Number based size distribution

A size distribution where the number of particles of a given size is used as the Y-axis (visually this emphasises smaller particles)

PPSD (Primary Particle Size Distribution)

PSD (Particle Size Distribution)

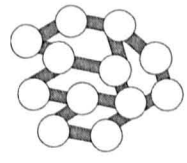

Pendular (bonding)

Plastic

Relating to permanent deformation (in this thesis plastic deformation will be used to refer to inelastic deformation, such as in brittle material, and the more classical definition of plastic – the movement of dislocations)

Ploughing

Ductile material removal characterised by material flowing to the sides and front of the impression.

Poissons ratio

Elastic constant. Ratio of lateral contraction per unit breadth to the longitudinal extension per unit length, when a piece of material is stretched. For most substances its value lies between 0.2 and 0.4. The relationship between poissons ratio, ν, Young's modulus, E, and rigidity, G, is given by:

$$\nu = \frac{E}{2G} - 1$$

Porosity

The ratio (usually expressed as a percentage) of the volume of the pore space to the total volume. Porosity refers to air space only, whereas inter-particle space refers to fraction of granule occupied by binder and air.

Primary Particle

The small solid particles that are agglomerated to form granules

Primary Particle size distribution (PPSD)

The size distribution of the particles used as the feed stock for a granulation process or the size distribution of the actual particles within a granule

Processing parameter

The way a granulation process is operated, e.g. impellor speed, run time, addition method, chopper speed and temperature

Projected Diameter

The diameter of a sphere having the same projected area as the particle

Range

The simplest measure of dispersion. The difference between the largest and smallest value of the sample observations

Shear Stress

The intensity of shear force per unit area of cross-section

Sphericity

The ratio of the surface area of a particle to the surface area of a sphere having the same volume as the particle

Standard Deviation

Square root of the variance (root mean squared deviation from the mean)

Strength

The maximum stress that a material can withstand before failure. For ductile material the strength is the stress at the onset of necking. For brittle material there is little or no necking and the strength ≈ yield stress

Stress

The force per unit area acting on a material and tending to change its dimensions, i.e. cause a strain

Substrate

The underlying base material onto which a stain or coating is attached

Surface free energy

Free energy per unit area. Surface tension multiplied by surface area

Surface Pressure

The 2-dimensional analogue of gas pressure. The difference between the surface tension of a pure liquid and that of a surface active solution, it represents the tendency of the adsorbed surfactant molecules to spread over the liquid surface

Surface tension

A property possessed by liquid surfaces whereby they appear to be covered in a thin elastic membrane in a state of tension, it is measured by the force acting normally across unit length in the surface. The phenomena is due to unbalanced molecular cohesive forces near the surface

Toughness

Defined as the work required to propagate unit area of crack within a material. KiloJoules per unit area. Glass is a very hard material but not very tough

Variance

The average of the squared deviations from the sample mean

Viscosity

The resistance of a fluid to shear forces – The shear stress per unit velocity gradient N s /m^2. (Kinematic Viscosity is the coefficient of viscosity divided by density, $m^2 s^{-1}$.)

Wettability

The extent to which a solid is wetted by a liquid, measured by the force of adhesion between the solid and the liquid

Yield Stress

The stress at the onset of plastic deformation, the end of the linear region of a stress-strain curve

Youngs modulus

Defined as the ratio of stress to strain over the linear region of a stress-strain curve

Appendix A

Predicting dynamic failure of dense granules from static compression tests

Available online at www.sciencedirect.com
SCIENCE DIRECT®
ELSEVIER
Int. J. Miner. Process. 79 (2006) 188–197
INTERNATIONAL JOURNAL OF MINERAL PROCESSING
www.elsevier.com/locate/ijminpro

Predicting dynamic failure of dense granules from static compression tests

R.E. Maxim, A.D. Salman *, M.J. Hounslow

Particle Products Group, The Department of Chemical and Process Engineering, University of Sheffield, Sheffield, S1 3JD, UK

Received 10 February 2006; accepted 24 February 2006
Available online 5 April 2006

Abstract

This paper shows how static failure loads can be used to predict impact failure of granules. A theoretical model is presented that gives the maximum force experienced during impact and equates this to experimentally measured static failure load to define a critical impact velocity for impact failure. A granule will fail if the predicted theoretical maximum force during impact due to the impact velocity is greater than the real force required to produce failure in that particular granule.

The random nature of granules produces a spread of velocities at which granules of a given size will fail; this spread is the failure distribution. In this paper it is shown that the failure distribution of a series of impact experiments can be represented by a 2-parameter Weibull equation. The important c-parameter is related to the impact angle and the critical normal impact velocity that is found from static compression tests. Thus the number of granules failing by impact at each velocity can be found by performing static failure tests.

Keywords: failure; granule; granules; high-shear granulation; compression; static; impact failure; dynamic failure; impact velocity; critical normal impact velocity; Hertzian failure; dense granules; dense granule; static failure; granulation

1. Introduction

Granulation has been an important powder production process in industry for the past few decades. There are many advantages to using granulated material, for example improved flow-ability and improved dissolution characteristics. As granules are so important to so many industries it is desirable to know as much as possible about efficient processing and transportation of granular material. Granules can impact upon each other and process equipment, potentially leading to granule breakage. It would be of useful if we could predict whether granule breakage will occur and, if so, the rate of granule breakage. Granule breakage on impact with a rigid surface depends upon material properties of the granule and the surface as well as the velocity and angle of impact. Despite the long history of research into granulation, it has been difficult to predict granule breakage during processing without using a statistical approach involving extensive impact experiments. This is largely due to the random nature of the number and position of flaws/pores within granules. This leads to a spread of impact velocities required to induce failure within a given sample of granules.

This random spread of failure velocity is indirectly apparent when particles of identical size and material are

* Corresponding author.
E-mail address: a.d.salman@sheffield.ac.uk (A.D. Salman).

0301-7516/$ - see front matter © 2006 Elsevier B.V. All rights reserved.
doi:10.1016/j.minpro.2006.02.003

fired at a rigid surface and the number of undamaged granules is counted as shown by Salman et al. (2001) in Fig. 1. In real-life granule processing industries it would be extremely useful to be able to predict the impact failure distribution without the need for extensive impact failure experiments. If the relationship between a granule's material properties, impact velocity and the resulting failure distribution were known then industries could predict the effects that process changes, such as transportation velocity, and material changes have on the amount of granule breakage. The model presented in this paper does just this: predicts the number of undamaged granules after impact from knowledge of impact velocity and angle, granule size and material properties of the granule and impact surface.

It is sensible that for any given granule there is a specific force required to cause the granule to fail by impact loading and a different specific force required to cause the granule to fail under static compression. Further, if a granule's properties are changed such that it becomes stronger and is more resistant to dynamic failure it is intuitive that it should become more resistant to static failure. It is well known that many granules fail by rupture of their interparticle bonds, Subero et al. (1999), and it has long been held that dynamic failure forces are not equal in value to static failure forces. This belief in the inequality between static failure force and dynamic failure force is largely due to the acceptance of creep (permanent deformation caused when certain materials experience low static forces for long periods of time) and high strain rate effects (increased resistance to deformation in some materials when exposed to high forces over very short periods). However it is believed that static failure loads can (in certain cases) be used to represent dynamic failure loads. The model and experimental results presented in this paper support this; as does previous work by Schonert (1979), who compared measured impact strains to evaluated static strains. By conducting static failure tests with relatively high loading rates (increase in force per time) the effects of creep can be ignored. Strain rate effects generally only have significance at high loading rates. It is believed that in this work either; the strain rate is not high enough in the dynamic impact to produce a difference between dynamic failure loads and static failure loads, or the spread in failure distribution as impact velocity increases incorporates the effects of strain rate as well as velocity increase. In either case the assertion that static failure loads can be used to predict dynamic failure distributions holds.

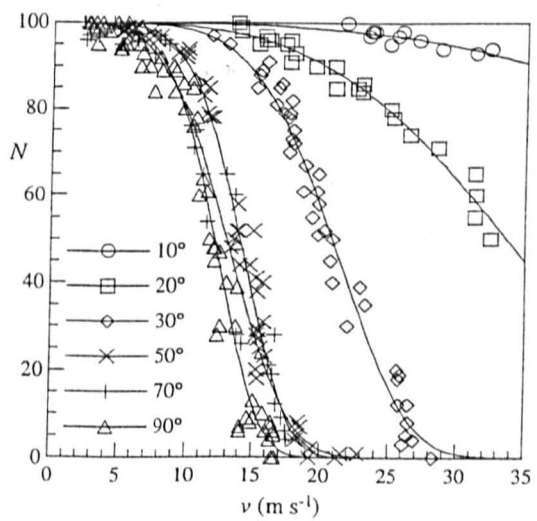

Fig. 1. Undamaged granules, N, as a function of impact velocity and angle.

Thornton et al. (1996) have used numerical solutions to analyse the failure of granules. This is based on simulations of discrete particles within granules and uses models representing the interparticle bonds and the subsequent rupture of these bonds when forces are applied. Another approach, applicable to granules of low porosity and ceramics, is to consider them as brittle elastic material, Galvez et al. (1997). This is the approach adopted in this work, as the porosity of the granules is $\approx 0.03\%$. Brittle elastic material allows the use of predicted forces based on the 'Hertzian elastic theory', work originally done by Hertz at the turn of the last century. Granules with porosity greater than those used in the experiments by Salman et al. (2001) will tend to move away from ideal Hertzian Elastic behaviour as the number and size of pores increase. The derivation of the critical normal impact velocity given in this paper should be used with dense granules, and is not applicable to porous granules.

The majority of work on brittle elastic failure assumes spherical particles and deals with elastic failure based on the original Hertzian theory, trying to relate induced stress fields to conventionally measured yield stresses in order to predict failure. Shipway and Hutchings (1993) present a method to find the internal and surface stress fields of a sphere as a function of applied load and contact area. The internal and surface stresses are different functions of the applied load and diameter of the sphere, and thus change at different rates as the load and diameter change.

This paper takes a slightly different approach and uses the predictions by Laugier (1984), dealing with

the force of impact in the platen, to find the relation between impact velocity and the force acting on the sphere by Newton's law. A previous paper by Maxim et al. (2002) gives some of the preliminary work to that which is presented in this paper. Other similar work includes that of Austin et al. (1992), who examined impact of cylindrical pellets of Al_2O_3, and that of Knight et al. (1977), who examined the failure of the impact platen. The critical normal impact velocity is defined by equating the force due to impact to a critical static failure load. Rather than trying to find the critical normal impact velocity by matching the yield stress of the material to the failure stress fields, a static failure force is measured and then related directly to the maximum force induced by normal impact velocity to find the critical normal impact velocity needed to induce failure. This method requires some simple static compression failure experiments to be conducted on granules of the material in question to find the static critical failure load.

1.1. 2-Parameter Weibull distribution

Salman et al. (2001) have characterised the failure of spherical fertilizer granules by firing them at a rigid platen at various velocities, v, and incident angles, θ (90° being perpendicular). The experiments tested 5.3 mm granules with the number of undamaged granules, N, being counted and plotted against impact velocity for each incident angle. Fig. 1 shows a typical set of data, also shown is the Weibull distribution curve fits using Eq. (1) below.

A 2-parameter Weibull distribution is used to relate the number of undamaged granules, N, to the impact velocity, v, as given below:

$$N = 100\exp\left[-\left(\frac{v}{c}\right)^{m}\right] \tag{1}$$

The Weibull distribution can be fitted to existing experimental impact data to find the values of c and m and then used to predict failure at other velocities of interest.

The parameter, m, does not vary with impact angle and has an average value of 4.50. The parameter, c, is interpreted as the critical impact velocity inducing 63.2% failure, further related to the critical normal impact velocity, u_f, by:

$$c = \frac{u_f}{\sin\theta} \tag{2}$$

More usefully, the Weibull equation can be used to predict failure distributions of dense granules from static failure tests by finding the critical normal impact velocity, u_f, and subsequently the c-parameter (with the m-parameter assumed constant at 4.50). The 2-parameter Weibull distribution (Eq. (1)) should also be applicable to porous granules, as this is just an equation to describe the shape of the failure distributions. The c-parameter, for porous granules, will have to be found from impact experiments and cannot be derived from static failure tests using the equation for critical normal impact velocity (which is based on the Hertzian theory and assumes the granules are dense and have brittle elastic behaviour).

1.2. Critical normal impact velocity, u_f

The critical normal impact velocity, u_f, developed in the theory section later, is defined as 'the velocity causing 63.2% of granules impacting normally on a surface to fail'. It is a function of material properties and particle size; it is a process independent parameter. For granules undergoing elastic failure with no plastic deformation the theoretical derivation defines u_f as a function of:

Static critical load F_{cr}
Density ρ
Young's modulus of the granule E
k-constant k
Radius of granule R

$$u_f = \left[\frac{F_{cr}}{1.835R^2}\left(\frac{k^2}{\pi^3E^2\rho^3}\right)^{1/5}\right]^{5/6} \tag{3}$$

The critical normal impact velocity can then be used to find the c-parameter (Eq. (2)) for various angles of impact. The Weibull equation (Eq. (1)) then gives the impact failure distributions as a function of impact velocity.

1.3. How it works

To get the theoretical distributions of impact failure:

1. Measure the critical static load.
2. Calculate the critical normal impact velocity, u_f (Eq. (3))
3. Use the critical normal impact velocity and impact angle to find the c-parameter (Eq. (2))
4. Use the Weibull equation (Eq. (1)) to find the failure distribution.

The static compression tests in step 1 need to be performed on real granules of the same material that will be used in the processes of interest. To find the critical normal impact velocity in step 2 requires knowledge of the material properties of the granules as well as the impact surface.

2. Theory

The basic idea is that the failure distributions of granules impacting on a surface at various velocities can be represented by a 2-parameter Weibull distribution, with the important c-parameter being predicted from static compression tests or fitted to experimental impact data. The distribution shape accounts for the randomness in the structure of the granules. The m-parameter describes the 'width' or 'spread' of the distribution whereas the c-parameter describes the critical impact velocity inducing 63.2% failure.

As the granules are dense (porosity <0.03%) it can be assumed they behave like brittle elastic material. It is assumed that the dense granules in question are spherical and thus Hertzian elastic theory can be used to predict the forces felt within the granule based on the size of the impact contact area (Laugier, 1984). Newton's laws of motion and simple trigonometry are applied to the sphere and combined with the force predicted by the Hertzian theory to give an expression, in terms of physical properties, for the effective acceleration in size of the contact area.

This acceleration expression is then manipulated and non-dimensionalised to give a dimensionless set of equations of motion for the impacting sphere. The numerical solution of which, for a non-failing sphere, yields real values for; total time of impact, maximum contact radius and maximum contact force.

A failure criterion is then applied that "a granule will fail if the theoretical maximum force is greater than the real force required to produce failure in that particular granule". The real force required to induce failure cannot be calculated and is difficult to measure exactly by impact experiments, thus it is suggested that the static critical load, F_{cr}, should be used as the equivalent real force inducing failure. The static critical load is found from static loading experiments and combined with the expression for maximum force of impact to give a critical normal impact velocity. The critical normal impact velocity is interpreted as the normal velocity creating a maximum force on impact that just equals the static failure load.

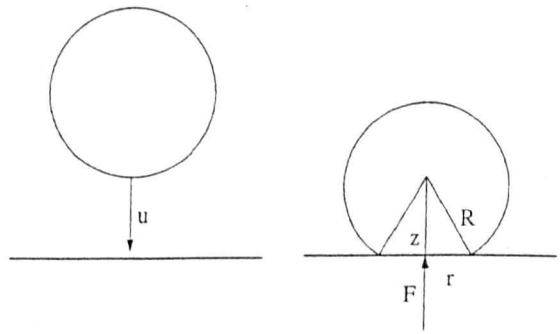

Fig. 2. Schematic of collision.

2.1. Derivation

Consider a sphere of radius, R, travelling at velocity, u, impacting on a rigid platen as shown in Fig. 2 below.

When the sphere impacts on the platen there is a force, F, acting to slow it down.

Assume the force acting on the sphere is given by (based on Laugier, 1984):

$$F = \frac{3}{4} r^3 \frac{E}{kR} \tag{4}$$

where:

$$k = \frac{9}{16}\left[\left(1-\gamma^2\right) + \left(1-\gamma_1^2\right)\frac{E}{E_1}\right] \tag{5}$$

k is simply a constant dependent on the material properties of the impacting sphere and the platen. E, E_1 and γ,γ_1 are the Young's moduli and Poisson's ratios of the sample and platen, respectively. R is the sphere radius and r is the contact radius.

Denoting the height of the centre of mass of the sphere above the platen surface as, z, and making the assumption that the squashed material has a negligible effect on the sphere radius then by trigonometry:

$$z = R\left(1 - \frac{r^2}{R^2}\right)^{1/2}$$

$$\text{if } r \ll R \text{ then } \frac{z}{R} \approx 1 - 1/2\left(\frac{r}{R}\right)^2 \tag{6}$$

The motion of the sphere must satisfy Newton's laws of motion where:

$$\text{Acceleration} \quad \ddot{z} = \frac{\partial^2 z}{\partial t^2} \tag{7}$$

$$\text{Mass} \quad \text{mass} = \frac{4}{3}\rho\pi R^3 \tag{8}$$

Using Eqs. (4) and (8) with Newton's law gives

$$\frac{3}{4}r^3\frac{E}{kR} = \frac{3}{4}\rho\pi R^3 \cdot \frac{d^2z}{dt^2} \tag{9}$$

Differentiation of Eq. (6):

$$\frac{d^2z}{dt^2} = -\frac{1}{2R}\frac{d^2r^2}{dt^2} \tag{10}$$

and substitution in Eq. (9) gives

$$\frac{d^2r^2}{dt^2} = -\frac{9}{8}r^3\frac{E}{k\rho\pi R^3} \tag{11}$$

If we introduce an area, a, and a constant, M, such that

$a = r^2$ and

$$M = \frac{9}{8}\frac{E}{8k\rho\pi R^3} \tag{12}$$

then Eq. (11) becomes

$$\ddot{a} = -Ma^{3/2} \tag{13}$$

Boundary conditions, with time, for Eq. (12) are given below. The contact area, a, at time (0)=0. The rate of change in the height, z, of the centre of mass above the impact platen, at time (0) is equal to the impact velocity, u.

$$a(0) = 0 \tag{14}$$

$$-\dot{z}(0) = u \tag{15}$$

For small deformation, differentiation of Eq. (6) and substitution into Eq. (14) gives

$$\dot{a}(0) = 2uR \tag{16}$$

Non-dimensionalising the area, a, and time, t, using

$$\bar{a} = \frac{a}{A} \tag{17}$$

$$\bar{t} = \frac{t}{T} \tag{18}$$

we can non-dimensionalise Eqs. (13), (14) and (16) giving

$$\ddot{\bar{a}} = -MT^2A^{1/2}\bar{a}^{3/2} \tag{19}$$

$$\bar{a}(0) = 0 \tag{20}$$

$$\dot{\bar{a}}(0) = 2uR\frac{T}{A} \tag{21}$$

where A and T are the dimensionless area constant and dimensionless time constant, respectively. These are effectively the dimensionless boundary conditions for the impact of the sphere on a platen.

A convenient choice for T and A is that which makes

$$MT^2A^{1/2} = 1 \tag{22}$$

$$2uR\frac{T}{A} = 1 \tag{23}$$

Solving Eqs. (22) and (23) simultaneously and substituting for M using Eq. (12) gives

$$A = 4R^2\left(\frac{u^2\rho k\pi}{9E}\right)^{2/5} \tag{24}$$

$$T = 2R\left(\frac{\rho\pi k}{9E\sqrt{u}}\right)^{2/5} \tag{25}$$

Eqs. (19), (20) and (21) now become:

$$\ddot{\bar{a}} = -\bar{a}^{3/2} \tag{26}$$

$$\bar{a}(0) = 0 \tag{27}$$

$$\dot{\bar{a}}(0) = 1 \tag{28}$$

Eq. (26) can be rewritten as:

$$\ddot{\bar{a}} = \dot{\bar{a}}\frac{d\dot{\bar{a}}}{d\bar{a}} = -\bar{a}^{3/2} \tag{29}$$

Integration of Eq. (28) using the boundary conditions given by Eqs. (27) and (28) yields:

$$\dot{\bar{a}}^2 = 1 - \frac{4\bar{a}^{5/2}}{5} \tag{30}$$

At $\bar{a}_{max}\dot{\bar{a}} = 0$ so that, from Eq. (30)

$$\bar{a}_{max}^{5/2} = \frac{5}{4} \text{ and } \bar{a} = 1.093 \tag{31}$$

We can now define a dimensionless force, $\bar{F}$, such that:

$$\bar{F} = \bar{a}^{3/2} \tag{32}$$

From the definition of $\bar{a}$ (Eq. (17)) and using $a=r^2$ gives:

$$\bar{F} = \frac{r^3}{A^{3/2}} \tag{33}$$

and, from Eq. (4):

$$r^3 = \frac{4}{3}\frac{kR}{E}F \tag{34}$$

Substitution for r^3 from Eq. (34) and for A from Eq. (24) leads to the dimensionless force:

$$\bar{F} = \frac{1}{2R^2}\left(\frac{3k^2}{\pi^3\rho^3E^2u^6}\right)^{1/5}F \tag{35}$$

The force reaches its maximum value when $\bar{a}=\bar{a}_{\max}$. It follows from Eqs. (31) and (32) that:

$$\bar{F}_{\max} = \left(\frac{5}{4}\right)^{3/5}1.143 \tag{36}$$

The maximum force is an especially important parameter as we can define the failure criterion as "a granule will fail if the theoretical maximum force is greater than the real force required to produce failure in that particular granule".

The maximum force can be found by substituting the dimensionless maximum force, Eq. (36), into Eq. (37) thus:

$$F_{\max} = 1.835R^2\left(\frac{\pi^3\rho^3E^2u^6}{k^2}\right)^{1/5} \tag{37}$$

The radius of maximum contact area can be found by:

$$r_{\max} = \sqrt{1.093A} = 2.091R\left(\frac{u^2\rho\pi k}{9E}\right)^{1/5} \tag{38}$$

The total collision time without failure can be obtained by numerical integration of Eq. (30) which gives the dimensionless time as $\bar{t}=3.218$ so that

$$\text{Time} = 3.218T = 6.436R\left(\frac{k\rho\pi}{9E\sqrt{u}}\right)^{2/5} \tag{39}$$

We now have an equation relating the maximum force, felt by a granule on impact, to:

The radius of the granule R
The material properties of the granule ρ, E, γ
The material properties of the impact surface E_1, γ_1
The velocity of impact u

A particular granule will fail if this maximum force is greater than the static critical load, F_{cr}, required to induce failure under static compression.

Failure criterion is $F_{\max} \geq F_{cr}$ (40)

For any granule impacting on a given surface the only variable that affects the failure force of that specific granule is the velocity of impact. It can clearly be seen from Eq. (37) that the maximum force felt on impact varies with velocity as $u^{6/5}$, thus a critical normal impact velocity, u_f, must exist above which failure of the granule will occur. This critical normal impact velocity is a process independent parameter used for predicting granule failure.

Eq. (37) and the failure criterion that the maximum force must equal or exceed the static critical load implies that the critical normal impact velocity can be written as Eq. (3).

This is the important result that allows the prediction of the critical impact velocity (parameter c) and subsequently the failure distributions using the Weibull distribution model. The static critical load can be found from static compression tests conducted on samples of granules. Steps (1) and (2) are shown clearly in Static compression experiments whilst steps (3) and (4) in Predicted impact failure distributions show how the predicted failure distribution using static compression tests matches the failure distribution obtained from impact experiments.

3. Experimental results and discussion

3.1. Weibull distribution—impact experiments

Salman et al. (2001) have characterised the failure of 5.3 mm (mean size) spherical granules of general purpose fertiliser (30% N, 20% P_2O_5, 20% K_2O). This is a weak material. The granules are roughly spherical with grain sizes ranging between 40 and 120 μm. This characterisation was done by firing them at a rigid platen at various velocities, v, and incident angles, θ (90° being perpendicular). The number of undamaged granules, N, were counted and plotted against impact velocity for each incident angle. A typical set of data and curve fits of the form given by the 2-parameter Weibull distribution (Eq. (1)) is shown in Fig. 1. Each point represents the number of undamaged granules, N, from 100 fired at the platen for that given velocity and angle.

The single particle impact experiments were carried out using a continuous flow gas gun as shown in Fig. 3. Initially a steady gas flow is established. Particles are then introduced one by one into the open breech and accelerated along a 300-mm-long section of the 8-mm diameter acceleration tube with a driving pressure up to 2 bars. The impact velocity was determined using two timing signals. The first timing signal was a photodiode switch at the end of the acceleration tube and the second was an electromagnetic vibration transducer attached to the target. The timer was connected to a computer, and the velocity was automatically measured for each impact from the measured timing interval.

3.2. Weibull distribution—fitting

For all angles used the curve fit parameters obtained are shown in Table 1.

Parameter, m, shows no significant variation with impact angle and has an average value of 4.50.

The c-parameter is interpreted as a measure of the velocity required to induce 63.2% failure. Further related to the critical normal impact velocity by:

$$u_f = c\sin\theta$$

In which case we should find that c should be directly proportional to $1/\sin\theta$. Fig. 4 shows that this is indeed the case. Parameter, c, declines as the incident angle approaches the perpendicular.

As the c-parameter is proportional to $1/\sin\theta$, it should be possible to represent all the data for a fixed granule size with N as a function of $u_f = c\sin\theta$ only. This is shown in Fig. 5 (symbols represent different angles, same as in Fig. 1, but the data has all been normalised).

3.3. Static compression experiments

It has already been shown that the Weibull equation accurately describes the failure distribution of impacting fertilizer granules and the theoretical model suggests it is possible to predict the critical normal impact velocity from material properties and static compression failure tests. The theory was verified using similar granules to those used in the original impact experiments and conducting static compression experiments on them. The measured static critical loads were then used to find the critical normal impact velocity and subsequently a theoretical failure distribution using the Weibull equation.

Table 1
Curve fit parameters for Weibull distribution

θ	c	m
90°	12.94±0.11	5.11±0.29
70°	14.18±0.2	4.03±0.29
50°	14.91±0.08	5.49±0.29
30°	22.22±0.15	5.19±0.22
20°	37.14±0.56	3.66±0.17
10°	67.34±12.03	3.54±0.73

The granules were placed between 2 rigid hard platens and a compressive load applied. The static failure loads were measured and Eq. (3) used to calculate the critical normal impact velocity for the granules using a density of 2000 kg/m^3, a Young's modulus of 2.48×10^9 N m^{-2} and a k value of 0.5. The results of individual tests are shown as points in Fig. 6. Also shown as a dashed straight line is the average critical normal impact velocity found from static failure tests and as a solid straight line the critical normal impact velocity found by fitting the Weibull equation to measured values from impact experiments. It can be seen that the fitted u_f value from impact experiments lies close to the theoretically predicted values from static compression experiments. Also, all u_f values calculated from static compression experiments lie within the range of velocities causing failure from Fig. 1. The random spread in static failure loads is due to the random nature of the granules as discussed in Introduction.

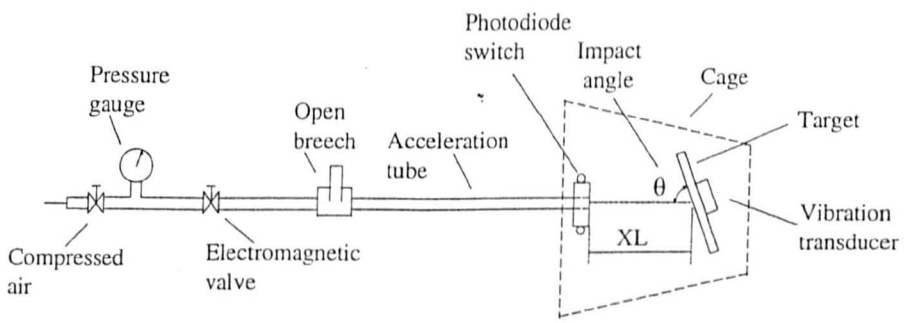

Fig. 3. Single-impact test apparatus and arrangement of measuring systems.

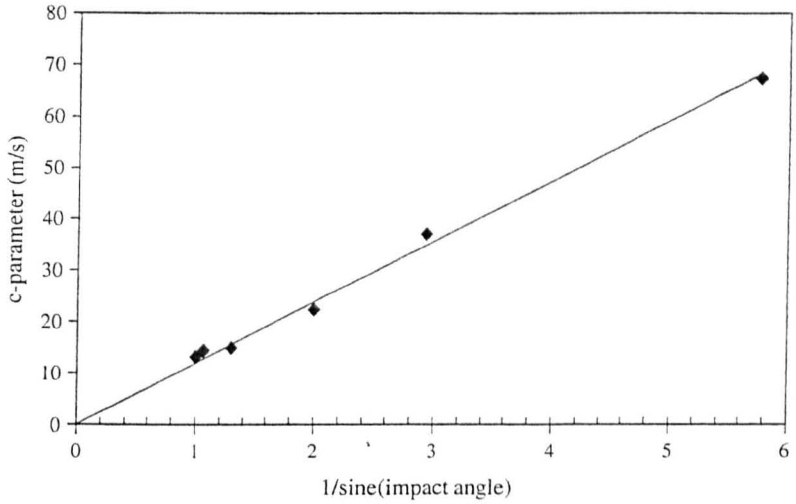

Fig. 4. *c*-parameter as a function of 1/sine angle.

3.4. Predicted impact failure distributions

The critical normal impact velocities calculated from the static compression tests were used to find the *c*-parameter using Eq. (2), an impact angle of 90° was assumed so the *c*-parameter was equal to the critical normal impact velocity. The predicted failure distributions were plotted for impact velocities from 0 to 20 m/s using Eq. (1), a constant *m*-parameter value of 4.50 was used and *c*-parameter values taken from the static compression tests. Fig. 7 shows predicted failure distributions based on: the highest and lowest recorded static failure load; the average failure load of all the static compression tests; and the original experimental impact data.

As can be seen the predicted failure distribution based on the average value from the static compression tests fits fairly closely to the experimental impact data.

4. Conclusion

It has been demonstrated that real experimental impact failure distributions for dense granules can be

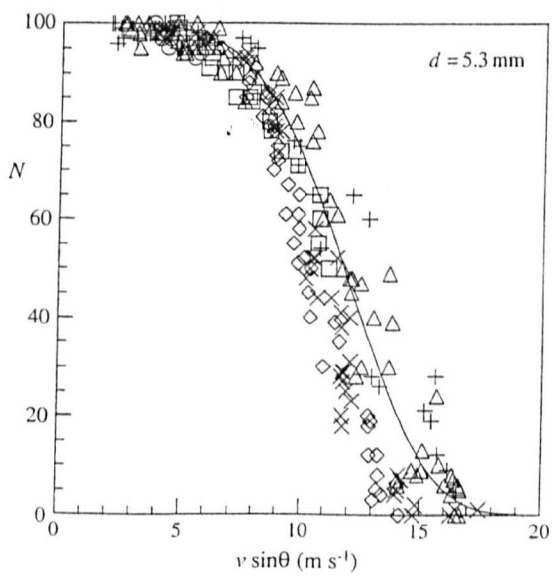

Fig. 5. All data for 5.3 mm granules plotting *N* as a function of normal velocity.

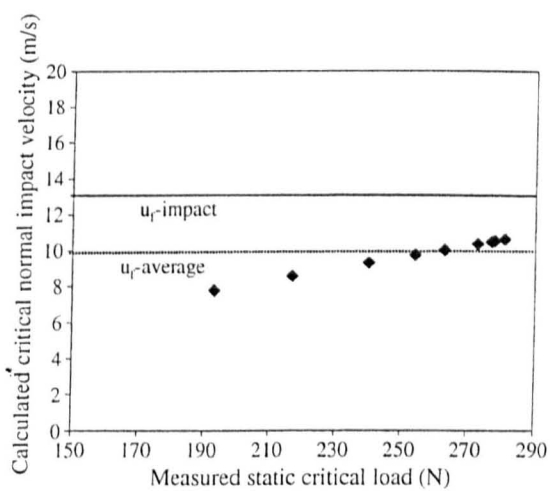

Fig. 6. Critical normal impact velocity, u_f, for 5.3 mm granules, derived from impact experiments compared to the average and individual values derived from static compression loading.

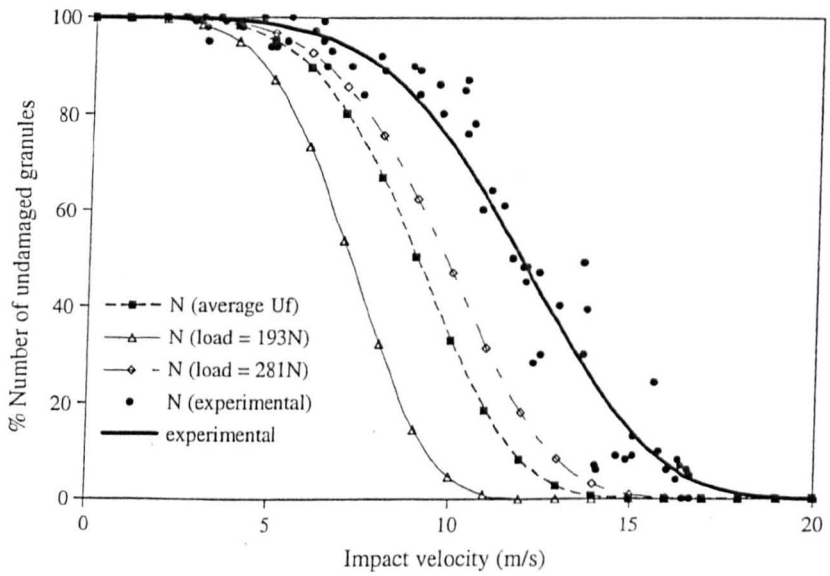

Fig. 7. Failure distributions of 5.3 mm granules comparing the experimental impact data to predicted distribution from individual and average static compression loading.

suitably represented by the 2-parameter Weibull equation. It was further demonstrated that the important parameter, the *c*-parameter, is related to the angle of impact and the critical normal impact velocity. This critical normal impact velocity can be found from knowledge of the granule material properties and failure loads found by experimental static compression tests. A fairly good agreement between the theoretical critical velocities calculated using these static critical loads and the values obtained from impact experiments supports the applicability of the theory. This is an important point; this paper shows that it is possible to and how to use static failure results to predict dynamic impact failure.

Nomenclature

a	Area (m^2)
$\dot{a}$	da/dt ($m^2\ s^{-1}$)
$\ddot{a}$	d^2a/dt^2 ($m^2\ s^{-2}$)
$\bar{a}$	Dimensionless area
A	Dimensionless area constant (m^{-2})
c	Parameter in Weibull distribution—critical impact velocity
D	Diameter of granule (m)
E	Young's modulus of granule ($N\ m^{-2}$)
E_1	Young's modulus of platen ($N\ m^{-2}$)
F	Force (N)
$\bar{F}$	Dimensionless force
F_{cr}	Static critical load (N)
k	Constant—Laugier equation
L	Dimension of Length (m)
M	constant $= \frac{9}{8k\rho\pi R^3}\frac{E}{}$ ($m^{-1}\ s^{-2}$)
m	Parameter in Weibull distribution
N	Number of undamaged granules per 100 fired
r	Radius of circle of contact (m)
R	Radius of granule (m)
T	Dimensionless time constant (s^{-1})
T'	Dimension of time (s)
$\bar{t}$	Dimensionless time
u	Normal velocity ($m\ s^{-1}$)
u_f	Critical normal failure velocity ($m\ s^{-1}$)
z	Elevation of the centroid of a granule above the platen (m)
v	Velocity of granule ($m\ s^{-1}$)
θ	Angle of impact with platen (90° being perpendicular)
ρ	Density ($kg\ m^{-3}$)
σ	Normal stress ($N\ m^{-2}$)
γ	Poisson's ratio of granule
γ_1	Poisson's ratio of platen

References

Austin, L.G., Trubelja, P.M., Scarlett, B., 1992. A study of the fracture of pellets fired against a target. Particle & Particle Systems Characterization 10, 347–352.

Galvez, F., Rodriguez, J., Sanchez, V., 1997. Tensile strength measurements of ceramic materials at high rates of strain. Journal de Physique IV France 7 C3, 151–156 (Colloque C3, supplement au Journal de Physique III d'aout 1997).

Knight, C.G., Swain, M.V., Chaudhri, M.M., 1977. Impact of small steel spheres on glass surfaces. Journal of Materials Science 12, 1573–1586.

Laugier, M.T., 1984. Hertzian indentation of sintered alumina. Journal of Materials Science 19, 254–258.

Maxim, R.E., Salman, A.D., Hounslow, M.J., 2002. Impact of granules: failure distribution. 4th World Congress of Particle Technology Sydney. Aus. Paper Number, vol. 113.

Salman, A.D., Fu, J., Gorham, D.A., Hounslow, M.J., 2001. Impact breakage of fertilizer granules. 7th International Symposium on Agglomeration, Albi, vol. 1. European Federation of Chemical Engineering, pp. 451–461.

Schonert, K., 1979. Aspects of physics of breakage relevant to comminution. Fourth Tewksbury Symposium, Melbourne, Aus.

Shipway, P.H., Hutchings, I.M., 1993. Fracture of brittle sphere under compression and impact loading: 1. Elastic stress distributions. Philosophical Magazine. A 67 (6), 1389–1404.

Subero, J., Ning, Z., Ghadiri, M., Thornton, C., 1999. Effect of interface energy on the impact strength of agglomerates. Powder Technology 105, 66–73.

Thornton, C., Yin, K.K., Adams, M.J., 1996. Numerical simulation of the impact fracture and fragmentation of agglomerates. Journal of Physics D: Applied Physics 29, 424–435.

Appendix B

Crushing Test Graphs

Chart 2 - Load per particle as a function of Size - constant dose mass

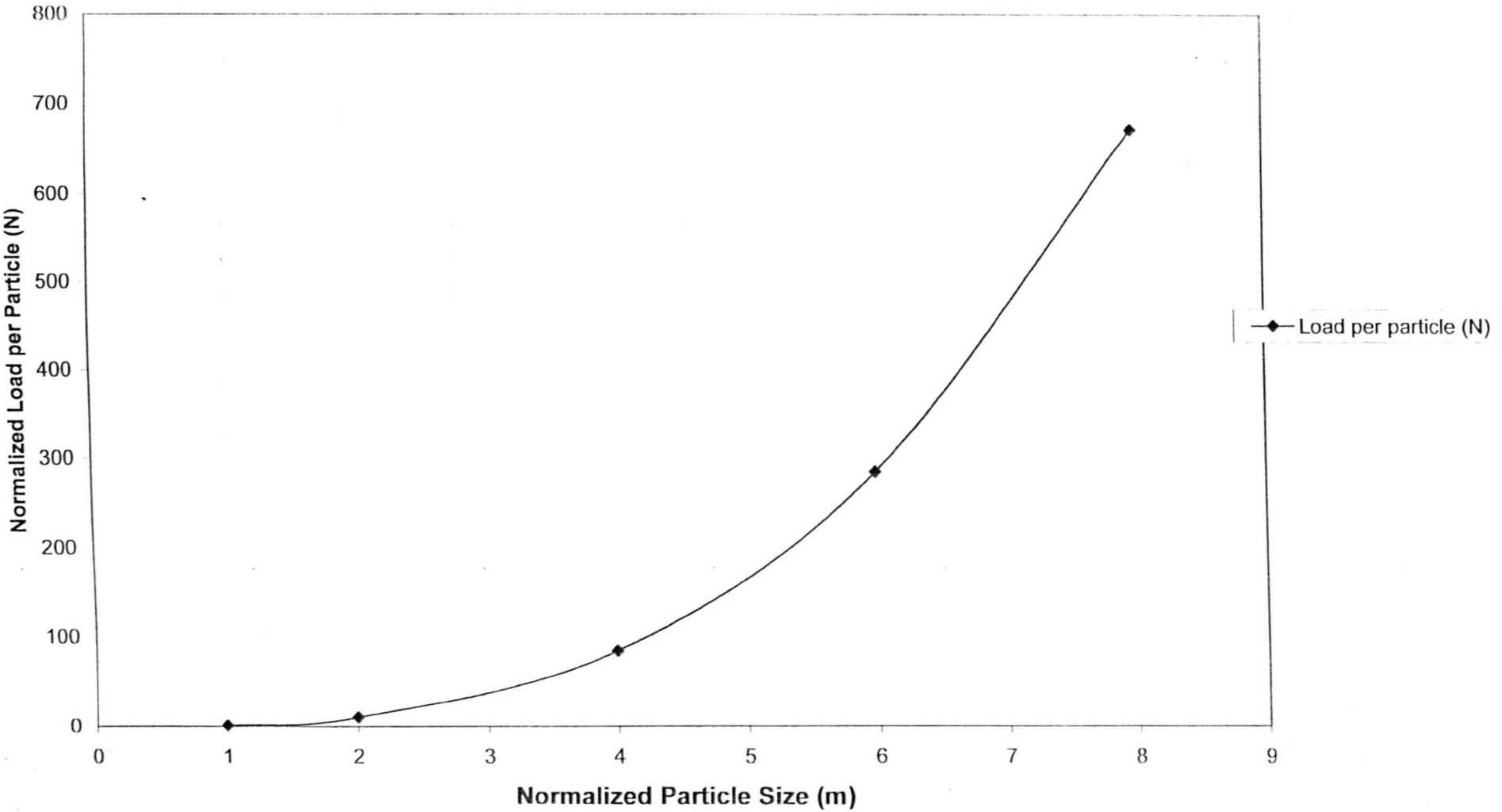

Chart 1 - Effect of mass dose and particle diameter on the total contact area of particles being crushed

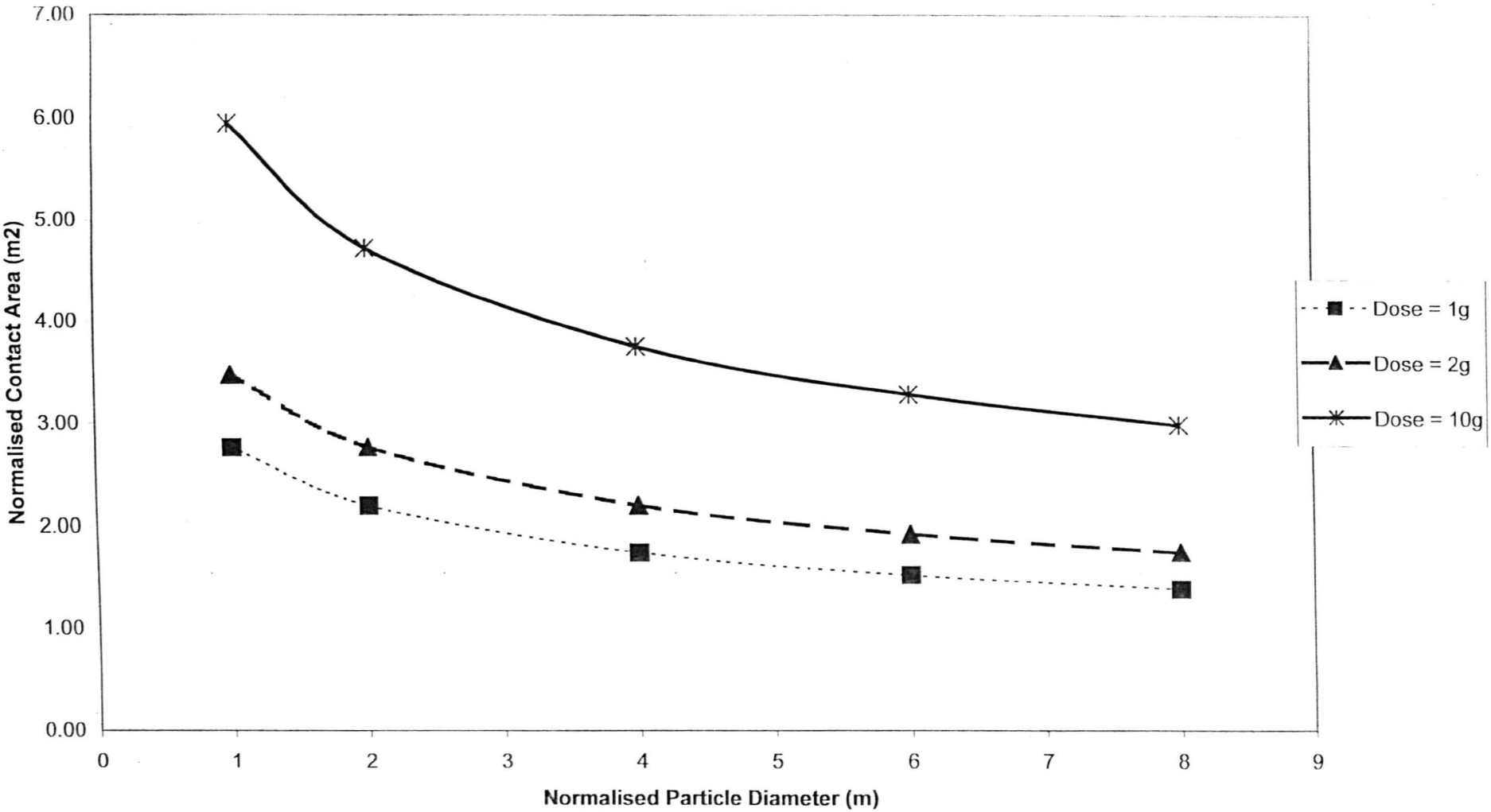

Chart 3 - Total Pressure on substrate as a function of size (constant dose mass)

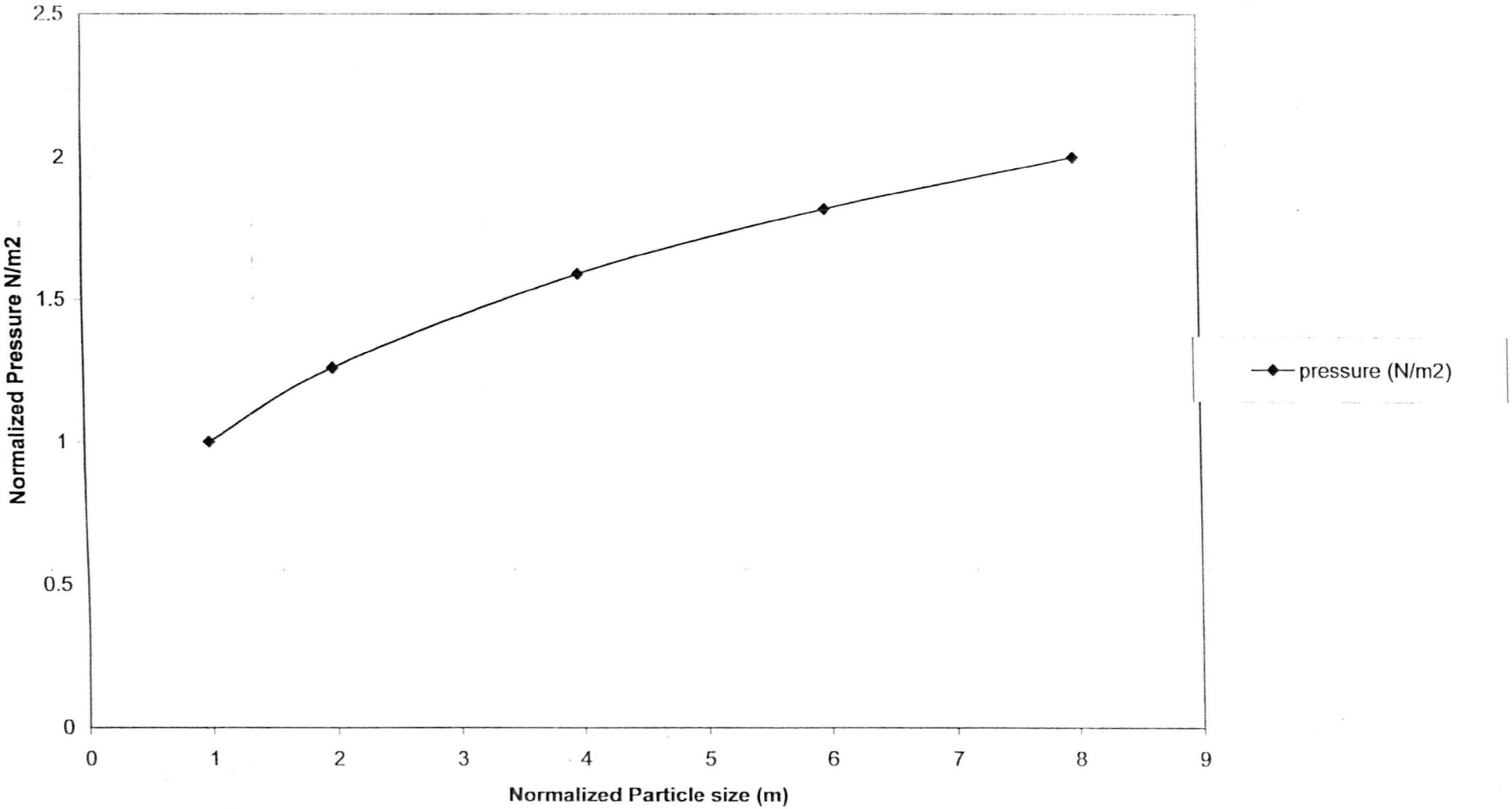

Chart 4 - Effect on total contact area and Pressure for particles changing size from large to small (constant number)

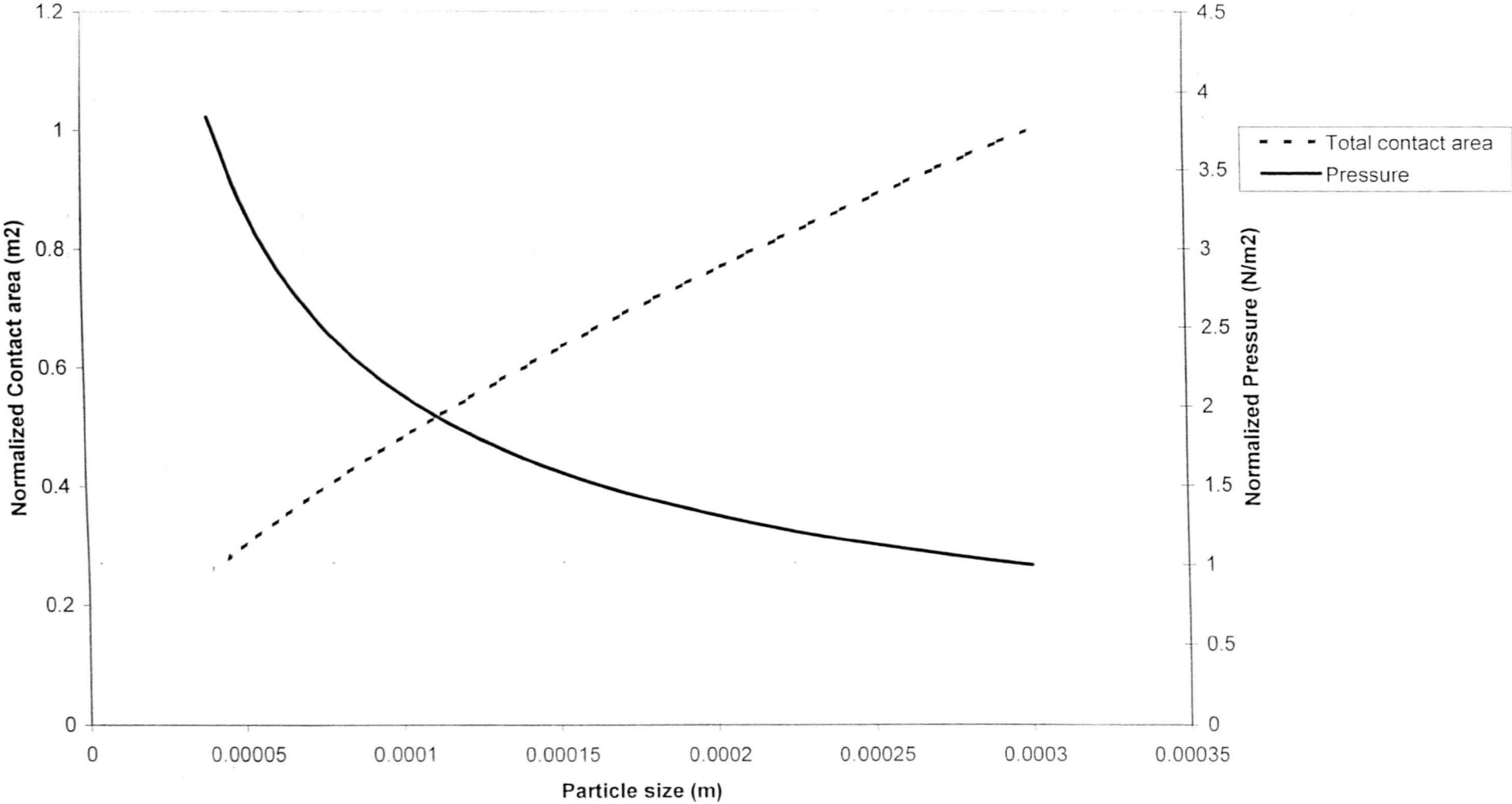

Chart 5 - Contact area as a Fuction of Particle Size and Applied Load

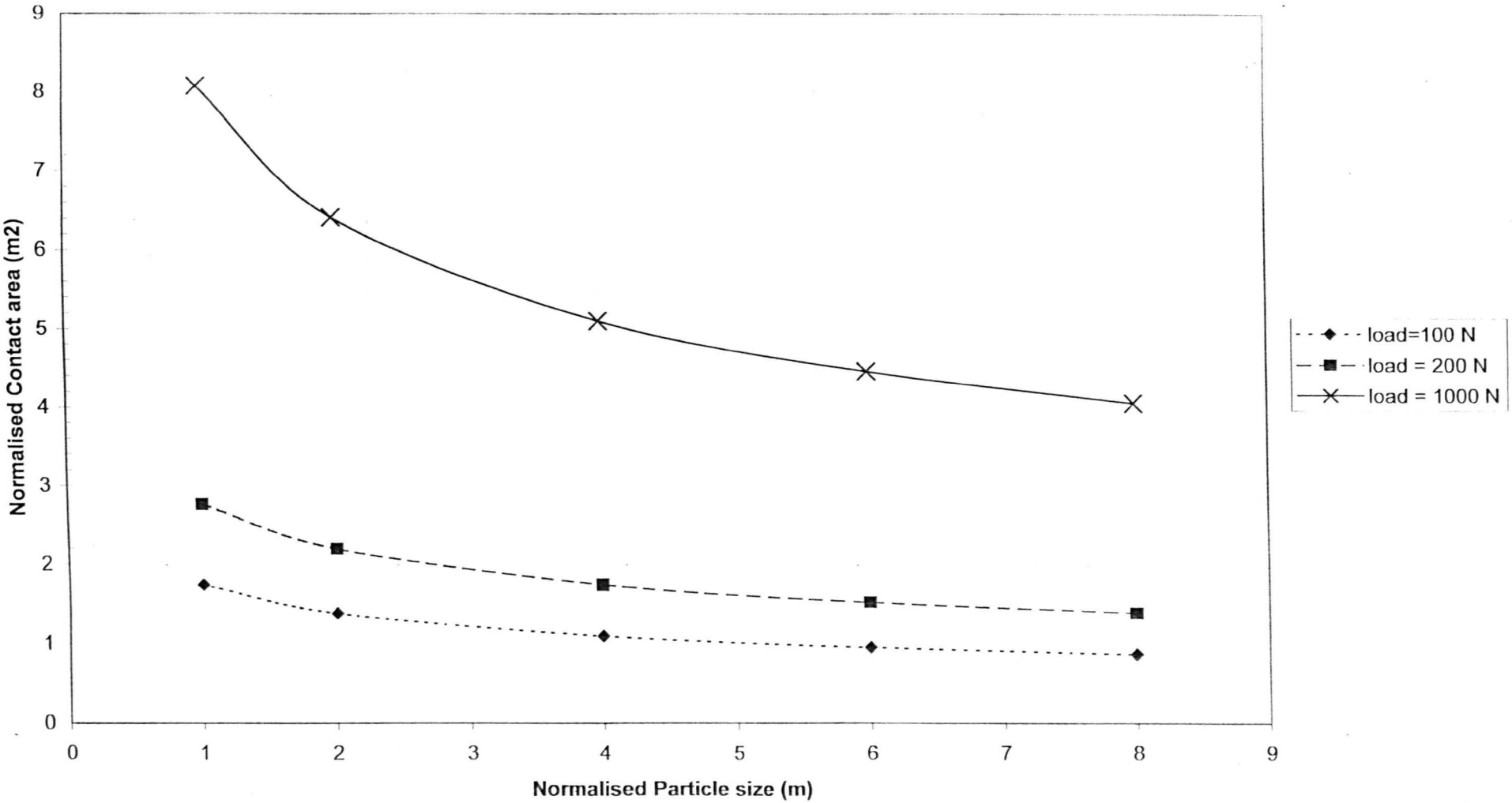

Appendix C

Derivation of Analysis of Binder Content and Packing Structure

Analysis of Binder Content of Orthorombic (Body-Centred-Cubic) packing of spherical particles.

Stage 1

Volume of a sphere:

$$= \frac{\pi}{6} d^3 \qquad (1)$$

A body-centred cubic packing arrangement will have a co-ordination number of 8. See diagram 1 below:

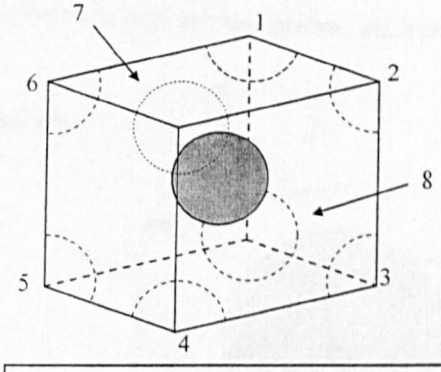

Diagram 1 showing the body-centred particle and the sections of 8 other particles contained in the control volume

According to the notes from the 2-day "agglomeration of powders" course by Prof. J. Seville and Prof. P. Knight of Birmingham University this should equate to a porosity of 0.395

Porosity is defined as:

$$Porosity = \frac{Volume\ of\ voids}{Total\ Volume}$$

For our cubic region let us assume that all the spherical particles at the corners are touching the central sphere. Assume the sphere has a radius of 1. Therefore the diagonal length across the sphere *xyz* will be length 4 (2 + 1 + 1). (2 radius' from the central sphere plus 1 radius from each sphere at the opposite corners.)

Let the length of 1 side of the cube be, *l*, then by trigonometry:

$$3l^2 = 4^2$$

$$l = 2.3094011$$

Thus the volume of the cube = 2.3094011^3

= 12.316806

Volume of spheres = $2 \times \frac{\pi}{6} d^3$

= 8.3775804

Volume of voids = 12.316806 – 8.3775804

= 3.9392253

=> Porosity = $\frac{3.9392253}{12.316806}$

= 0.3198252 (which is different from the quoted value in the text by Seville and Knight)

Stage 2

Imagine the spheres touch at their points, such that 1-2-3 is an unbroken line. (see diagram 2)

Line 1-2-3 = w

Diameter of sphere = d

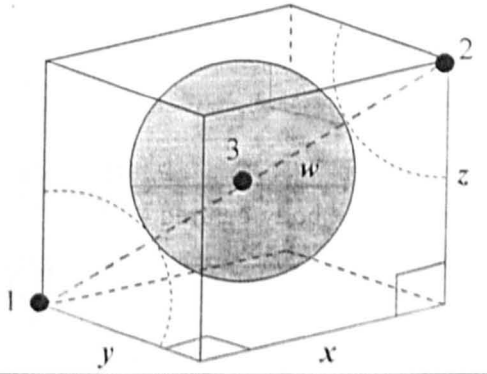

Diagram 2 – showing dimensions for calculation of control volume in terms of particle diameter 'd'

Length of line w

$$w^2 = x^2 + y^2 + z^2$$

but the CV (control volume) is a cube => x = y = z

thus:

$$w^2 = 3x^2 \qquad (2)$$

also

$$w = 2d$$

(2) implies $4d^2 = 3x^2$

$$\sqrt{\frac{4}{3}}d = x \qquad (3)$$

volume of cube, V_c = $3x^3$

= $\left(\sqrt{\frac{4}{3}}d\right)^3$

V_c = $\left(\sqrt{\frac{4}{3}}\right)^3 d^3$ (4)

Volume of spheres, V_s = $\frac{2\pi}{6}d^3$ = $\frac{\pi}{3}d^3$ (5)

Porosity (or space filled with binder), B_v (as fraction):

$$B_v = 1 - \frac{V_s}{V_c} \qquad (6)$$

(4) and (5) into (6) =>

$$B_v = 1 - \left(\frac{\pi d^3}{3} \div \sqrt{\frac{64}{27}}d^3\right)$$

$$B_v = 1 - \frac{\sqrt{3}\pi}{8}$$

General. B_v = 0.3198252 (7)

Therefore if there is no gap / space between the particles (spheres) at the points of contact (the point of closest approach between neighbouring particles) then the binder content as a ratio of the total volume is independent of the volume and independent of volume of individual granules (diameter of sphere drops out of equation (7).

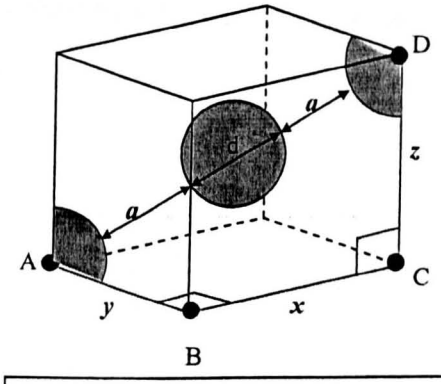

Diagram 3 – showing binder layer 'a'

Imagine a second case where there is a gap between the particles due to a binder film of thickness, a,. As shown in the diagram 3 above.

Again $x = y = z$

Length of line AD is given by:

$$AD^2 = y^2 + x^2 + z^2$$

$$AD^2 = 3x^2$$

$$(2d+2a)^2 = 3x^2$$

thus: $$\frac{2}{\sqrt{3}}(d+a) = x \qquad (8)$$

therefore volume of cube:

$$V_c = \frac{8}{3\sqrt{3}}(d+a)^3 \qquad (9)$$

Volume of sphere:

$$V_s = \frac{\pi}{3}d^3 \qquad (5)$$

(5) and (9) into (6) =>

$$B_v = 1 - \frac{\pi d^3 3\sqrt{3}}{3\times 8(d+a)^3}$$

$$B_v = 1 - \frac{\sqrt{3}}{8}\pi\frac{d^3}{(d+a)^3} \qquad (10)$$

This is the equation for the binder fraction of a cubic body-centred packing structure.

Analysis of Binder Content of a tetrahedronal shaped unit cell (non-Body-Centred) packing of spherical particles.

Packing state of a tetrahedron (4 sided pyramid with equilateral triangles) see diagram 4. Each vertices A, B, C and D represents the centre of a spherical particle.

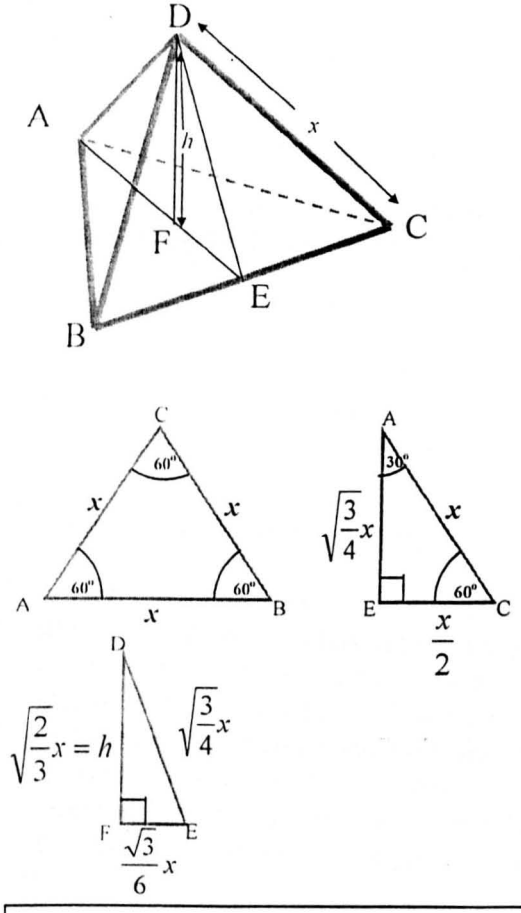

Diagram 4 – tetrahedronal packing structure and dimensions

Volume of any cone is given by:

Volume = 1/3 (area of base) x (height)

For our case:

$$\text{Area of base} = \frac{1}{2}x\sqrt{\frac{3}{4}}x$$

$$= \frac{\sqrt{3}}{4}x^2$$

Therefore volume of tetrahedron:

$$\frac{1}{3}\cdot\frac{\sqrt{3}}{4}x^2\cdot\sqrt{\frac{2}{3}}x$$

$$V_{tetrahedron} = \frac{\sqrt{2}}{12}x^3 \qquad (11)$$

Thus if we imagine the control volume for the packing is a tetrahedron of side, x, and the particles (spheres) are of diameter, d, then:

$$x = d$$

$$V_{cv} = \frac{\sqrt{2}}{12}d^3 \qquad (12)$$

Volume of a sphere is given by (5)

A single vertices of the control volume contains approximately $1/20^{th}$ of a sphere (This is an approximation as it has not been possible to calculate or find the exact fraction of a sphere that will be contained at the apex of a Tetrahedron – Tetrahedron pack approximately to a regular 20 faced ICOSAHEDRON, however the internal axis of the pyramids forming an icosahedron are shortened. When Tetrahedron are packed around a central point you can fit 20 with a small amount of space let over → the actual volume of a sphere contained at each vertice will be slightly less than 120^{th} of a sphere). Using this approximation the volume of particles in the control volume is approximately $4/20 = 1/5^{th}$ of a sphere.

Volume of solid particles in the control volume:

$$V_s = \frac{\pi}{30}d^3 \qquad (13)$$

The space filled by binder (binder fraction) is given by (6).

(12) and (13) => $$B_v = 1-\left(\frac{\pi d^3}{30}\div\frac{\sqrt{2}}{12}d^3\right)$$

$$B_v = 1-\frac{\sqrt{2}}{5}\pi$$

General $B_v = 0.1114234$ (14)

Imagine a further case where the control volume is still a tetrahedron and the primary particles are spheres of diameter, *d*, but there is a gap between the particles due to a binder film of thickness, *a*.

The length of side, *x*, of the control volume is now given by:

$$x = d + a \quad (15)$$

Thus the control volume is now given by:

$$V_c = \frac{\sqrt{2}}{12}(d+a)^3 \quad (16)$$

The volume of the particles stays the same (13).
Equation (6) => Binder fraction:

$$B_v = 1 - \left(\frac{\pi}{30} d^3 . \frac{12}{\sqrt{2}} (d+a)^{-3} \right)$$

$$B_v = 1 - \frac{\sqrt{2}}{5} \pi \frac{d^3}{(d+a)^3} \quad (17)$$

This is the equation for the binder fraction of a tetrahedronal packing structure.

When comparing eqn (10) and (17) it can be seen that for a generic packing of identical spherical particles the fraction of the total packed volume (ignoring edge conditions) is dependent on the diameter of the particles, *d*, the binder thickness, a, and a packing factor, *k*, relating to the way the particles pack together. Such that:

$$B_v = 1 - \frac{k\, d^3}{(d+a)^3} \quad (18)$$

Where: for body-centred-cubic packing:

$$k = \frac{\sqrt{3}}{8} \pi$$

For packing based on a tetrahedronal close packing (approximation):

$$k = \frac{\sqrt{2}}{5} \pi$$

It follows that the binder thickness, a, should be related to the flow properties of the binder, i.e. the viscosity, density and compressibility.
The diameter of particles, d, is obviously related to the size of particles being used.

In order visualize how the packing structure, particle diameter and binder thickness affect the interparticle space plots were produced of the generic packing equation using k-

values for tetrahedral packing (approximated as k= 0.88) and body-centred-cubic (k=0.68).

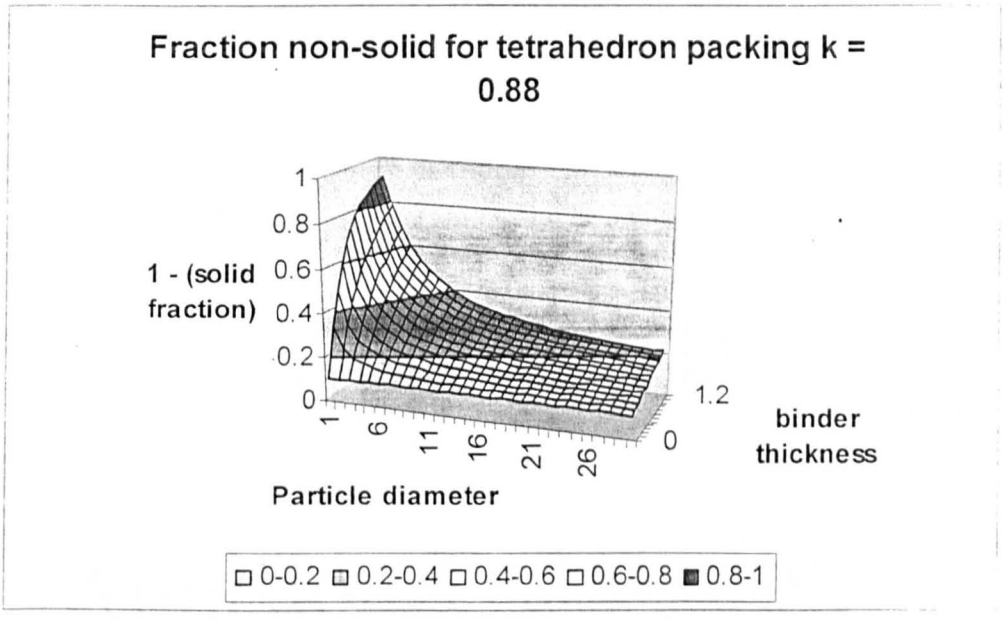

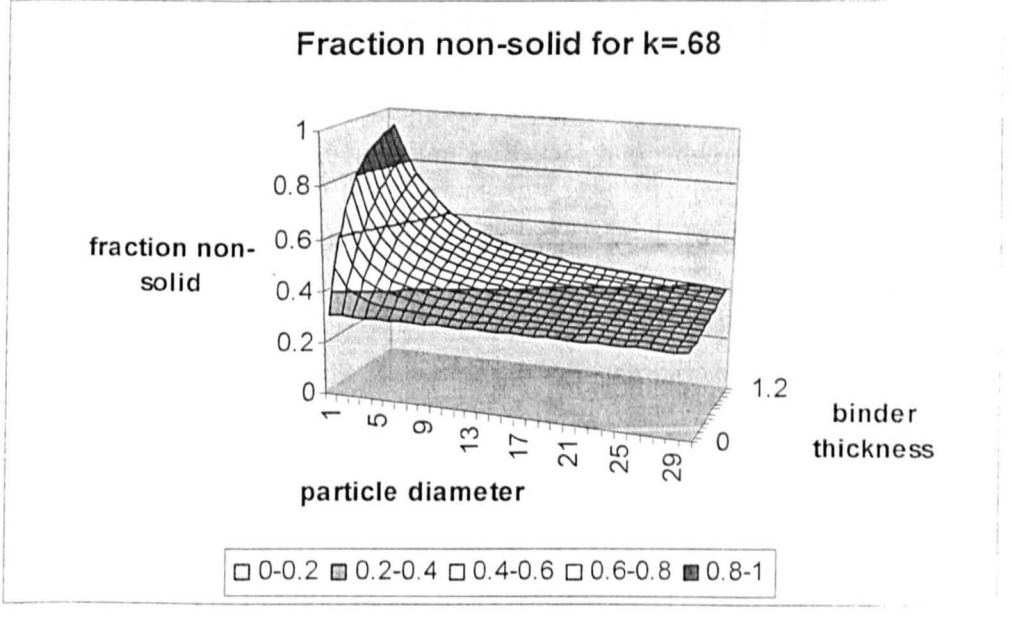

Appendix D

Abrasion Testing Report (early report)

Robert Maxim

Report: Abrasive testing of Granules (up to 12-08-03)

Introduction

The general aim of the research is to determine if it is possible to produce designer granules that have a specified abrasive strength. Granules have been made using a lab-scale high-shear mixer; the primary particles are $CaCO_3$ (Calcium Carbonate) and the binder is PEG (PolyEthyleneGlycol). The abrasive testing was done using 4 different toothbrush abrasion rigs:

1) Lissajous (swirling) motion abrasion rig at Port Sunlight research labs
2) Unilever Linear motion abrasion rig at Chemical Eng, Dept. Sheffield
3) In-House Linear motion abrasion rig at Chemical Eng. Dept. Sheffield
4) Random motion Hand-Held abrasion tester at Chemical Eng. Dept. Sheffield

The initial testing was done on the Lissajous rig using the standard Knoop indent testing method devised by Unilever (measures the amount of abrasion based on the change in length of a diamond shaped indent). Variation in the amount of abrasion generated by different granules and abrasion conditions was observed. Tests to determine the granule dose effect were carried out using the Hand-Held abrasion tester; these tests did not produce useful quantitative results for comparing the abrasive properties of the granules. Further tests were carried out on the Unilever Linear rig to compare it to the Lissajous rig; these tests produced visible scratching and grooving. Tests were then done using the In-House Linear rig to determine whether the toothbrush heads, the granules or a combination of both, generated the scratches. Tests were carried out to analyse the damage caused to the granules themselves during the abrasion process.

Testing Methods

This section describes the method used for the tests.

Lissajous Abrasion Rig

Square PMMA sample plates were indented with 4 diamond shaped Knoop indents and left to stand for 24hrs (for the PMMA to relax) before the length of the indents were measured. The indents were produced using a load of 1000 grams applied over 12 seconds. A suspension of granules in oil was made up using 6 grams in 60 grams of oil; 10 ml of this suspension was then dosed onto each sample plate. The Lissajous abrasion rig was then run for 400 strokes at 150 strokes per minute with a total downward load of 375 grams. The samples were then removed and the indents measured. The depth of abrasion was calculated from the change in length of the indent.

Hand-Held Abrasion Tester

Rectangular PMMA sample plates were indented with 4 diamond shaped Knoop indents and left to stand for 24hrs (for the PMMA to relax) before the length of the indents were measured using a computer aided microscope in the Materials Engineering Department. The indents were produced using a load of 100 grams applied over 15 seconds. 6 tests were conducted using the granule size and dose indicated in the table below.

No.	Granule Size	Dose
1	< 38 μm	0.5 g / 5 ml
2	< 38 μm	1 g / 5 ml
3	< 38 μm	2 g / 5 ml
4	> 300 μm	0.5 g / 5 ml
5	> 300 μm	1 g / 5 ml
6	> 300 μm	2 g / 5 ml

The Hand-Held abrasion rig was run for 3 minutes with a total downward load of between 4 and 10 grams. The samples were then removed and the indents measured using 2 separate computer aided microscopes; the same microscope that was used to measure the initial indents and a second microscope located in the Chemical Engineering Department. The depth of abrasion was calculated from the change in length of the indent.

Unilever Linear Motion Abrasion Rig

2 Square PMMA sample plates were used without Knoop indents. Separate suspensions of < 38 μm and > 212 μm granules in oil were made up using 0.6 grams in 5 ml of oil and dosed onto each sample plate. The abrasion rig was then run for 1000 strokes at speed setting 5 with a total downward load of 15.5 grams. The samples were then removed and the damage to the granules and the sample plate observed under a microscope.

In-House Linear Motion Abrasion Rig

Square PMMA sample plates were used without Knoop indents. A suspension of 106 – 300 μm granules in oil made up using 0.5 grams in 2 ml of oil was dosed onto each sample plate. The abrasion rig was then run for 10 minutes at 140 strokes per minute. Tests were run with a total downward load of: 103.2 grams, 153.2 grams, 203.2 grams and 303.2 grams. The samples were then removed and the damage observed under a microscope. A separate test was conducted using oil only without granules and a total downward load of 103.2 grams.

Size analysis of granules before and after abrasion

A suspension of 63 – 106 μm granules in oil was made up using 0.6 grams in 5 ml of oil. This was stirred using a pipette to agitate the granules and keep them in suspension. 2 separate samples were taken and measured using the Sympatec (laser scattering particle size distribution device) in a 6 ml cuvette that was stirred by hand. A separate sample was taken and measured using the Sympatec in a 25 ml cuvette that was stirred mechanically. Roughly 3 ml of the granule suspension was then abraded for 3 minutes using the Hand-Held abrasion rig. The abraded particles were measured using the Sympatec, 2 samples using the 6 ml cuvette and 1 using the 25 ml cuvette.

Results

This section describes the results from each test.

Lissajous Abrasion Rig

Granules made from $CaCO_3$ and PEG all produced abrasion resulting in a calculated depth change of 3 to 4 times that produced by granules of the same size made from Wessalith (Zeolite) and PEG. The control test using oil only without any abrasive particles produced an average depth change of 0.1 μm compared to 1 μm for the Wessalith granules. For granules made from $CaCO_3$ and PEG there was a small decrease in the average of depth change as the size of the granules increased

Hand-Held Abrasion Tester

During the test the granules moved towards the sides of the sample plate holder leaving a barren area in the middle of the sample plates. The depth change caused by abrasion increases with increasing mass of dose and smaller granules produce more abrasion for a given mass of dose. This is based on measurements of the indents before and after abrasion using different microscopes.
When the same microscope is used to measure the indents before and after abrasion the results are very scattered and there are no obvious trends.

Unilever Linear Motion Abrasion Rig

For the > 212 μm granules most of the granules were pushed to each end of the sample trough and were not taking part in the abrasion. The images of the > 212 μm granules before abrasion show the presence of lots of relatively small particles on the surface of the granules, this makes the granules look like surface rough spheroids. There is no sign of small granules / particles present in the oil that are not attached to large granules. Images of the > 212 μm granules after abrasion show that the large granules are smooth spheroids. There are also lots of smaller particles present in the oil.
For the small granules the images before abrasion show small sharp edged granules with some completely opaque granules and some with translucent sections. After abrasion the granules appear more rounded and there is a greater portion of translucent granules and sections of granules. There are also lots of smaller particles present floating in the oil.
The surface of the sample plates moved over by the brush head had lots of straight scratches and gouges in the surface all running parallel to the direction of the linear brush motion. They had a pattern similar to a bar code, with some sections having lots of scratches and others with very few. On one sample there was also a single, un-broken abrasion line in an area with no other scratches.

In-House Linear Motion Abrasion Rig

The PMMA sample plates were examined before abrasion and no scratches were present on any of the plates. After abrasion all the sample plates had scratches and grooves running parallel to the direction of the brush strokes. The sample plate that was brushed with oil only had grooves similar to those produced on the plate brushed with granules for the same loading. The thickness and depth of grooves appeared to

increase with loading, although this was difficult to tell using the 2-dimensional microscope.
The dry granules, before oil was added, were a mixture of sizes and looked like large rough spheroid granules aggregated with smaller angular granules attached to their surfaces. After oil was added most of the smaller granules detached from the larger spheroid granules leaving the larger granules appearing smooth.
In all tests granules were pushed to each end of the sample holder, with large granules collecting together close to the brushing region and small granules collecting together near the edges of the sample holder. When the granules were examined under a microscope after abrasion it was not possible to tell if damage had occurred to the large granules. The smaller angular granules appeared to have reduced in size, becoming smoother, rounder and more translucent. The images of granules in oil before and after abrasion show a similar number of floating small particles.

Size analysis of granules before and after abrasion

For granules measured before abrasion: The first test using the small 6 ml cuvette used 2 readings and gives a (mass based) mode size of ~ 90 μm, the second test used 6 readings and gives a (mass based) bi-modal size distribution with peaks at 90 – 100 μm and a higher peak at ~160 μm. There were a lot of particles smaller than the 63 μm sieve size that was used to classify the granules, but the majority of the mass was in the size region 60 – 112 μm. The test using the large 25 ml cuvette used 8 readings and gives a (mass based) mode size of 85 μm.
For granules measured after abrasion: The first test using the small 6 ml cuvette used 7 readings, after the initial stirring the sample was left to settle and 2 further readings were taken. After the 3rd reading the sample was re-stirred and 4 further readings were taken. Based on the readings taken immediately after stirring the mode size was 90 – 100 μm. The readings taken as the sample settles show a reducing mode size with time suggesting that larger particles are settling out faster than the smaller particles. The second test using the small 6 ml cuvette used 7 readings and gives a mode size of 90 – 100 μm, a few of the readings gave bi-modal distributions with a second smaller peak at 160 μm. The test using the large 25 ml cuvette used 8 readings and gives a mode size of ~ 90 μm.
When all the tests are taken together there is no obvious difference between the size distributions before and after abrasion.

Discussion

The experiments done using the Lissajous abrasion rig show that the primary particle type within the granule affects the amount of abrasion.
Smaller granules appear to produce more abrasion than larger granules, but this could be because the tests are being dosed by mass rather than surface area. Abrasion is relative to the area swept by the abrasive particles so a given mass of small particles will have a larger number of particles and a larger surface area to cause abrasion than the same mass of larger particles. A single large particle should cause more abrasion than a single small particle. It follows that increasing the mass of the abrasive dose will increase the amount of surface area available for abrasion and thus the amount of abrasion; the tests using the Hand-Held abrasion tester that appear to support this for the measurements taken before and after on different microscopes. However there is doubt as to the accuracy of these measurements, as when the indents are measured after abrasion using the same microscope that measured them at the start the results show no such relation. This is assumed to be because of either human error in measuring the ends of the indent or improper calibration of the computer aided microscopes. In a separate investigation the human error in measuring the length of the Knoop indents was investigated and this gave standard deviation of 6.03 μm for the length of the indents, which when combined with the typical values of indent lengths before and after abrasion gives calculated errors on the abrasion of ± 50 %.
The scratches and gouges produced using the linear abrasion rigs will run perpendicular to any Knoop indents and may obscure the ends of the indents making accurate measurements of indent length and calculation of the depth change less accurate when using the linear abrasion rigs. The Hand-Held abrasion tester is not really a good test method as the granules being pushed to the sides will not be taking part in the abrasion test, it is difficult to clean the brush between each test as water cannot be used and the bristles on the brush are not all the same length (they are shorter in the centre).

For the linear abrasion rigs: the bristles on the toothbrush head and not the granules must produce the scratches and gouges, as they are present with and without abrasive granules. The increasing width of the scratches with load indicates that they are deeper and is probably due to the bristles on the brush being pushed in to the surface with a greater force, they could also be caused by granules becoming trapped under the bristle and dragged along the surface. The unevenness in the distribution of the scratches is probably due to bristles of different length on the toothbrush heads. The single, un-broken abrasion line could be caused by a single abrasive particle, a long bristle sticking out proud of the rest or a groove that fills with fresh granules on each stroke.
Some sort of segregation process is occurring during abrasion to produce the separate groups of large and small granules at the end. It is possible that the bristles are filtering out the large particles and the smaller particles get carried along with the oil. This segregation makes it impossible to analyse the size distribution before and after abrasion using image analysis because the location of the image taken on the sample plate will affect the size distribution. The images of granules before and after abrasion suggest that some form of erosion is taking place, as all the granules (small and large) become rounded and surface smooth after abrasion. The presence of more very small particles after abrasion using the Unilever linear abrasion rig supports this and could

be primary particles worn from the surface of larger granules. The presence of small particles before abrasion using the In-House abrasion rig could be caused by primary particles aggregated onto the larger granules that become dislodged when the oil is added, it is too difficult to tell whether the number of these small particles increases with abrasion indicating erosion or whether there is the same number. It is not clear what happens to the small angular granules that are present at the start of abrasion; these seem to become smaller, more rounded and more translucent. It is possible that the images of the granules before abrasion using the Unilever rig were taken dry and not in oil and that would explain the lack of presence of small particles before abrasion, as they would be aggregated onto the larger granules.
Wider scratches and gouges indicates that the more abrasion is occurring, however it is not clear whether this is due to increased abrasion from the granules or the bristles on the toothbrush. It is likely that the increased damage is due to the bristles as the pattern of the damage remains consistent with that caused by bristles and there is no evidence of increased damage to the granules with increased load. This is sensible as if the bristles are filtering the large granules and the small granules are getting swept along by the oil then they are not in a position to have the extra load transferred to them. Any granules that do get caught and dragged underneath a bristle tip will feel the increased load and possibly suffer greater damage and cause more abrasion in the PMMA surface (hence a possible explanation for the few deeper scratches), but the number of these granules will be small and any damage will be masked by the presence of many more un-damaged granules.

The size analysis of the granules before and after abrasion using the Sympatec was an attempt to quantify the damage to the granules, but this did not prove that the granules are breaking or being eroded during abrasion. It did show that larger granules settle quickly in oil, thus the sampling method and measuring method need to be strictly controlled in order to get reproducible and comparable results. The presence of bi-modal size distributions could be caused by 1 of 3 things:

1. The presence of a few large particles
2. Dust on the lens or the cuvette
3. Particles being counted together due to overlap caused by:
    - Too high concentration
    - Stirrer speed too high

Conclusion

The Linear abrasion rigs are not suitable for analysing the quantitative abrasion of granules using a toothbrush as the second body. The material used for the primary particles has a greater effect on the abrasion than the size and dose of the granules. Increasing the number of abrasive particles will increase the amount of abrasion. Increasing the load will increase the amount of damage to the substrate. The Knoop indent approach is not accurate due to the large variation in length measurements arising from human error, this should be unaffected by the total load used to produce the indent (and thus depth). However, it appears to be accurate enough to give trends when enough tests are performed. Granules used for abrasion have small particles stuck to the surface when dry, which dislodge when mixed with oil. These are probably primary particles held in place by electrostatic forces. The damage to the abrasive granules is by erosion with very little, if any, measurable size reduction.

Future Work

This section describes the work and experiments that need to be carried out to take the knowledge in this area forward.

An alternative approach to the linear abrasion rig, using a toothbrush head as the second body, needs to be found in order to produce quantitative abrasion data. Possible alternatives are to use a soft block with imbedded particles or a completely different device such as the pin-on-disk or the ball cratering method.
The Knoop indent method needs to be assessed to determine it validity, an alternative would be to use a Vickers indent as this has 2 axes to measure rather than the one (both of which should be the same length if uniform surface wear is occurring).
Size distributions of granules before and after abrasion need to be determined under strict control, it is suggested that letting the large particles settle out for a given time period and then decanting the top layer (including the smaller particles) for size analysis will give more meaningful results.
Once a satisfactory abrasion test has been found the affect of loading needs to be re-investigated. Knowledge of the mechanisms of abrasion and the different circumstances under which variables such as load become more or less dominant on the amount of abrasion is necessary in order to conduct meaningful tests to assess the relative abrasive strength of granules.

Appendix E

Original Drawings for Design of Abrasion Rig

Original Drawings for Design of Abrasion Rig

Specifications:

Brush Movement	38mm (reciprocating)
Angle of Brush Head	5° (to direction of reciprocating motion) – (Changed to 10° or 25° on actual machine)
Speed of Movement	150 cycles per minute (changed to 81 cycles per minute due to fixed speed on motor)
Duration of Test	5 minutes
Toothbrush head size (original)	28 mm x 11 mm x 5 mm (plus bristles)
Metal Counterbody size	28 mm x 11 mm x 11 mm
Applied Load	200N (Counterbody + Holder + added mass)
Sample Plate size (PMMA)	54 mm x 54 mm x 5 mm
Samples per test	5
Clearance in Sample plate holder	10 mm

A diagram of the original counterbody (toothbrush head) and the sample plate are shown on Page 1 of appendix F.

The dimensions of the counterbody holder head attachment are shown on page 2, this shows the screw holes which allow the metal block (counterbody) to be removed and wrapped in cloth and subsequently refitted and held in place.

The dimensions of the sample plate holders are shown on page 2, there are 5 of these used on each abrasion test run. The sample plate holders are mounted onto the base plate of the abrasion rig as shown on page 3, they are removable for cleaning. The sample plate holders have a square cavity into which the sample plates are pushed, there is a very close fit between the walls of the sample plate holder and the sample plate to ensure no oil and granules leak out during the abrasion test. In order to remove the sample plate there is a hole in the bottom of the sample plate holder to allow the sample plate to be pushed out.

The counterbody holder is shown on page 3. This includes the counterbody holder head attachment which is welded to a central rod, above this is a fixed circular plate with two retaining holes drilled into it. The retaining holes are such that when the counterbody

holder is attached to the top plate the counterbody holder head is able to pass through the slots in the top plate and the mounting pegs locate into the retaining holes. The retaining holes and mounting pegs are aligned such that the angle of the counterbody is held at 5° to the direction of reciprocating motion.

Page 4 shows the tope plate with the dimensions of the slots and the location of the mounting pegs. The top plate is mounted on runners above the base plate and attached to a motor with a reciprocating motion.

Page 5 shows the abrasion rig set-up from cross-section. The motor is attached to the top plate and has a reciprocating motion with 38mm of travel. Additional weight can be added to each of the counterbody holders to increase or decrease the applied load during abrasion. The top plate is fully removable to allow access to the sample plate holders mounted on the base plate.

NOTES:
An angle of 5° was used as this was based on the BS 5136:1981 standard, it is believed to be set at this angle to maximise the wear area and so that toothbrush bristles are slightly offset from those in front (the original tests use toothbrushes as a counterbody and the bristles are all aligned in straight rows so if the counterbody is not offset they would be scratching the same surface as those immediately in front and behind).

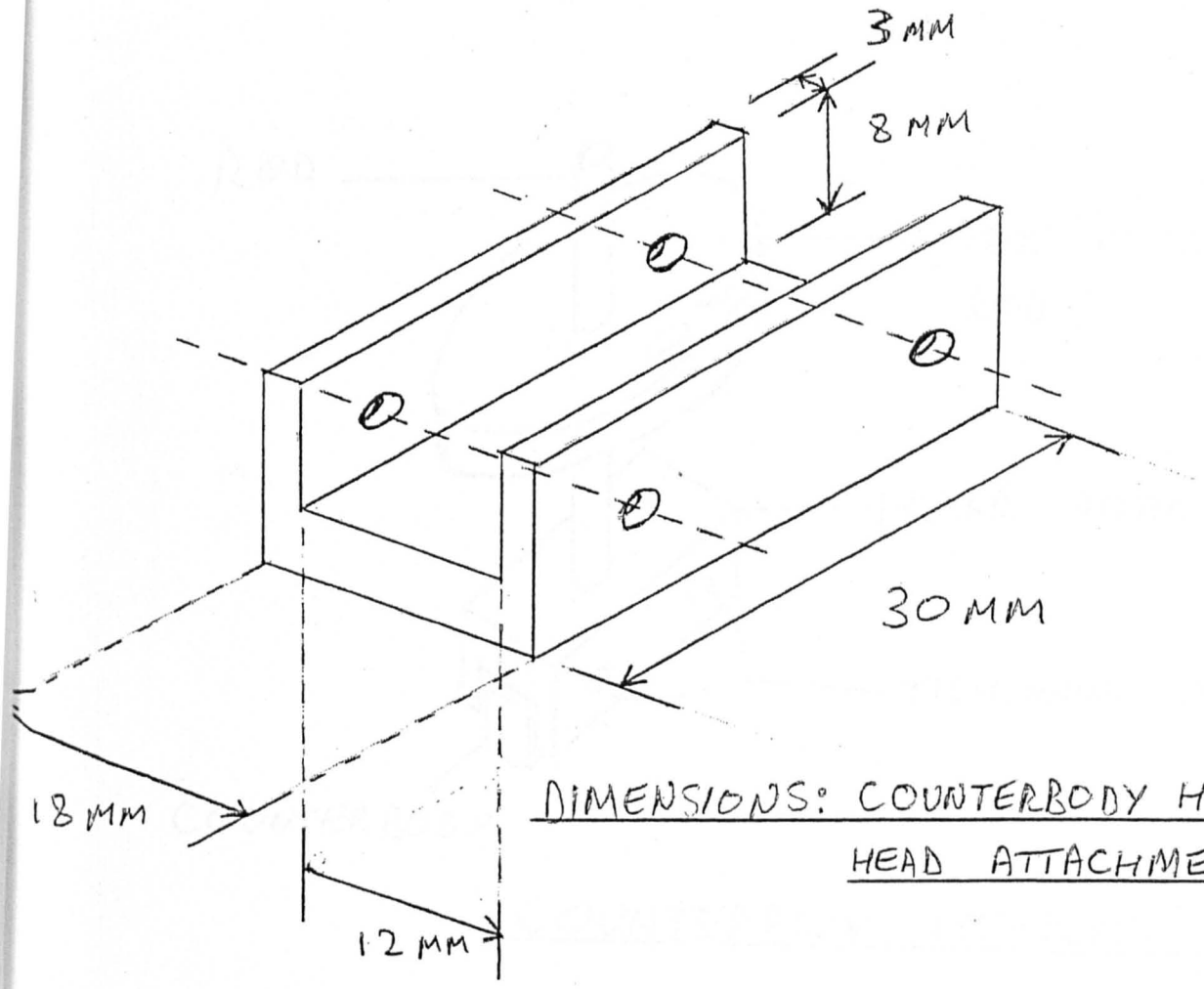

DIMENSIONS: COUNTERBODY HOLDER HEAD ATTACHMENT

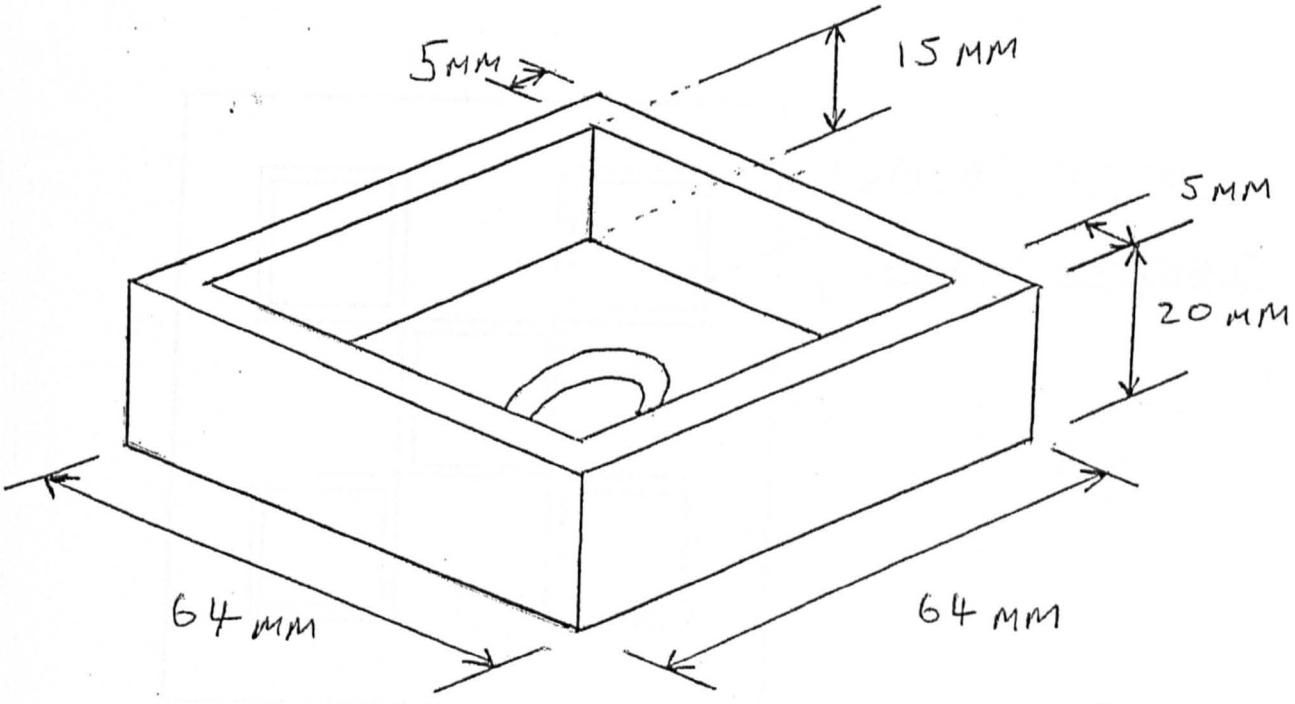

DIMENSIONS: SAMPLE PLATE HOLDER

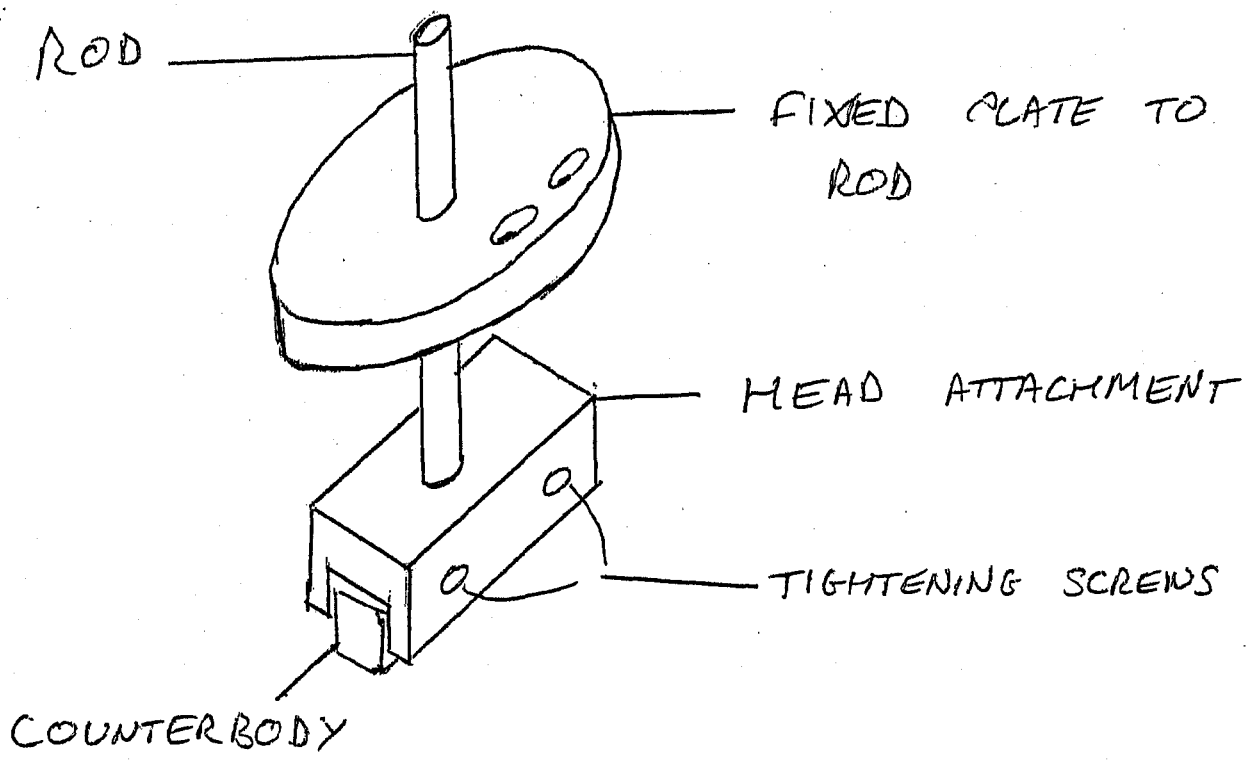

COUNTERBODY HOLDER

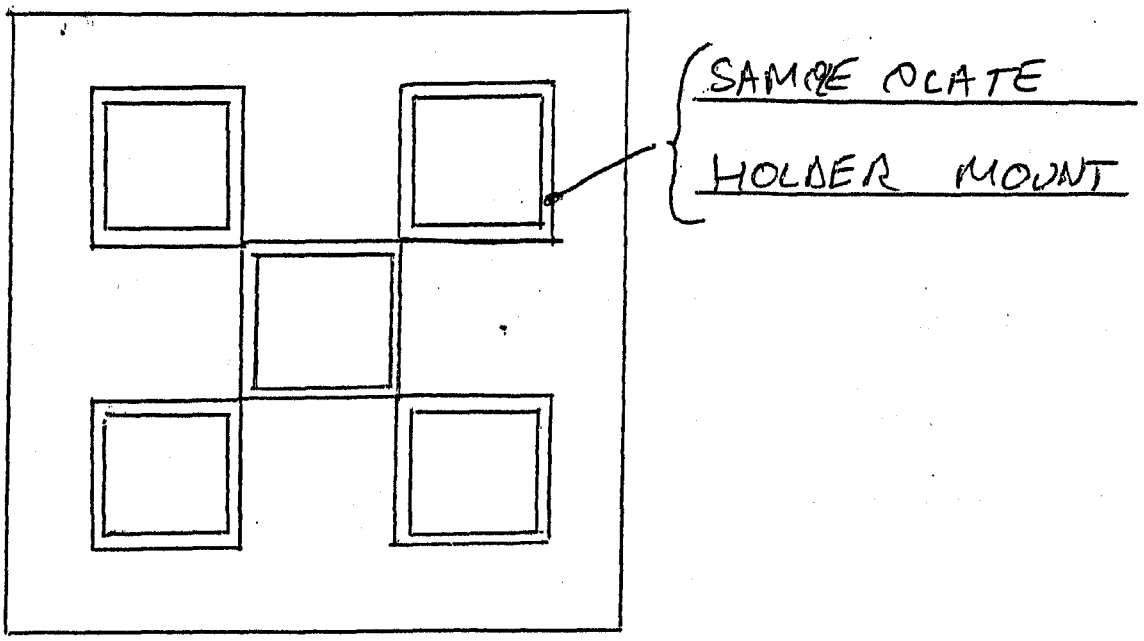

BASE PLATE

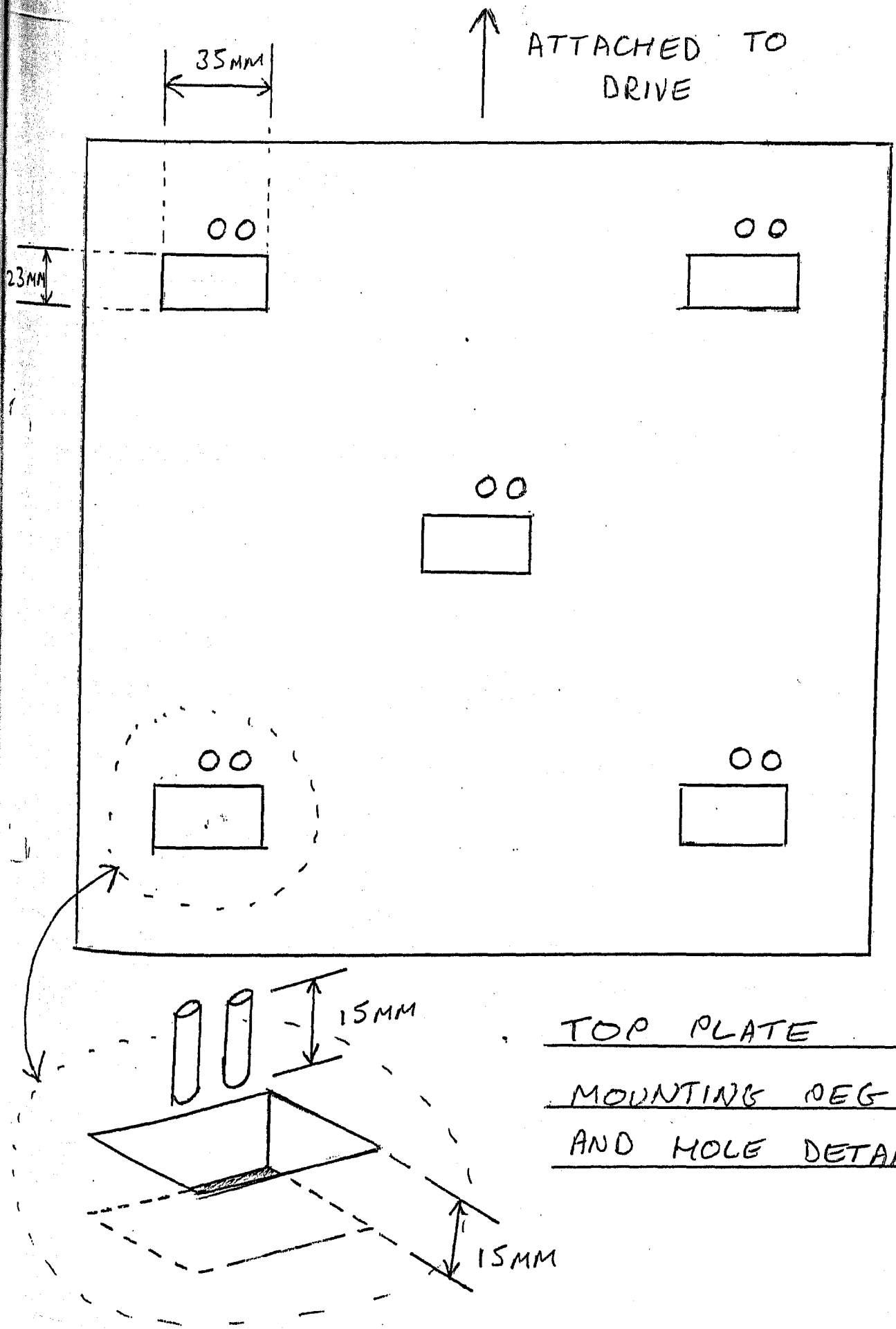

TOP PLATE MOUNTING OEG AND HOLE DETAIL

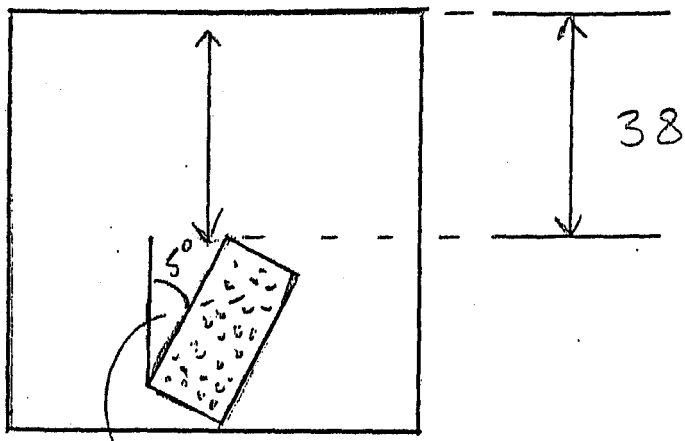

5° ANGLE . TO DIRECTION OF TRAVEL

COUNTERBODY MOTION ON SAMPLE PLATE

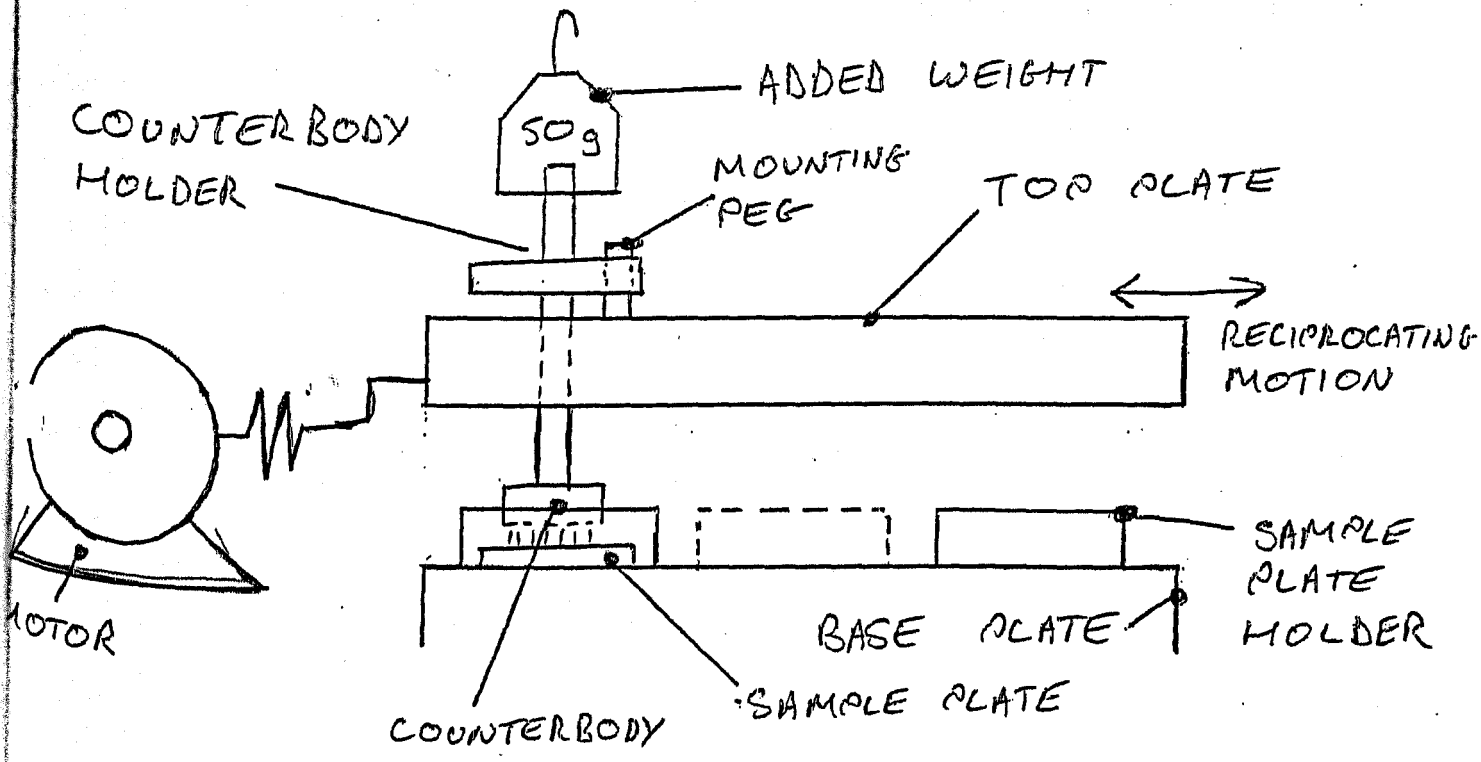

ABRASION RIG SET - UP

Appendix F

Binder Content Verification

Binder Content Verification

The test method outlined in the main body of the thesis was originally proposed by Peter Knight and adopted by the PPG group at Sheffield without any verification. It was just assumed that burning the granules at 600°C for 2 hours would burn off ALL the PEG and NONE of the Calcium Carbonate. It was not clear whether this test method was applicable to other primary particle types such as Zeolite (Wessalith and Wessalith P) or that it was indeed valid for Calcium Carbonate and PEG.

I was concerned about time constraints relating to the amount of experiments that needed to be carried out and so set about verifying the test method and trying to accelerate the experimental method by using a higher temperature at shorter time periods.

Initially PEG was burned at 750°C. This resulted in the entire PEG being burnt and no residue remaining in the crucibles. Calcium Carbonate samples were then burned for 1 hour at 900°C and 1 hour at 750°C, the hope was that none of the Calcium Carbonate would disappear. Unfortunately when Calcium Carbonate is burned at these elevated temperatures it produces degradation and some mass is lost, this mass loss is not accounted for by trapped moisture alone (the test at 100°C was used to determine the percentage moisture in these samples). Thus the protocol could not be accelerated by elevating the temperature.

This did not prove that the original protocol is acceptable so a series of tests were conducted. Burning PEG on its own at 600°C and Calcium Carbonate on its own at 600°C and finally by adding a known mass of pure PEG and putting a known mass of Calcium Carbonate on top and burning that at 600°C. The results are interesting.
For burning Calcium Carbonate on its own at 600°C results in a greater mass loss than would be the results of moisture loss alone, this indicates that some material degradation and mass loss of the Calcium Carbonate itself is occurring. However this mass loss is very small only about 1% and is about 20 times less mass loss than occurs at 750 and 900°C. More interesting is the fact that when the PEG and Calcium Carbonate are burnt together the mass loss is significantly greater and between 12% and 20% by mass is lost from the Calcium Carbonate. This is indicative that carry out of the fines is occurring, in other words as the PEG burns and the vapours rise the momentum of the gases is carrying out the fine particles of the Calcium Carbonate. Alternatively it could mean that a reaction is occurring with the hot PEG that results in Calcium Carbonate degradation. This brings into question the validity of this testing method and the accuracy of the results quoted in the sections of this thesis relating to the Binder content.

Another discovery was that Zeolite degrades significantly at 600°C. This test method is not appropriate for testing other primary particle types that were used in this study.

As further evidence of the above, when complete granules were burned at 750°C and 600°C with the results analysed using the analytical method in this thesis it was found that they gave different values for the amount of binder content. Burning at 750°C indicated a far higher binder content.

Experimental Protocol for Liquid-Binder content of Granules – ($CaCO_3$ and PolyEthylene Glycol –PEG)

There is a need to determine the liquid binder to solid ratio of individual granules in order to determine if there is an even distribution of binder in all sizes of granules or if there is a change in the ratio of solid-liquid as the granule size changes.

For the analysis of the system $CaCO_3$ and PEG an experimental protocol has been suggested on the basis that PEG burns completely leaving no residue at 600°C whilst $CaCO_3$ remains unaffected.
Method:
The mass of an empty crucible is recorded W_6.
A scoop of granules is added to the crucible and weighed W_7
The crucible and granules are placed in an oven at 600°C for 1hr.
The crucible and content are then re-weighed W_9 – we can now find the mass of Calcium Carbonate left in the crucible by difference, and the weight that has burnt off is the PEG and moisture.

The moisture content of the granules needs to be determined:
The mass of an empty crucible is recorded W_{10}
A scoop of granules is added to the crucible and weighed W_{11}
The crucible and granules are placed in an oven at 105°C for 1 hr.
The crucible and content are then re-weighed W_{12}

The percentage moisture by mass is given by:

$$Moisture = \frac{W_{11} - W_{12}}{W_{11} - W_{10}} \times 100\%$$

The percentage binder by mass is given by:

$$Binder = \left(\frac{W_7 - W_9}{W_7 - W_6} \times 100\% \right) - moisture\%$$

The binder : solid ratio by mass is then given by:

$$= \frac{Binder\%}{100 - Binder\%}$$

NOTE: This assumes that:

A) The binder completely volatilises at 600°C
B) No decomposition of $CaCO_3$ takes place at this temperature.
C) All moisture is surface moisture and none is bound up granules
D) No volatilisation of PEG occurs at 105°C

To test the assumptions made and to find at what temperature and time volatilisation of PEG takes place a series of short experiments are planned. These will test several of the solid PEG available in the department as well as the 2 liquid PEG. The moisture content of the PEG will also be analysed using standard Thermogravimetric methods.

The proposed oven temperatures are:
105°C
600°C
750°C
925°C

These temperatures were chosen because they are readily available in the labs.

Experiment 1
Samples of all types of PEG will be tested at all four temperatures. 13 samples of each will be weighed into pre-weighed crucibles for each temperature. After 10 minutes and at 10 minute intervals thereafter 2 crucibles will be removed and weighed to record the weight loss. The last sample will be left until to see if the contents completely volatiles at that temperature if it has not done so already.

Experiment 2
Samples of all sizes of DURCAL will be tested at all four temperatures. 12 samples of each will be weighed into pre-weighed crucibles for each temperature. After 10 minutes and at 10 minute intervals thereafter 2 crucibles will be removed and weighed to record the weight loss.

Experiment 3
Samples of PEG will be weighed into pre-weighed crucibles and placed in a dessicator and the atmosphere evacuated using a vacuum pump. The samples will then be left to dry for 24 hrs. The samples will then be transferred to the oven at 105°C. After 1 hr the samples will be removed and weighed to record the weight loss. Any weight loss should be due to decomposition of volatiles being released not moisture as all the moisture will have been removed in the dessicator.

Appendix G

Database – electronic form

Appendix H

Plots from queries from results database

Plot 55 - Granule Size Distribution (Camsizer) BN/04/14 (unrealistic distribution)

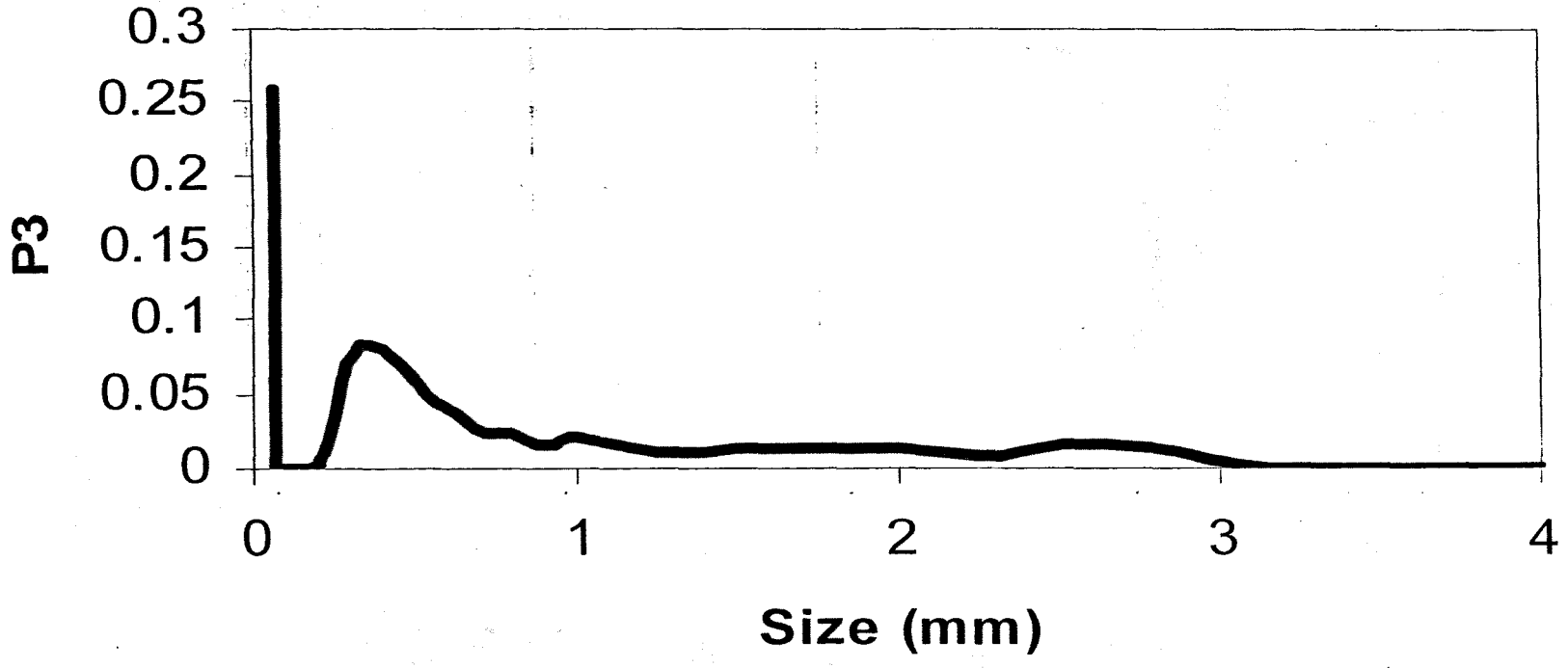

Plot 54 - Granule Size Distribution (Camsizer) BN/04/XB-2

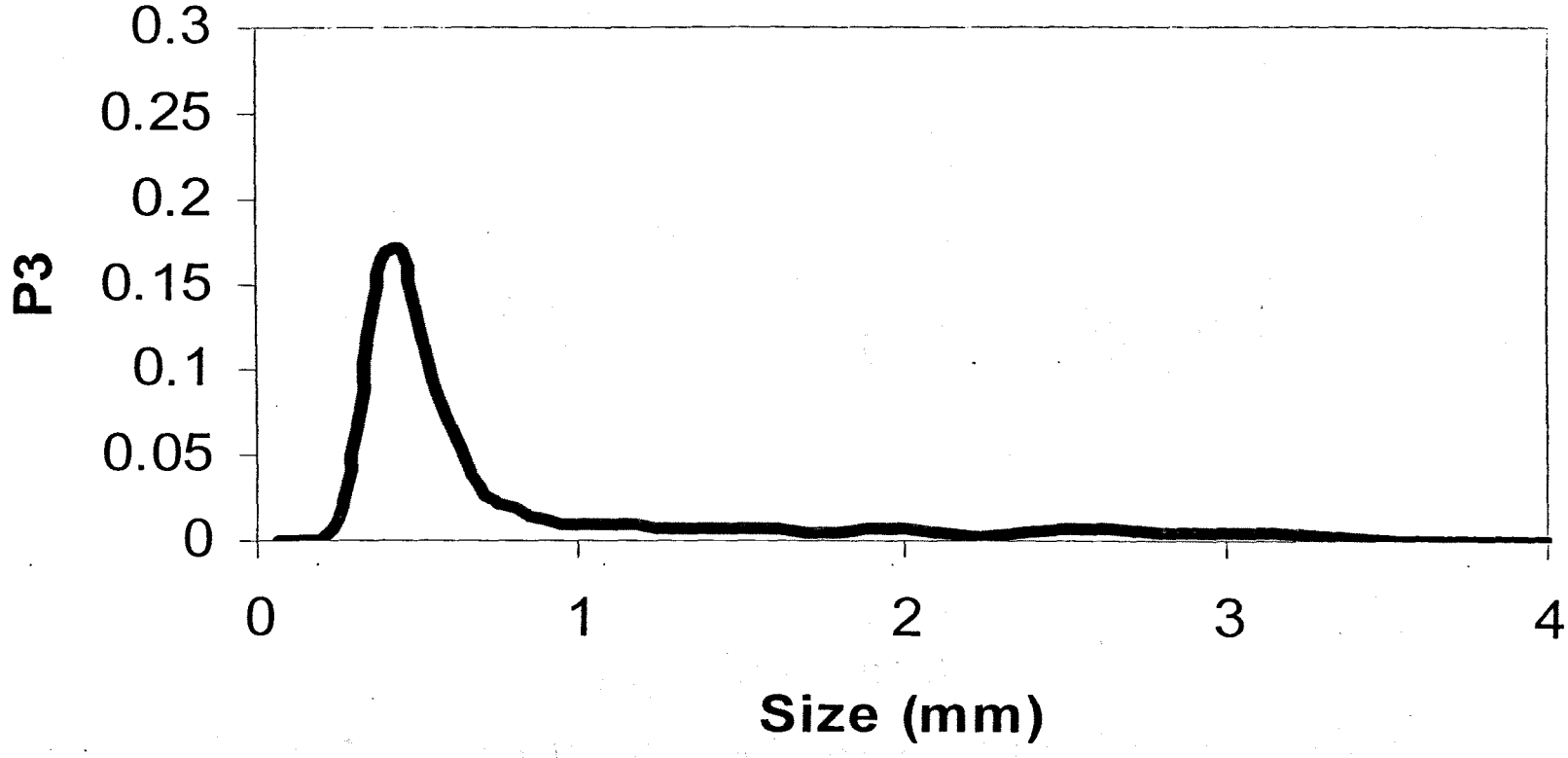

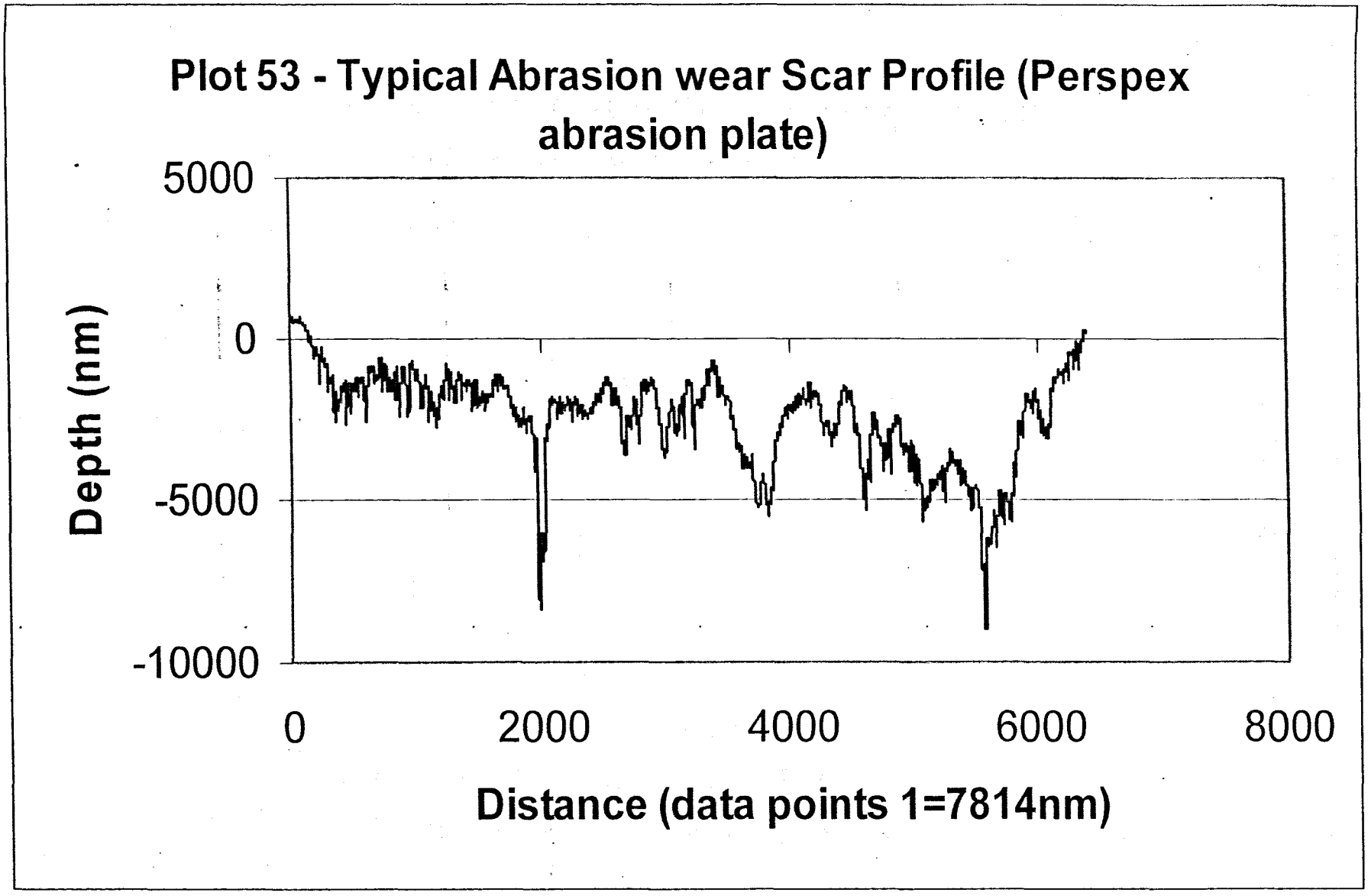
Plot 53 - Typical Abrasion wear Scar Profile (Perspex abrasion plate)
Depth (nm)
5000
0
-5000
-10000
0
2000
4000
6000
8000
Distance (data points 1=7814nm)

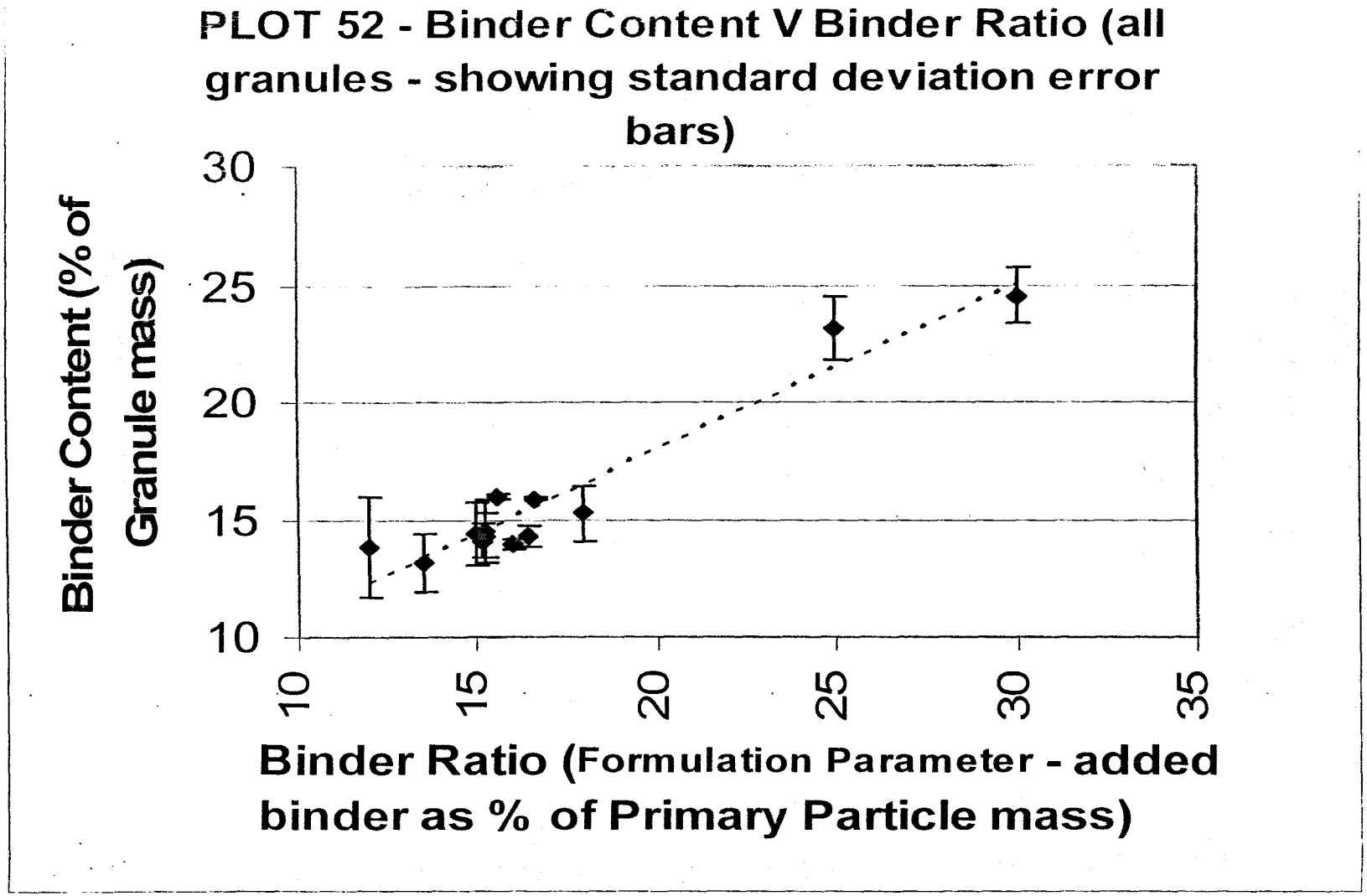
PLOT 52 - Binder Content V Binder Ratio (all granules - showing standard deviation error bars)
Binder Content (% of Granule mass)
30
25
20
15
10
10
15
20
25
30
35
Binder Ratio (Formulation Parameter - added binder as % of Primary Particle mass)

PLOT 51 - Abrasion V Binder Ratio (106-212) - showing estimated average error

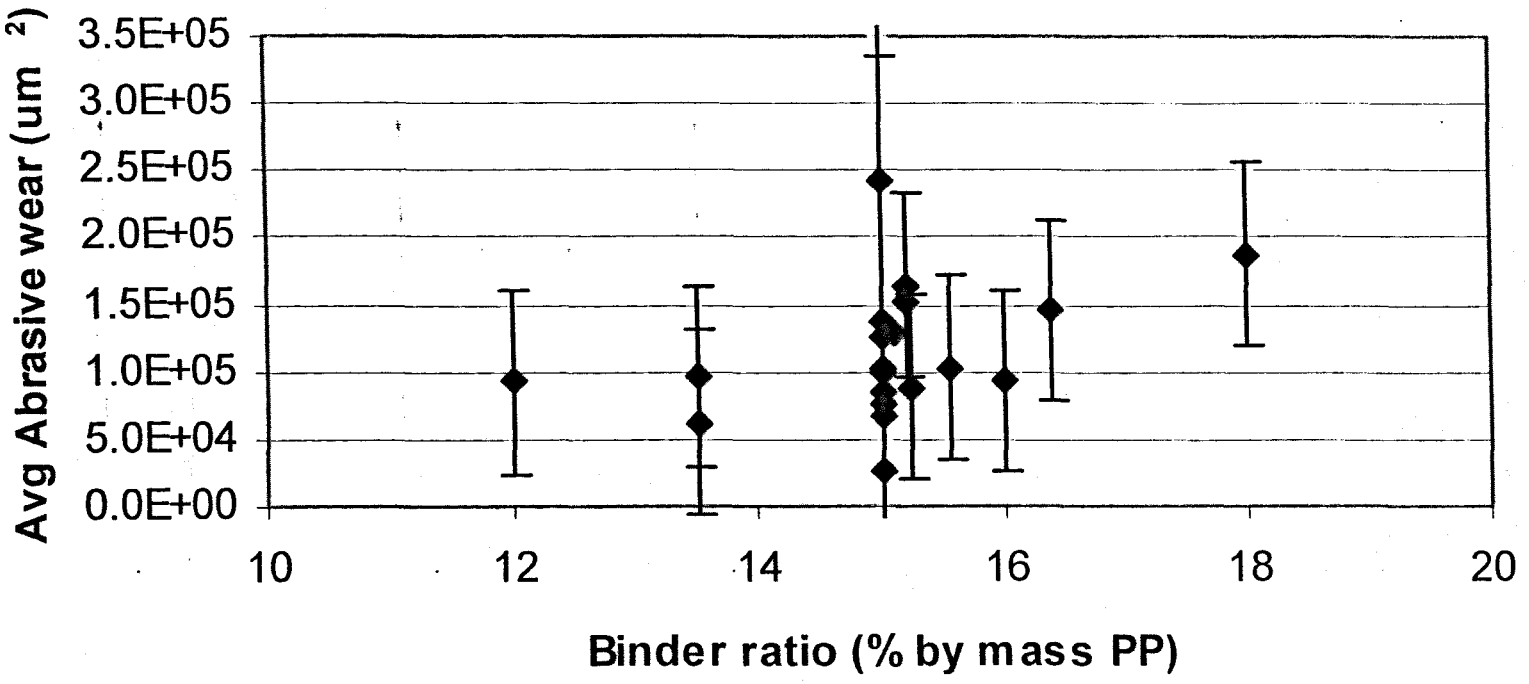

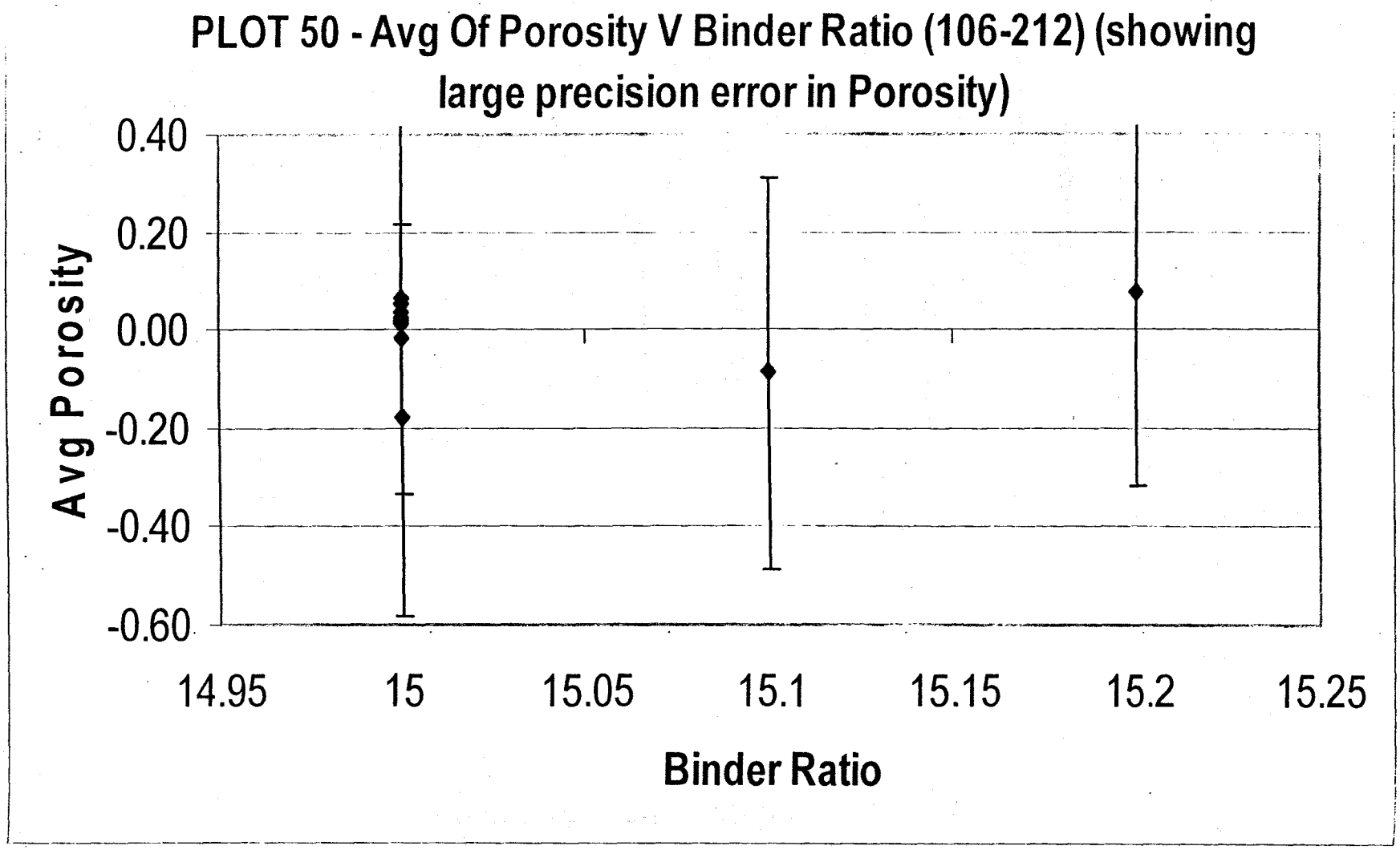
PLOT 50 - Avg Of Porosity V Binder Ratio (106-212) (showing large precision error in Porosity)
Avg Porosity
0.40
0.20
0.00
-0.20
-0.40
-0.60
14.95
15
15.05
15.1
15.15
15.2
15.25
Binder Ratio

PLOT 48 - Avg Strength V Primary Particle Type (showing 95% confidence limits - where applicable)

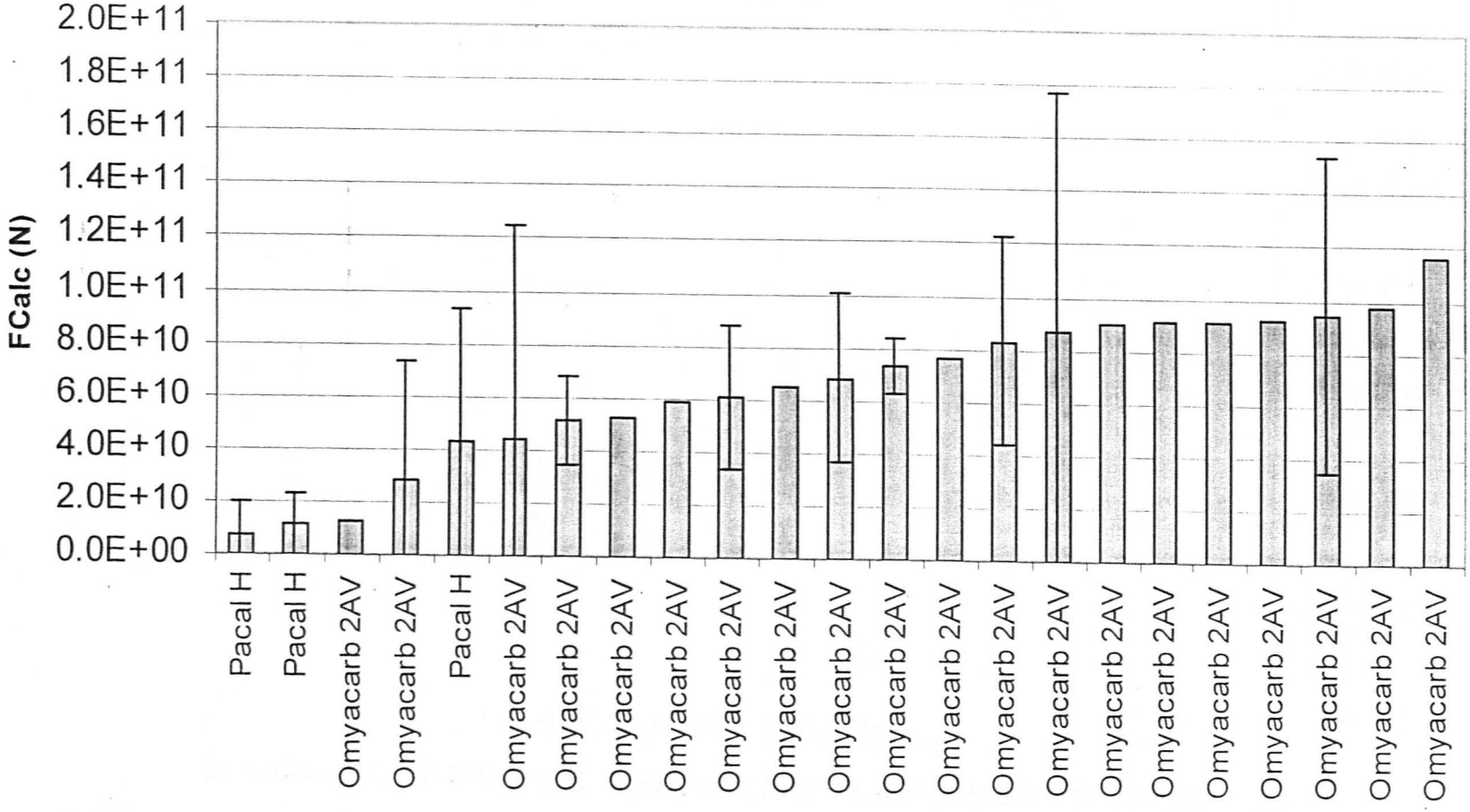

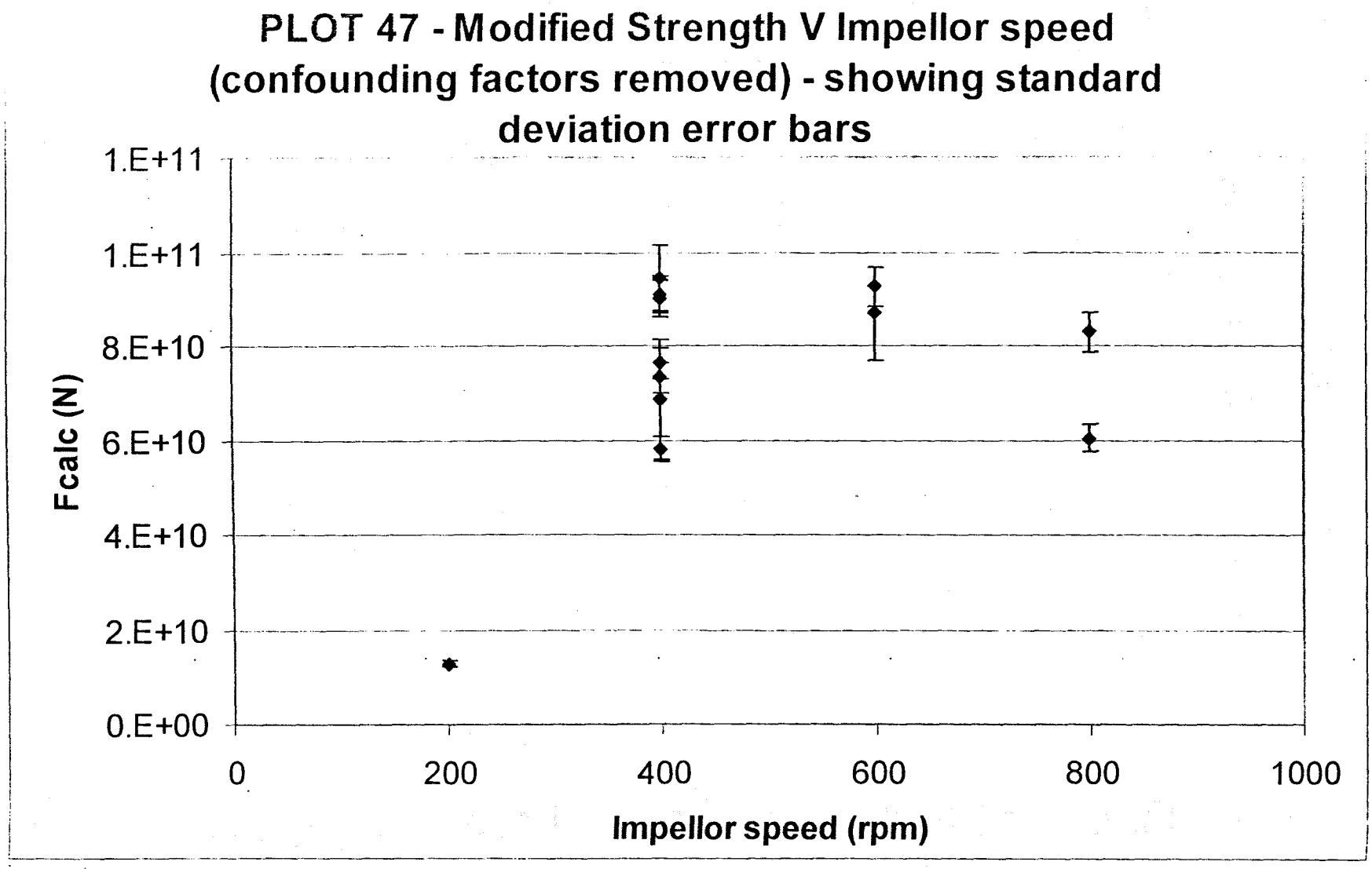
PLOT 47 - Modified Strength V Impellor speed (confounding factors removed) - showing standard deviation error bars
1.E+11
1.E+11
8.E+10
6.E+10
4.E+10
2.E+10
0.E+00
Fcalc (N)
0
200
400
600
800
1000
Impellor speed (rpm)

PLOT 46 - Strength V impellor speed (106-212 all)

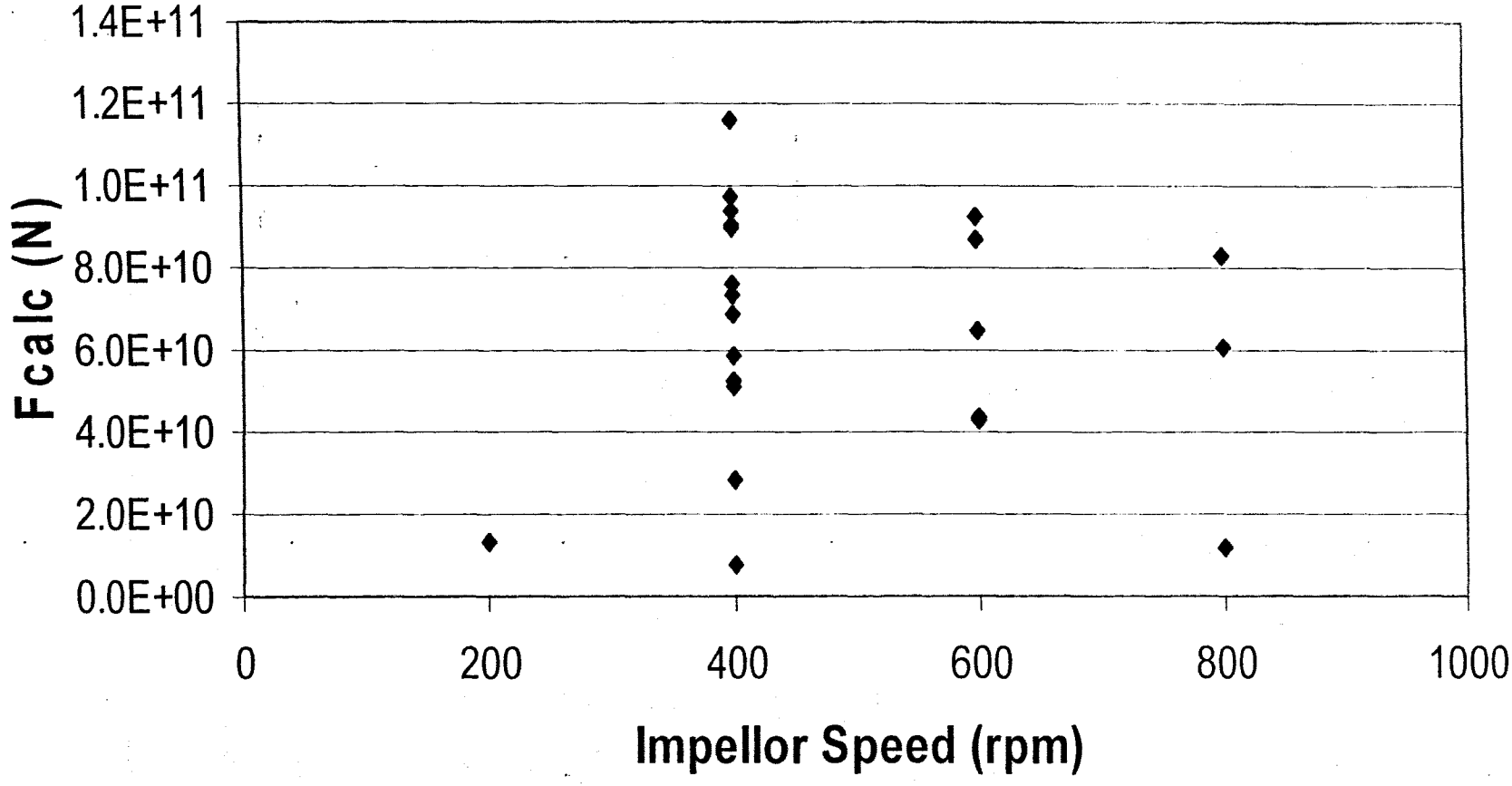

PLOT 45 - Strength V Binder Ratio (106-212) - (confounding / compounding data removed) showing standard deviations

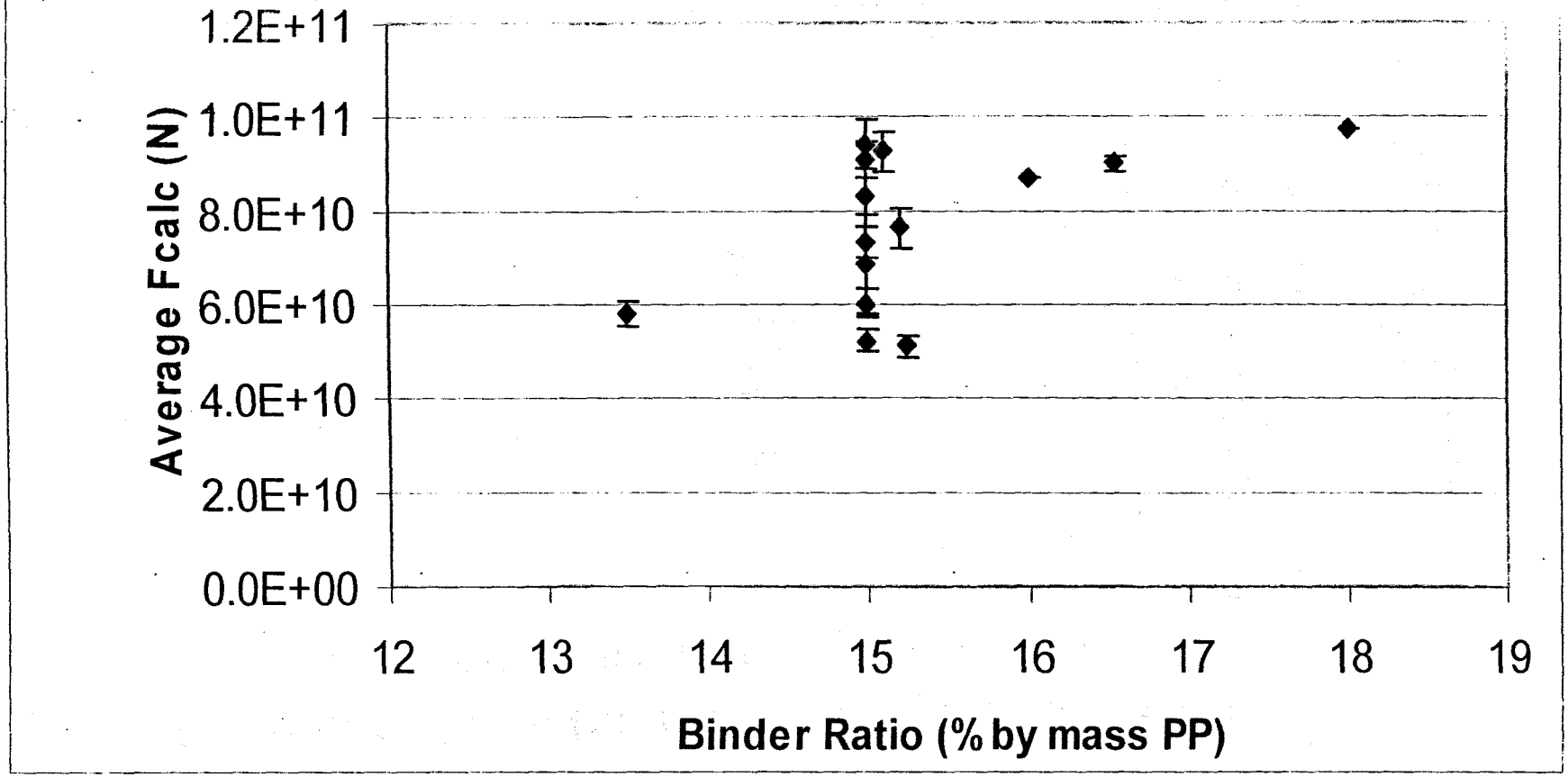

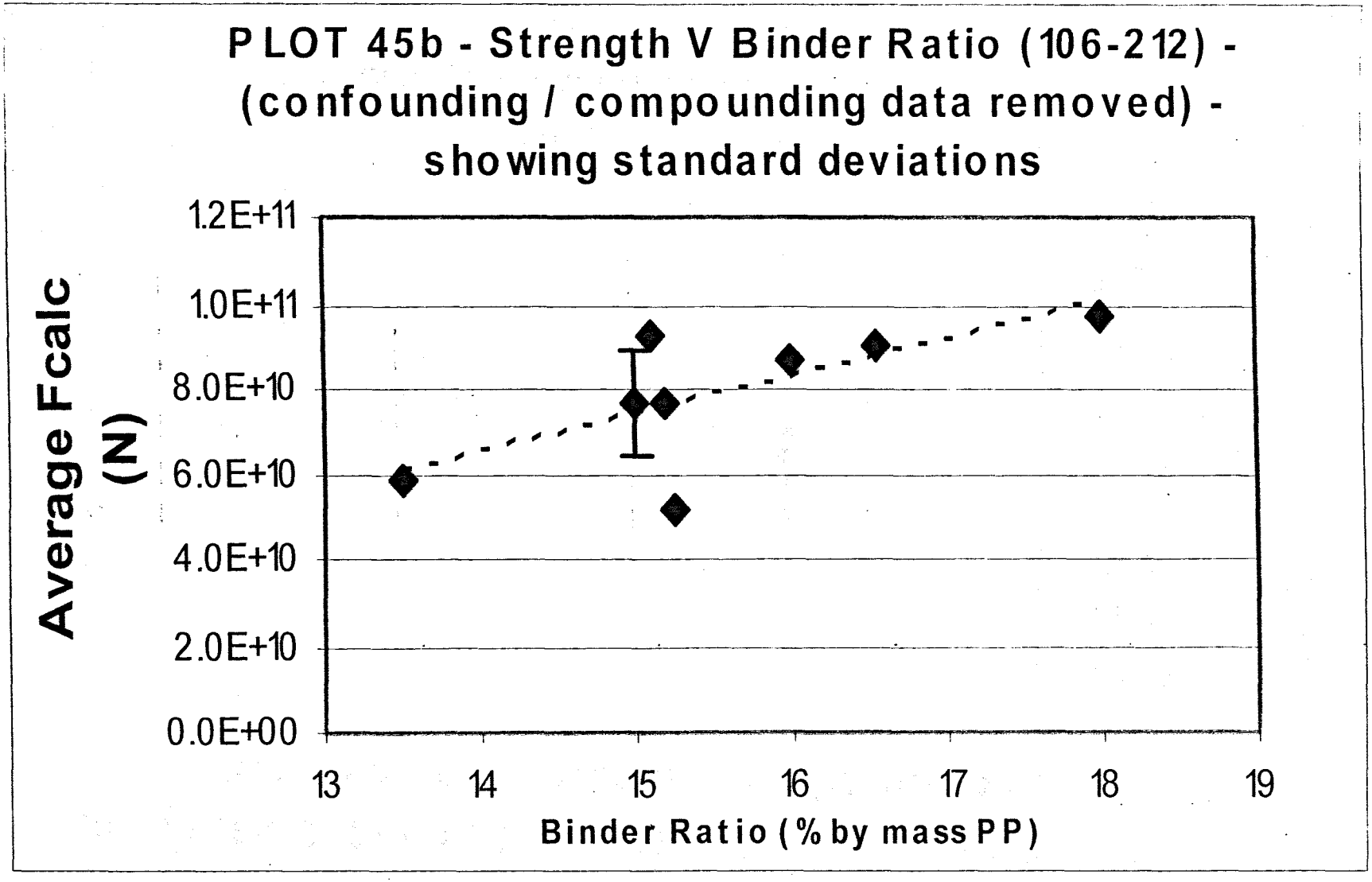
PLOT 45b - Strength V Binder Ratio (106-212) -
(confounding / compounding data removed) -
showing standard deviations
Average Fcalc (N)
1.2E+11
1.0E+11
8.0E+10
6.0E+10
4.0E+10
2.0E+10
0.0E+00
13
14
15
16
17
18
19
Binder Ratio (% by mass PP)

PLOT 44 - Strength V Binder Ratio (106-212) (inc. confounding / compounding batches)

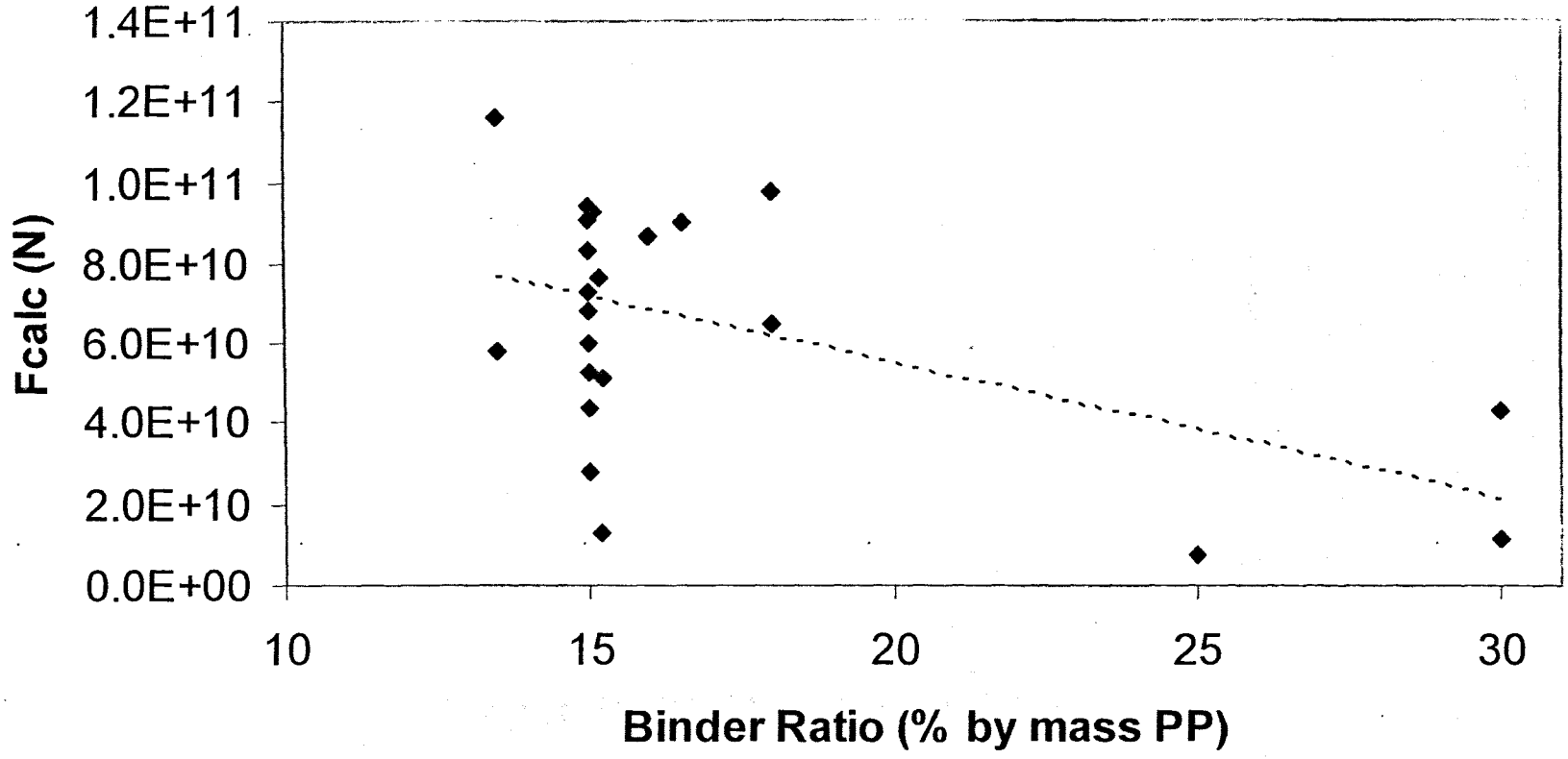

PLOT 43 - Abrasive Wear V Run Time
(95% confidence limits)

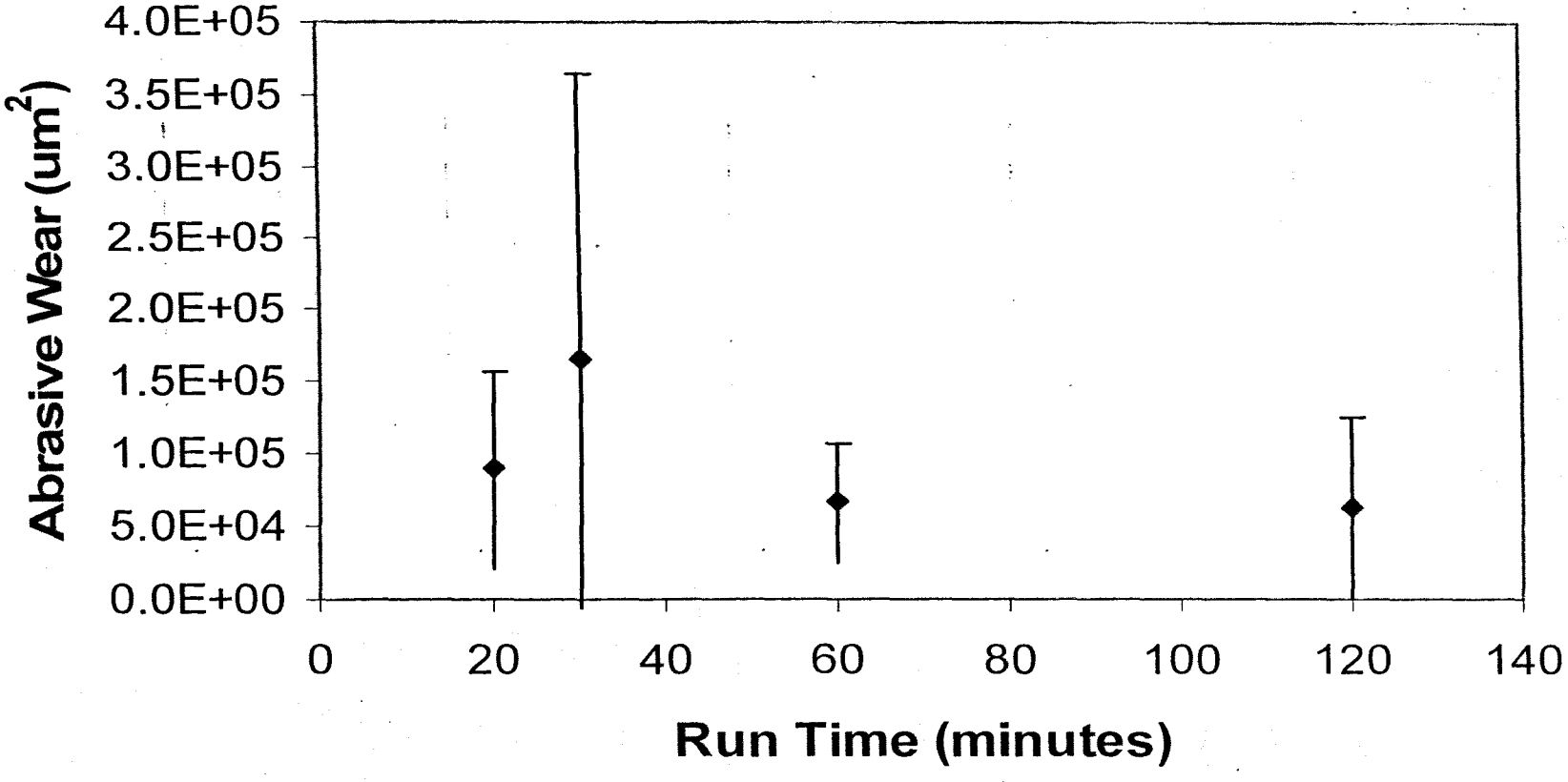

Plot 42 - Abrasion V Primary Particle Type - showing estimated average error

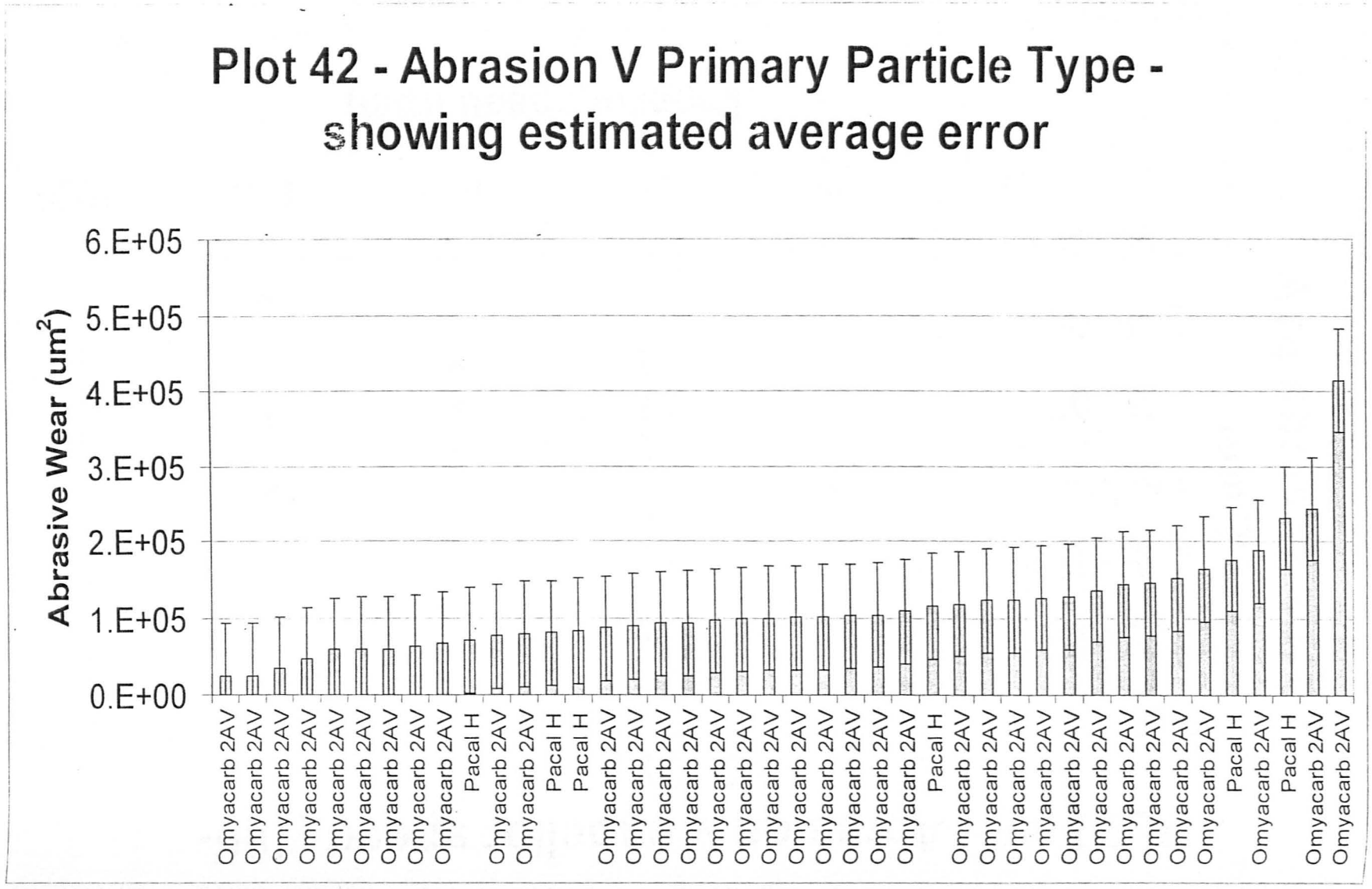

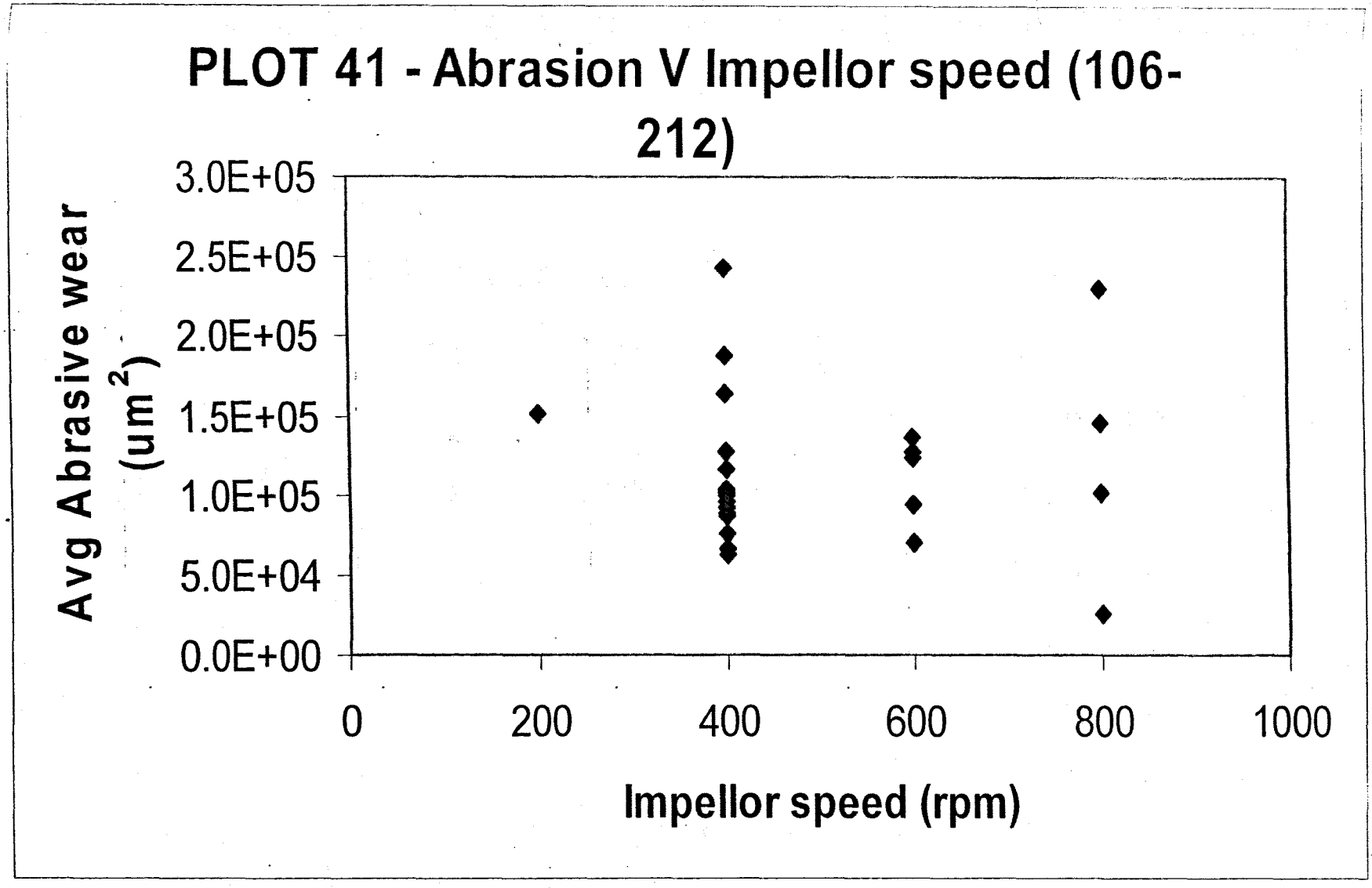
PLOT 41 - Abrasion V Impellor speed (106-212)
Avg Abrasive wear (um²)
3.0E+05
2.5E+05
2.0E+05
1.5E+05
1.0E+05
5.0E+04
0.0E+00
0
200
400
600
800
1000
Impellor speed (rpm)

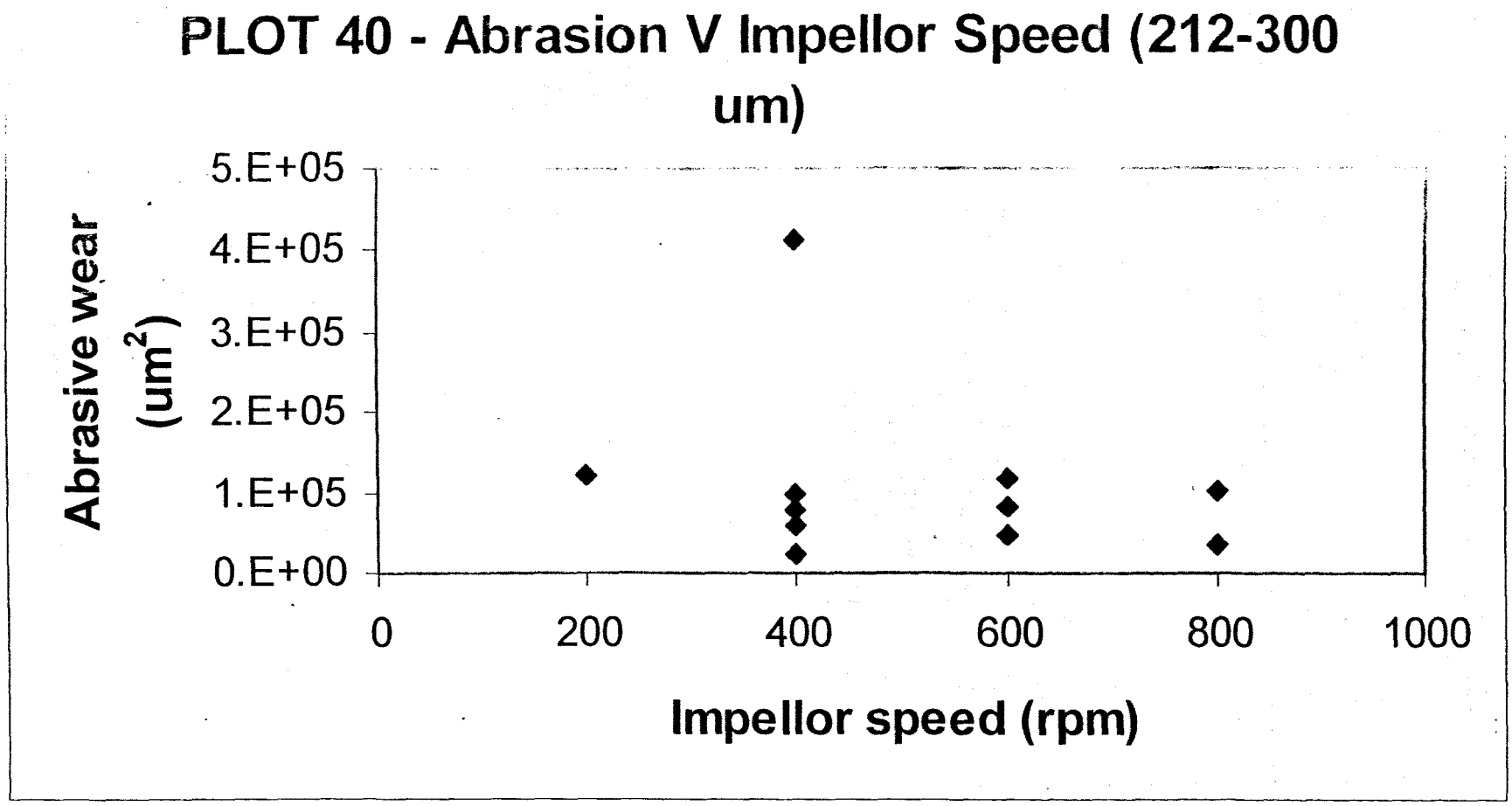
PLOT 40 - Abrasion V Impellor Speed (212-300 um)
Abrasive wear (um2)
5.E+05
4.E+05
3.E+05
2.E+05
1.E+05
0.E+00
0
200
400
600
800
1000
Impellor speed (rpm)

PLOT 23 - Load Strength V Binder Content (all) - showing estimated average error

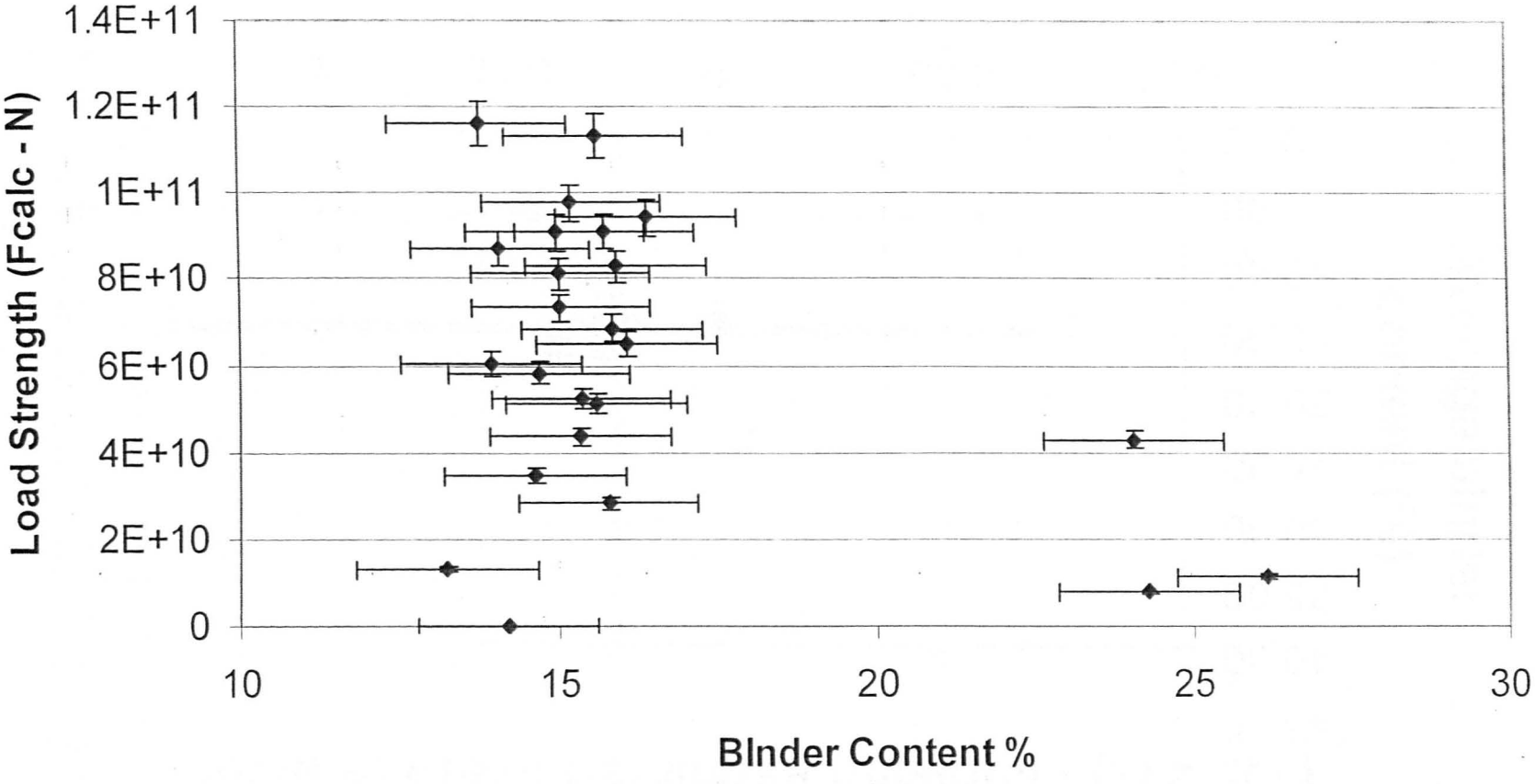

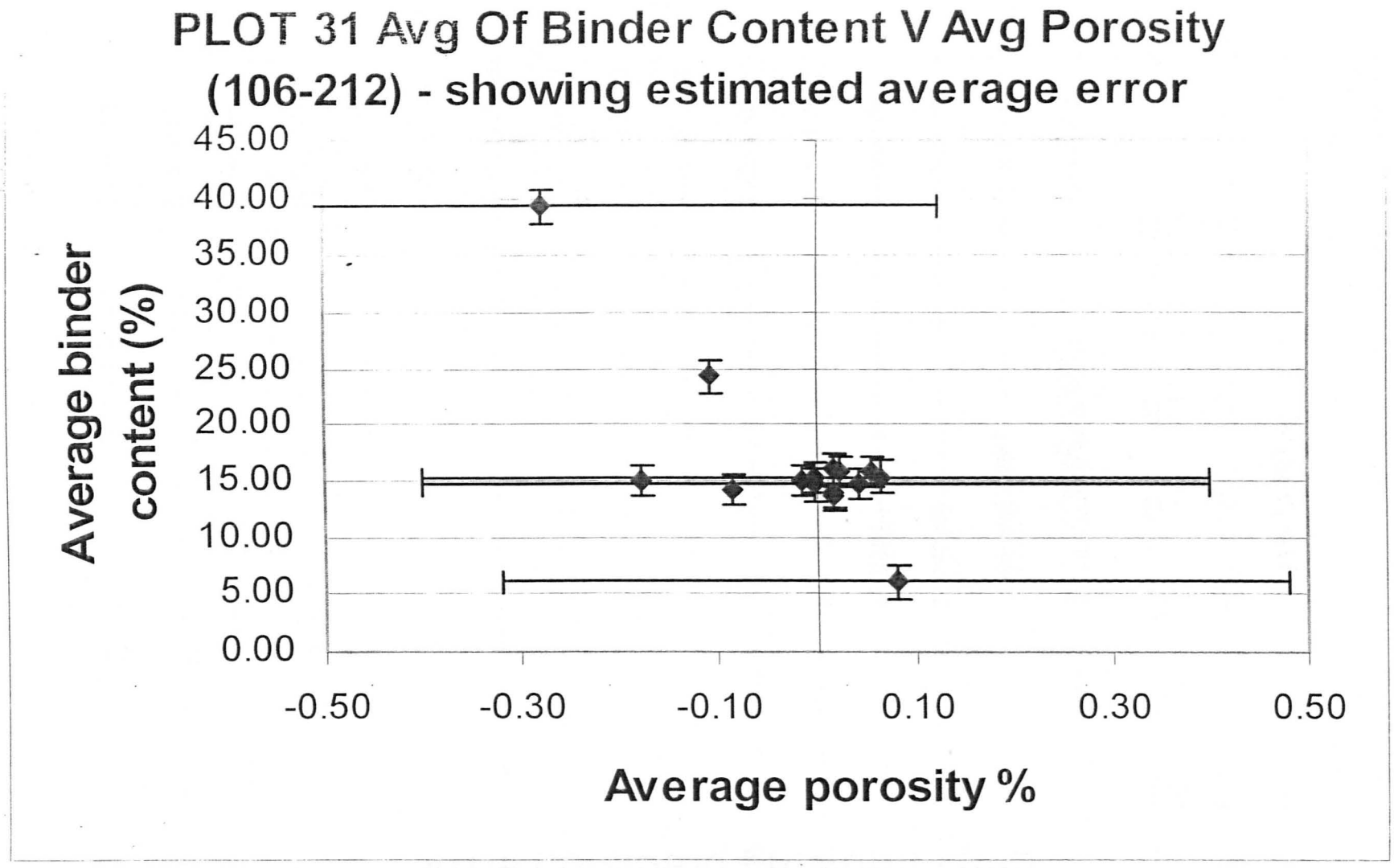
PLOT 31 Avg Of Binder Content V Avg Porosity
(106-212) - showing estimated average error
Average binder content (%)
45.00
40.00
35.00
30.00
25.00
20.00
15.00
10.00
5.00
0.00
-0.50
-0.30
-0.10
0.10
0.30
0.50
Average porosity %

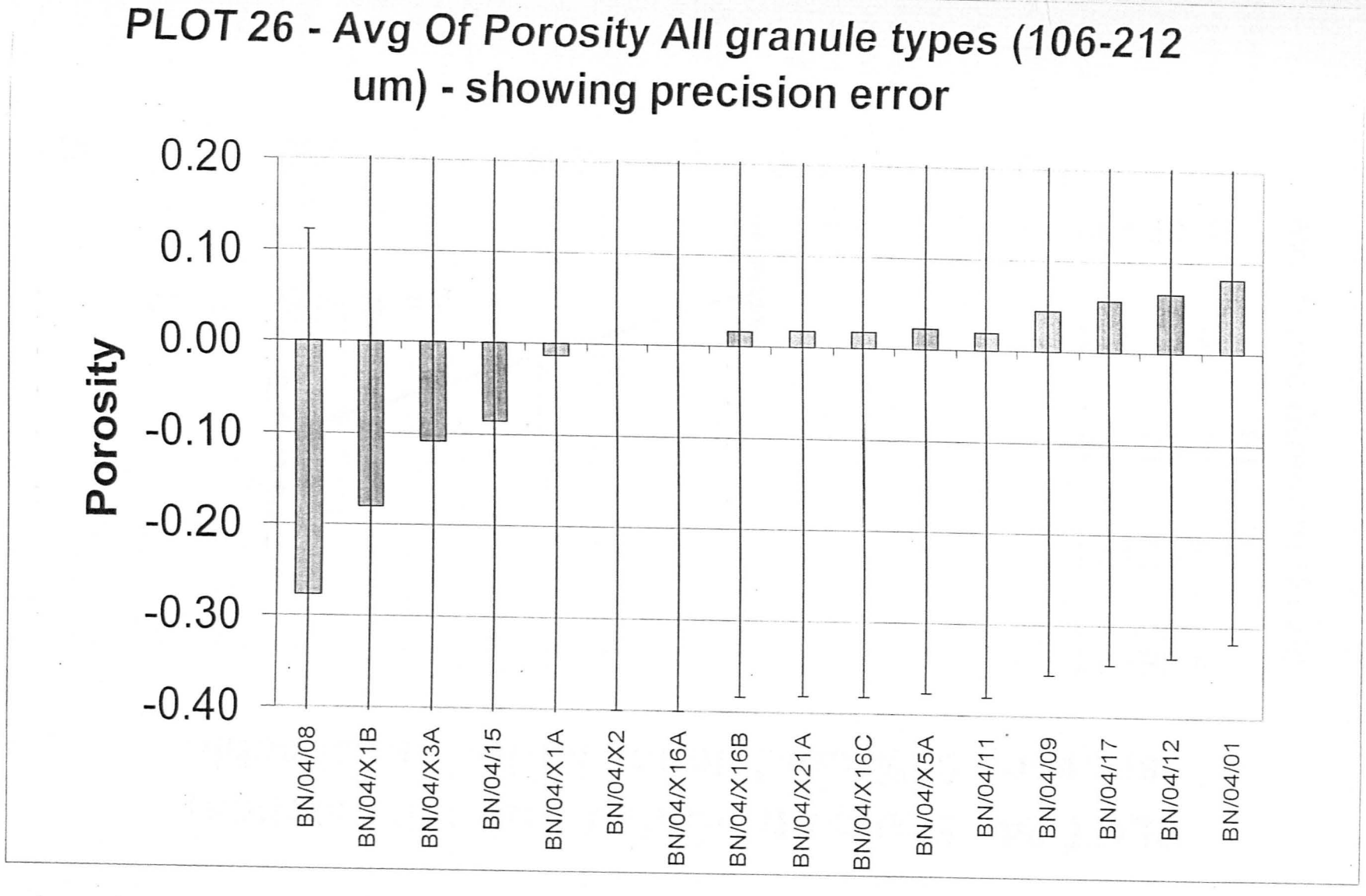
PLOT 26 - Avg Of Porosity All granule types (106-212 um) - showing precision error
Porosity
0.20
0.10
0.00
-0.10
-0.20
-0.30
-0.40
BN/04/08
BN/04/X1B
BN/04/X3A
BN/04/15
BN/04/X1A
BN/04/X2
BN/04/X16A
BN/04/X16B
BN/04/X21A
BN/04/X16C
BN/04/X5A
BN/04/11
BN/04/09
BN/04/17
BN/04/12
BN/04/01

PLOT 24 - Static Strength V Size (all batches) - showing 95% confidence limits if applicable

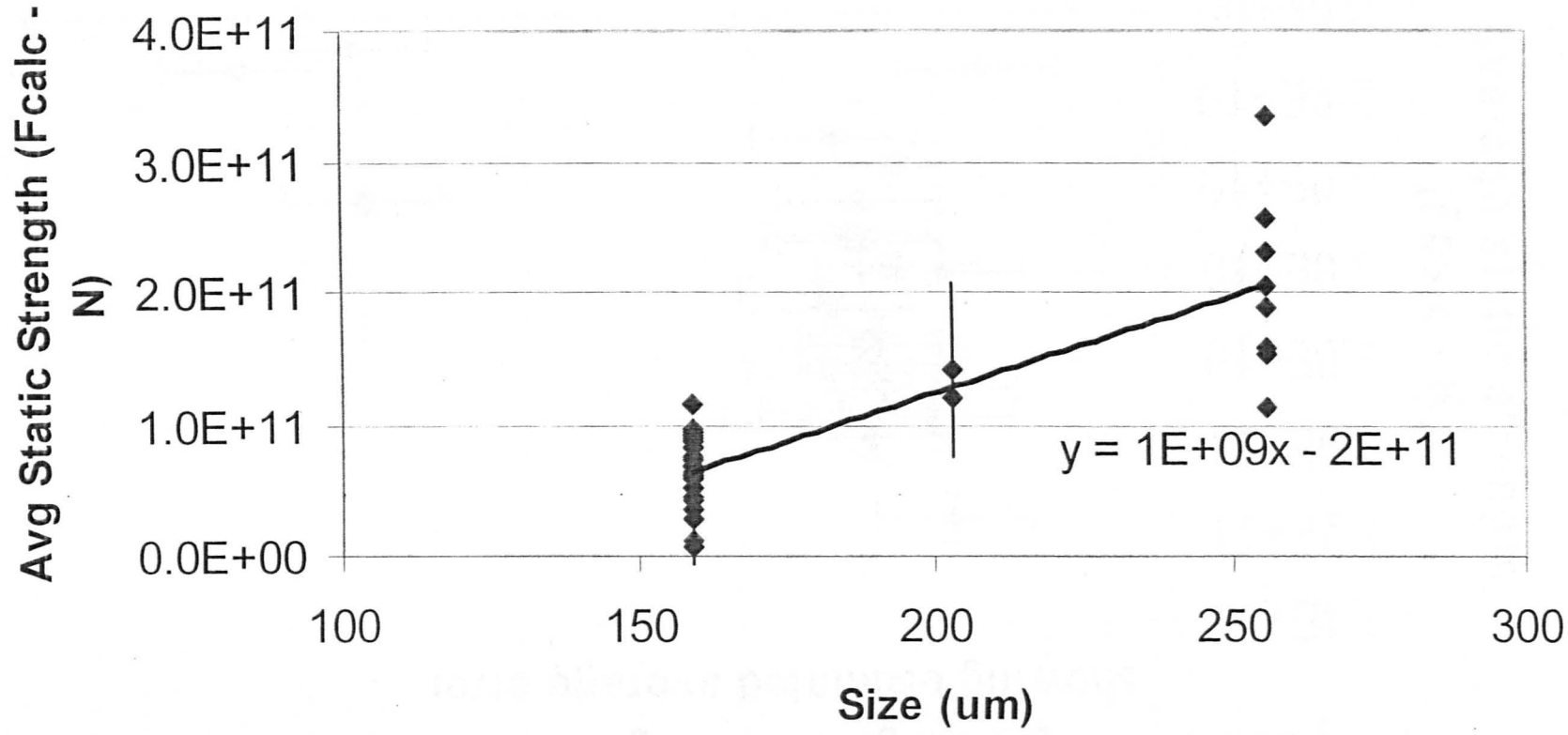

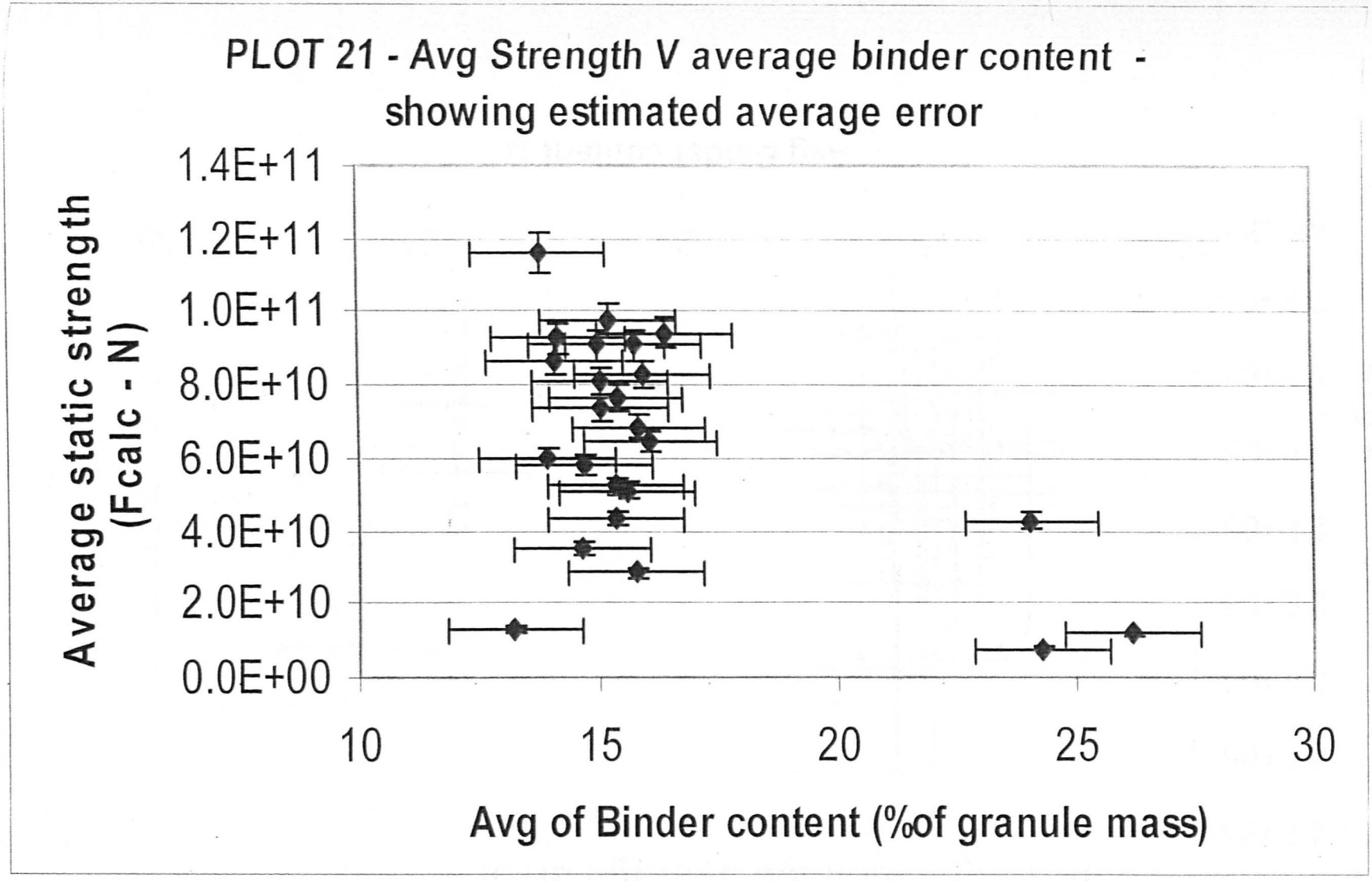
PLOT 21 - Avg Strength V average binder content - showing estimated average error
Average static strength (Fcalc - N)
1.4E+11
1.2E+11
1.0E+11
8.0E+10
6.0E+10
4.0E+10
2.0E+10
0.0E+00
10
15
20
25
30
Avg of Binder content (%of granule mass)

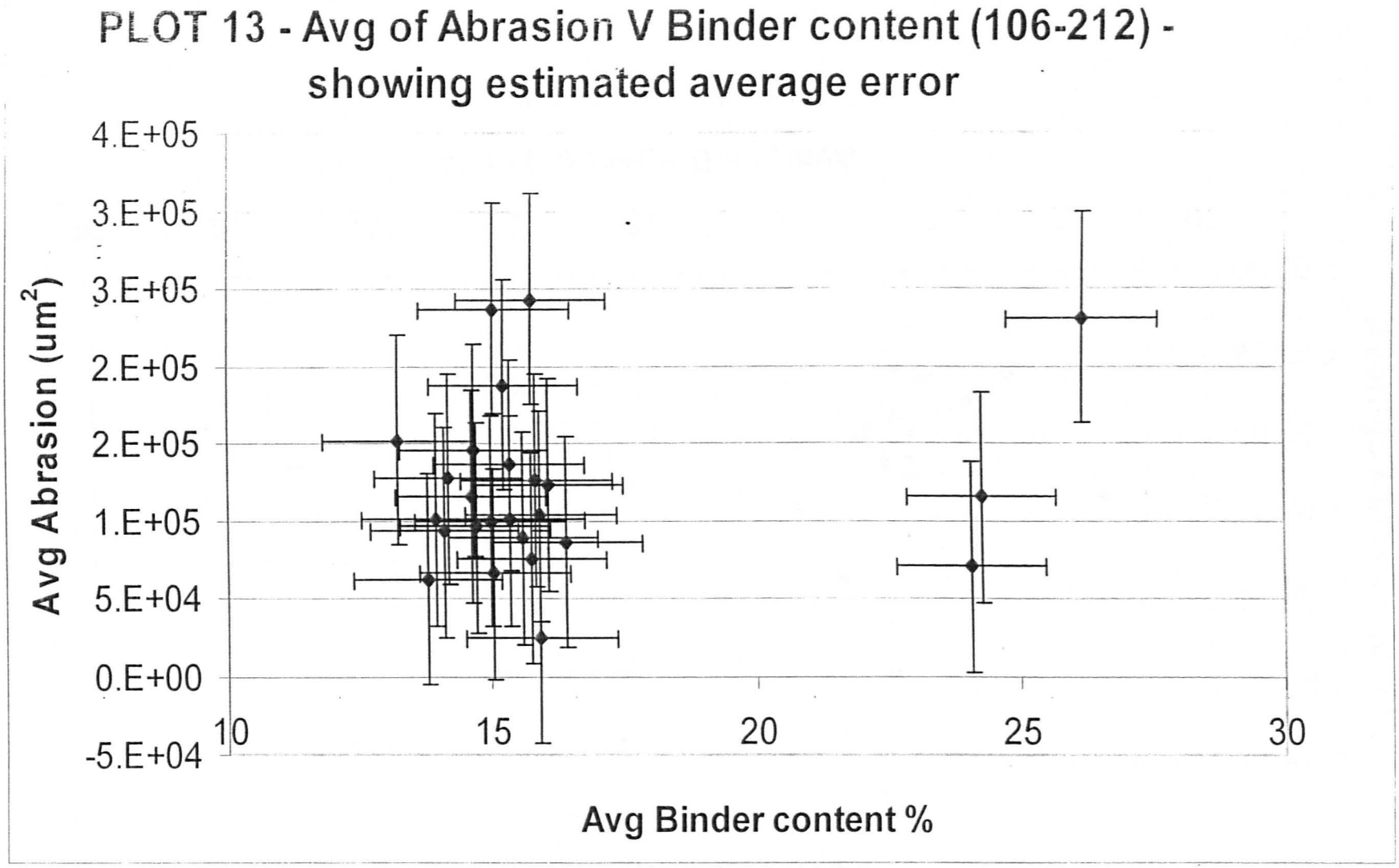
PLOT 13 - Avg of Abrasion V Binder content (106-212) - showing estimated average error
Avg Abrasion (um²)
4.E+05
3.E+05
3.E+05
2.E+05
2.E+05
1.E+05
5.E+04
0.E+00
-5.E+04
10
15
20
25
30
Avg Binder content %

PLOT 12 - Averages of Abrasion against Binder Content (all)

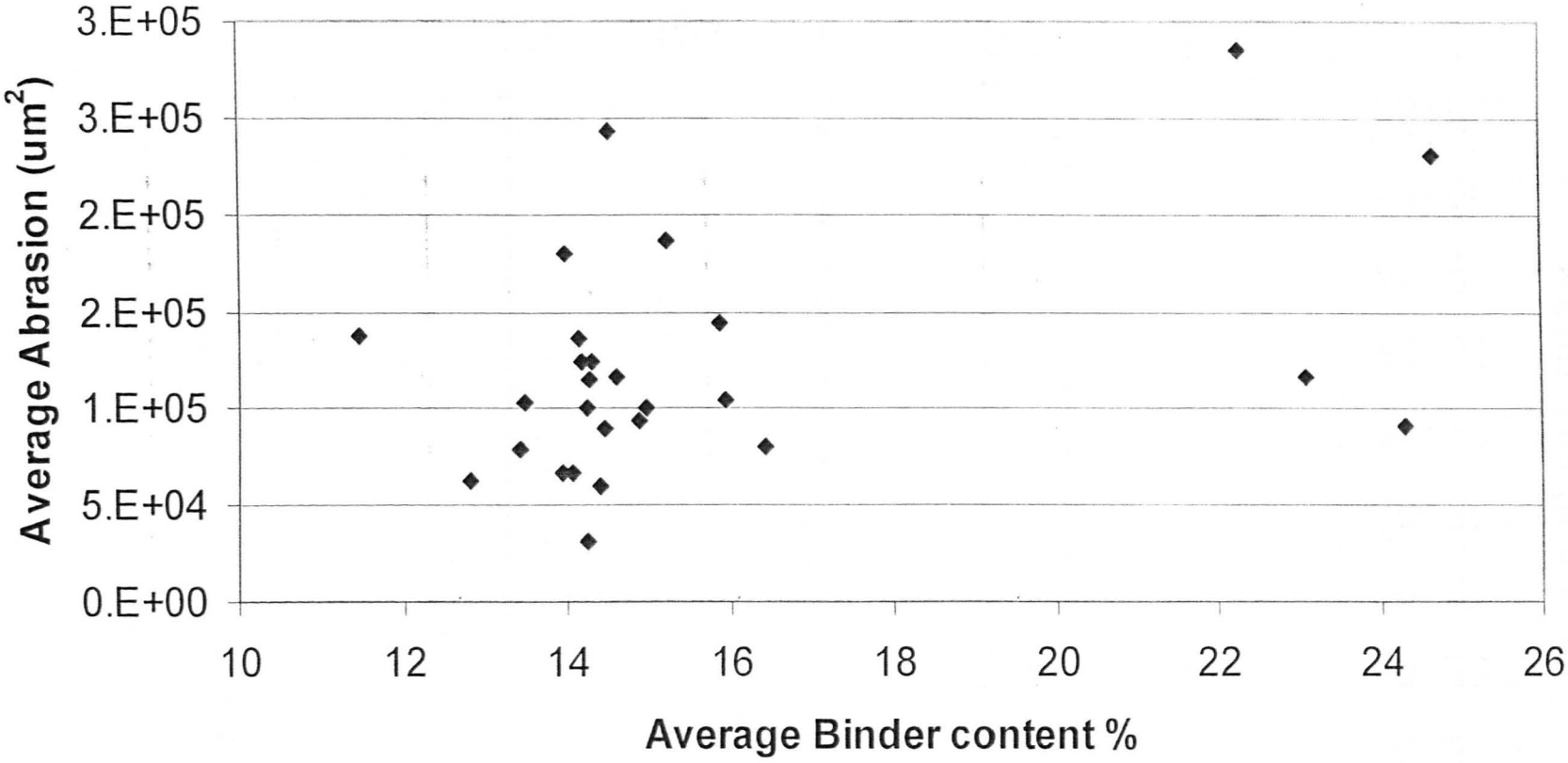

PLOT 5 - Abrasivity against Size (BN/04/X3B) - showing 95% confidence limits

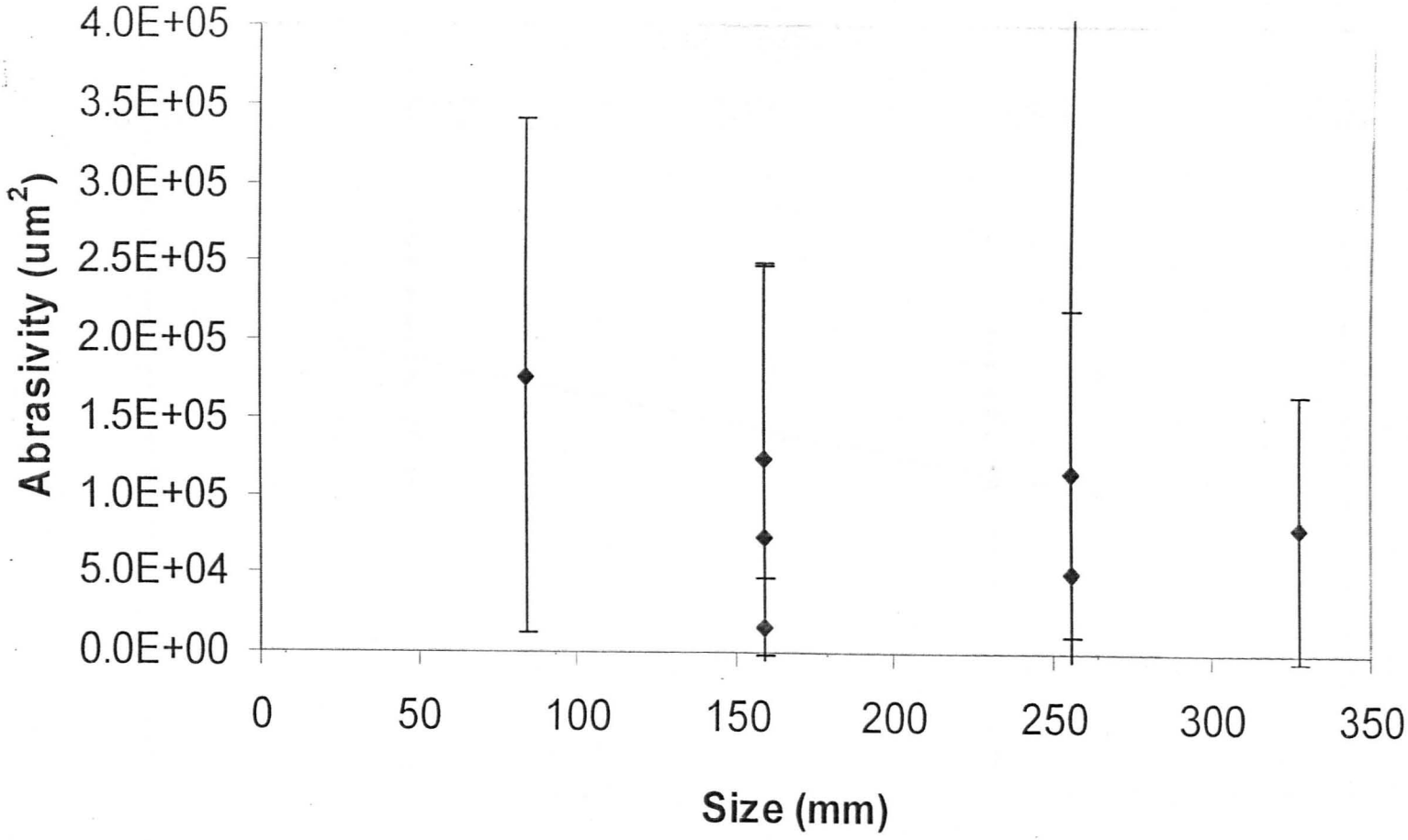

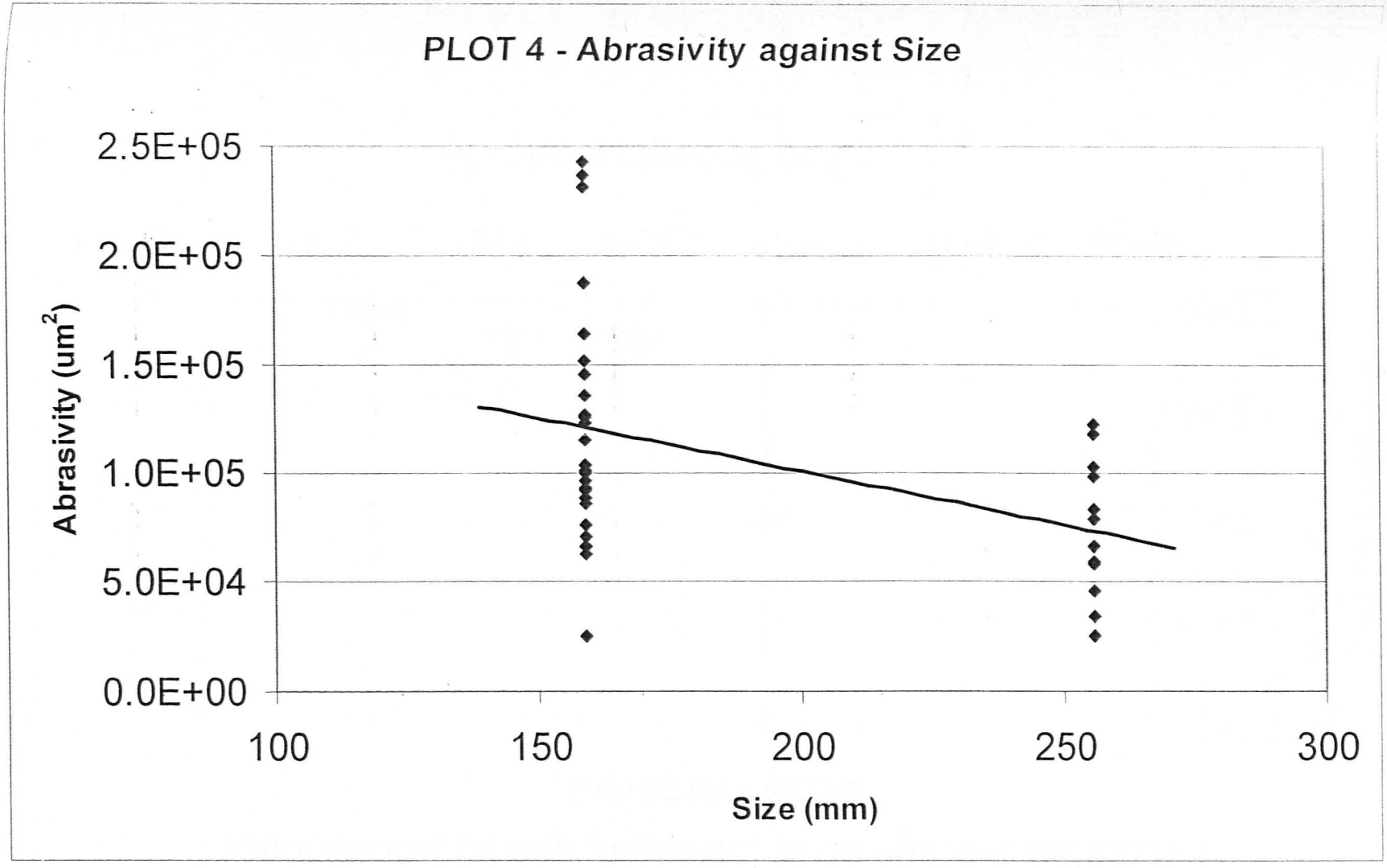
PLOT 4 - Abrasivity against Size
2.5E+05
2.0E+05
1.5E+05
1.0E+05
5.0E+04
0.0E+00
Abrasivity (um²)
100
150
200
250
300
Size (mm)

PLOT 3 - Abrasive wear V Strength (212-300) - showing estimated average error (strength) and 95% confidence limits (abrasion)

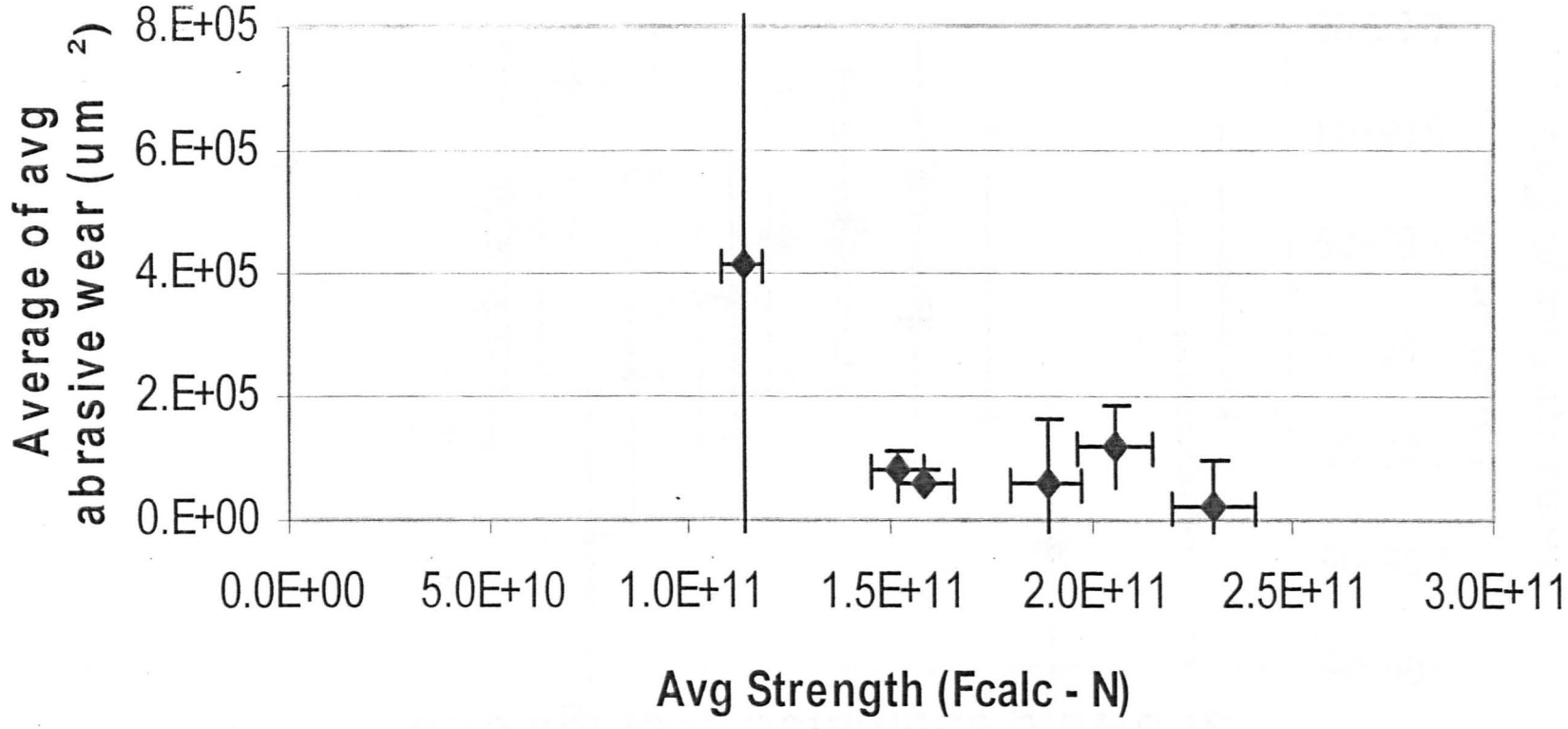

PLOT 2 - Abrasive wear V Strength (106-212um) - showing estimated average error

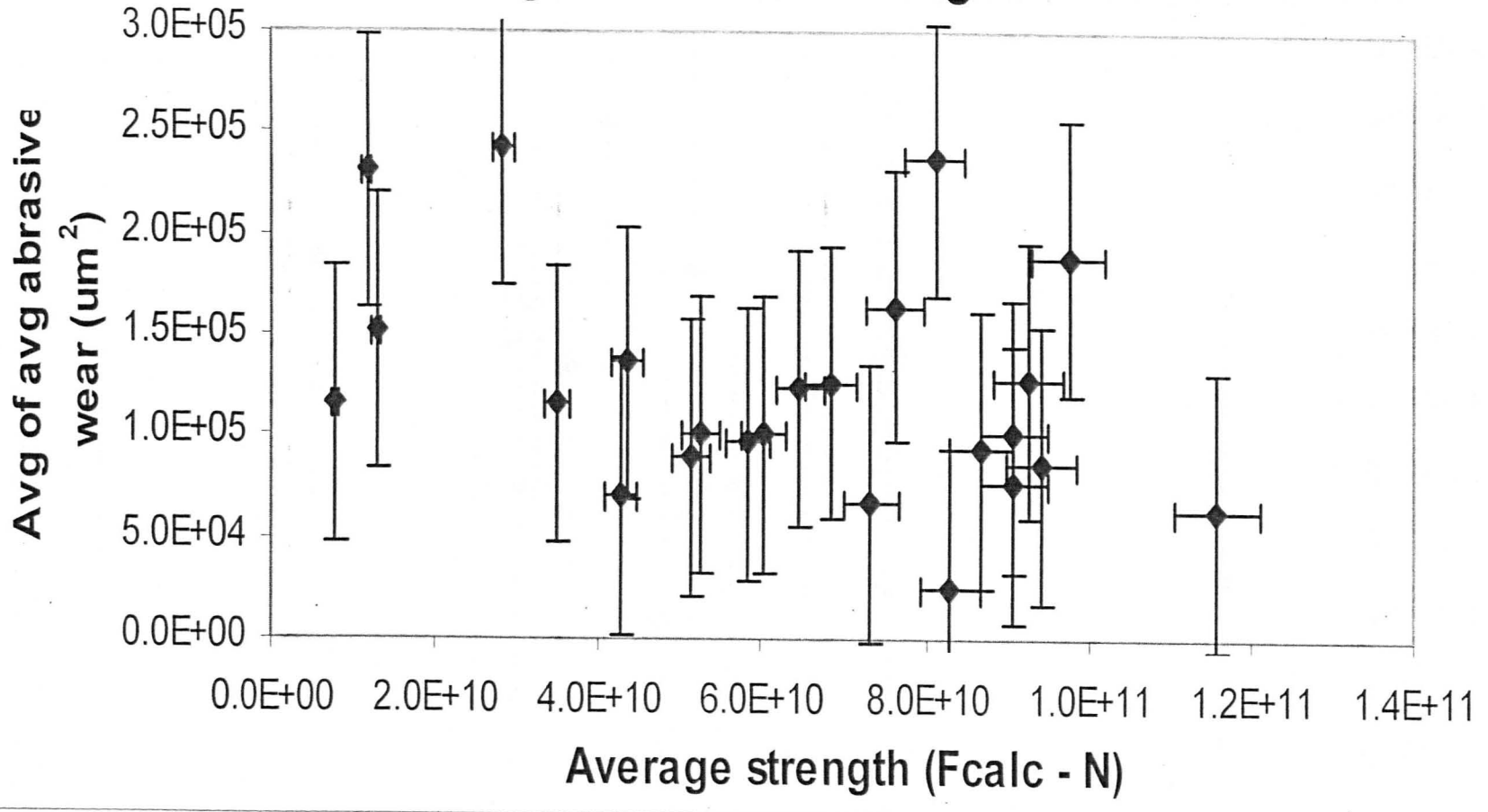

PLOT 1 - Abrasive Wear V Strength - showing estimated average error (106-212 - PEG 1500 / Omyacarb 2av)

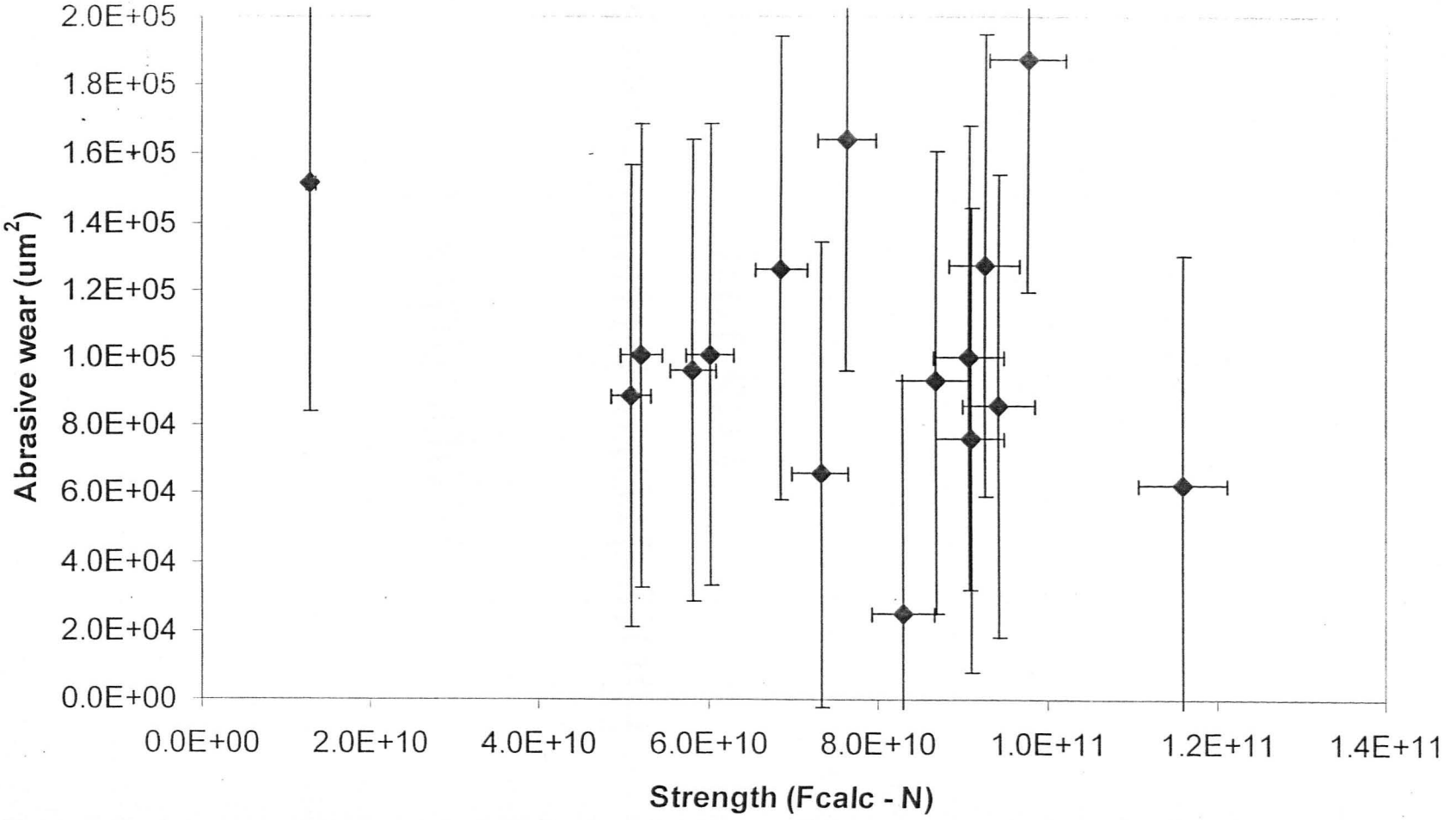

Appendix I

Plots from Preliminary Testing

micromeritics

Micromeritics Instrument Corporation

Sample: 2AV(2000) 63-106 um
Operator: DL
Submitter: MICROMERITICS FOR SHEFFIELD UNIVERSITY
File: C:\DEMO9500\DATA\MCA\MCA-844.SMP

LP Analysis Time:	9/5/2003 10:28:26AM	Sample Weight:	0.3000 g
HP Analysis Time:	9/5/2003 11:45:44AM	Correction Type:	Blank
Report Time:	9/6/2003 9:35:50AM	Show Neg. Int:	No

Summary Report

Penetrometer parameters

Penetrometer:	#s/n - (14) 3 Bulb, 0.412 Stem, Powder		
Pen. Constant:	10.790 µL/pF	Pen. Weight:	56.1912 g
Stem Volume:	0.4120 mL	Max. Head Pressure:	4.6800 psia
Pen. Volume:	3.2375 mL	Assembly Weight:	96.2768 g

Hg Parameters

Adv. Contact Angle:	140.000 degrees	Rec. Contact Angle:	140.000 degrees
Hg Surface Tension:	480.000 dynes/cm	Hg Density:	13.5335 g/mL

User Parameters

Param 1:	0.000	Param 2:	0.000	Param 3:	0.000

Low Pressure:

Evacuation Pressure:	50 µmHg
Evacuation Time:	5 mins
Mercury Filling Pressure:	0.27 psia
Equilibration Time:	10 secs
Maximum Intrusion Volume:	0.005 mL/g

High Pressure:

Equilibration Time:	10 secs
Maximum Intrusion Volume:	0.005 mL/g

Blank Correction Sample: C:\9500\DATA\BLANKS\MCA-237.SMP
Blank Correction ID: BLANK 14-0580

Intrusion Data Summary

Total Intrusion Volume =	0.5752 mL/g
Total Pore Area =	0.163 m^2/g
Median Pore Diameter (Volume) =	21.2081 µm
Median Pore Diameter (Area) =	12.8928 µm
Average Pore Diameter (4V/A) =	14.1027 µm
Bulk Density at 0.27 psia =	1.0072 g/mL
Apparent (skeletal) Density =	2.3972 g/mL
Porosity =	57.9642 %
Stem Volume Used =	42 %

Sample: 2AV(2000) 63-106 um
Operator: DL
Submitter: MICROMERITICS FOR SHEFFIELD UNIVERSITY
File: C:\DEMO9500\DATA\MCA\MCA-844.SMP

LP Analysis Time: 9/5/2003 10:28:26AM
HP Analysis Time: 9/5/2003 11:45:44AM
Report Time: 9/6/2003 9:35:50AM

Sample Weight: 0.3000 g
Correction Type: Blank
Show Neg. Int: No

Tabular Report

Pressure (psia)	Mean Diameter (µm)	Cumulative Pore Volume (mL/g)	Incremental Pore Volume (mL/g)	Cumulative Pore Area (m^2/g)	Incremental Pore Area (m^2/g)
0.27	796.6745	-0.0005	0.0000	0.000	0.000
0.33	723.9775	0.0019	0.0023	0.000	0.000
0.51	535.8391	0.0091	0.0072	0.000	0.000
0.75	352.2126	0.0153	0.0062	0.000	0.000
1.00	248.5718	0.0235	0.0082	0.000	0.000
1.50	177.6890	0.0332	0.0097	0.000	0.000
2.00	124.4650	0.0401	0.0068	0.001	0.000
2.01	106.4930	0.0403	0.0002	0.001	0.000
2.75	91.9171	0.0481	0.0078	0.001	0.000
3.00	74.3105	0.0503	0.0022	0.001	0.000
4.00	62.2230	0.0589	0.0086	0.002	0.001
4.00	53.3288	0.0593	0.0004	0.002	0.000
5.25	46.9927	0.0686	0.0094	0.003	0.001
5.49	39.7487	0.0706	0.0019	0.003	0.000
6.48	35.8797	0.0814	0.0108	0.004	0.001
7.00	31.7115	0.0880	0.0065	0.005	0.001
7.48	29.5030	0.0997	0.0117	0.006	0.002
7.96	27.6509	0.1174	0.0177	0.009	0.003
8.20	26.3965	0.1339	0.0165	0.011	0.003
8.44	25.6413	0.1552	0.0212	0.015	0.003
8.51	25.1696	0.1641	0.0090	0.016	0.001
8.75	24.7211	0.1856	0.0215	0.020	0.003
8.99	24.0579	0.2058	0.0202	0.023	0.003
9.23	23.4295	0.2263	0.0204	0.026	0.003
9.46	22.8333	0.2448	0.0185	0.030	0.003
9.70	22.2691	0.2624	0.0176	0.033	0.003
9.94	21.7318	0.2794	0.0170	0.036	0.003
10.17	21.2178	0.2949	0.0154	0.039	0.003
10.41	20.7321	0.3086	0.0137	0.042	0.003
10.51	20.4015	0.3148	0.0062	0.043	0.001
10.74	20.0835	0.3272	0.0124	0.045	0.002
10.98	19.6492	0.3389	0.0117	0.048	0.002
11.21	19.2338	0.3516	0.0127	0.050	0.003
11.44	18.8373	0.3620	0.0104	0.053	0.002
11.67	18.4595	0.3733	0.0112	0.055	0.002
11.91	18.0962	0.3831	0.0099	0.057	0.002
12.14	17.7456	0.3924	0.0093	0.059	0.002
12.37	17.4095	0.4006	0.0082	0.061	0.002
12.61	17.0841	0.4081	0.0074	0.063	0.002
12.84	16.7702	0.4153	0.0073	0.065	0.002

micromeritics

Micromeritics Instrument Corporation

Sample: 2AV(2000) 63-106 um
Operator: DL
Submitter: MICROMERITICS FOR SHEFFIELD UNIVERSITY
File: C:\DEMO9500\DATA\MCA\MCA-844.SMP

LP Analysis Time: 9/5/2003 10:28:26AM
HP Analysis Time: 9/5/2003 11:45:44AM
Report Time: 9/6/2003 9:35:50AM

Sample Weight: 0.3000 g
Correction Type: Blank
Show Neg. Int: No

Tabular Report

Pressure (psia)	Mean Diameter (μm)	Cumulative Pore Volume (mL/g)	Incremental Pore Volume (mL/g)	Cumulative Pore Area (m^2/g)	Incremental Pore Area (m^2/g)
12.99	16.5180	0.4193	0.0040	0.066	0.001
13.22	16.2767	0.4258	0.0065	0.067	0.002
13.69	15.8584	0.4352	0.0094	0.070	0.002
14.17	15.3205	0.4453	0.0100	0.072	0.003
14.64	14.8159	0.4534	0.0081	0.074	0.002
15.10	14.3479	0.4610	0.0076	0.076	0.002
15.58	13.9077	0.4674	0.0065	0.078	0.002
15.98	13.5203	0.4722	0.0048	0.080	0.001
16.69	13.0653	0.4797	0.0075	0.082	0.002
17.40	12.5212	0.4861	0.0064	0.084	0.002
18.35	11.9429	0.4936	0.0075	0.087	0.003
19.55	11.2694	0.5009	0.0074	0.089	0.003
19.97	10.7968	0.5036	0.0026	0.090	0.001
21.40	10.3238	0.5104	0.0068	0.093	0.003
22.95	9.6314	0.5165	0.0061	0.095	0.003
23.00	9.2856	0.5168	0.0003	0.095	0.000
24.96	8.9116	0.5227	0.0059	0.098	0.003
25.00	8.5401	0.5230	0.0004	0.098	0.000
27.67	8.1212	0.5295	0.0065	0.101	0.003
29.98	7.4123	0.5339	0.0044	0.104	0.002
30.70	7.0322	0.5401	0.0062	0.107	0.004
34.95	6.5266	0.5460	0.0059	0.111	0.004
36.31	5.9895	0.5472	0.0012	0.112	0.001
41.78	5.4908	0.5528	0.0056	0.116	0.004
46.49	4.8474	0.5556	0.0028	0.118	0.002
56.37	4.1863	0.5604	0.0049	0.123	0.005
71.80	3.3776	0.5645	0.0041	0.128	0.005
86.29	2.7216	0.5667	0.0022	0.131	0.003
111.39	2.1937	0.5696	0.0029	0.136	0.005
136.39	1.7396	0.5708	0.0012	0.139	0.003
171.21	1.4050	0.5722	0.0014	0.143	0.004
216.78	1.1150	0.5729	0.0007	0.146	0.003
266.91	0.8916	0.5733	0.0004	0.147	0.002
326.38	0.7264	0.5739	0.0006	0.150	0.003
416.13	0.5831	0.5743	0.0004	0.153	0.003
516.65	0.4628	0.5748	0.0005	0.157	0.004
636.67	0.3740	0.5749	0.0002	0.159	0.002
697.12	0.3205	0.5750	0.0000	0.160	0.001
796.82	0.2869	0.5751	0.0001	0.162	0.002
986.99	0.2419	0.5752	0.0001	0.163	0.001

micromeritics

Micromeritics Instrument Corporation

Sample: 2AV(2000) 63-106 um
Operator: DL
Submitter: MICROMERITICS FOR SHEFFIELD UNIVERSITY
File: C:\DEMO9500\DATA\MCA\MCA-844.SMP

LP Analysis Time: 9/5/2003 10:28:26AM
HP Analysis Time: 9/5/2003 11:45:44AM
Report Time: 9/6/2003 9:35:50AM

Sample Weight: 0.3000 g
Correction Type: Blank
Show Neg. Int: No

Tabular Report

Pressure (psia)	Mean Diameter (µm)	Cumulative Pore Volume (mL/g)	Incremental Pore Volume (mL/g)	Cumulative Pore Area (m^2/g)	Incremental Pore Area (m^2/g)
1198.28	0.1971	0.5752	0.0000	0.163	0.000
1297.20	0.1712	0.5752	-0.0000	0.163	-0.000
1396.95	0.1586	0.5752	-0.0000	0.163	-0.000
1498.04	0.1476	0.5752	-0.0000	0.163	-0.000
1596.66	0.1380	0.5752	-0.0000	0.163	-0.000
1696.72	0.1297	0.5752	-0.0000	0.163	-0.000
1897.04	0.1191	0.5752	-0.0000	0.163	-0.000
2046.03	0.1084	0.5752	-0.0000	0.163	-0.000
2195.59	0.1007	0.5752	-0.0000	0.163	-0.000
2345.71	0.0941	0.5752	-0.0000	0.163	-0.000
2502.84	0.0881	0.5752	-0.0000	0.163	-0.000
2640.66	0.0830	0.5752	-0.0000	0.163	-0.000
2692.05	0.0800	0.5752	-0.0000	0.163	-0.000
2840.67	0.0772	0.5752	-0.0000	0.163	-0.000
2991.48	0.0732	0.5752	-0.0000	0.163	-0.000
3239.62	0.0686	0.5752	-0.0000	0.163	-0.000
3488.69	0.0635	0.5752	-0.0000	0.163	-0.000
3738.95	0.0591	0.5752	-0.0000	0.163	-0.000
3987.85	0.0553	0.5752	-0.0000	0.163	-0.000
4237.34	0.0519	0.5752	-0.0000	0.163	-0.000
4486.25	0.0489	0.5752	-0.0000	0.163	-0.000
4725.15	0.0463	0.5752	-0.0000	0.163	-0.000
4985.08	0.0440	0.5752	-0.0000	0.163	-0.000
5282.10	0.0416	0.5752	-0.0000	0.163	-0.000
5480.82	0.0397	0.5752	-0.0000	0.163	-0.000
5733.61	0.0381	0.5752	-0.0000	0.163	-0.000
5980.31	0.0364	0.5752	-0.0000	0.163	-0.000
6229.86	0.0350	0.5752	-0.0000	0.163	-0.000
6478.48	0.0336	0.5752	-0.0000	0.163	-0.000
6727.64	0.0323	0.5752	-0.0000	0.163	-0.000
6976.04	0.0311	0.5752	-0.0000	0.163	-0.000
7476.53	0.0296	0.5752	-0.0000	0.163	-0.000
7963.53	0.0277	0.5752	-0.0000	0.163	-0.000
8477.80	0.0260	0.5752	-0.0000	0.163	-0.000
8966.72	0.0245	0.5752	-0.0000	0.163	-0.000
9270.22	0.0234	0.5752	-0.0000	0.163	-0.000
9562.35	0.0227	0.5752	-0.0000	0.163	-0.000
10010.23	0.0218	0.5752	-0.0000	0.163	-0.000
10459.19	0.0209	0.5752	-0.0000	0.163	-0.000
10961.41	0.0199	0.5752	-0.0000	0.163	-0.000

Sample: 2AV(2000) 63-106 um
Operator: DL
Submitter: MICROMERITICS FOR SHEFFIELD UNIVERSITY
File: C:\DEMO9500\DATA\MCA\MCA-844.SMP

LP Analysis Time: 9/5/2003 10:28:26AM
HP Analysis Time: 9/5/2003 11:45:44AM
Report Time: 9/6/2003 9:35:50AM

Sample Weight: 0.3000 g
Correction Type: Blank
Show Neg. Int: No

Tabular Report

Pressure (psia)	Mean Diameter (μm)	Cumulative Pore Volume (mL/g)	Incremental Pore Volume (mL/g)	Cumulative Pore Area (m^2/g)	Incremental Pore Area (m^2/g)
11458.22	0.0190	0.5752	-0.0000	0.163	-0.000
11960.49	0.0182	0.5752	-0.0000	0.163	-0.000
12560.33	0.0174	0.5752	-0.0000	0.163	-0.000
13061.94	0.0167	0.5752	-0.0000	0.163	-0.000
13607.83	0.0160	0.5752	-0.0000	0.163	-0.000
13958.00	0.0155	0.5752	-0.0000	0.163	-0.000
14297.03	0.0151	0.5752	-0.0000	0.163	-0.000
14551.61	0.0148	0.5752	-0.0000	0.163	-0.000
14957.48	0.0145	0.5752	-0.0000	0.163	-0.000
15401.24	0.0141	0.5752	-0.0000	0.163	-0.000
15754.40	0.0137	0.5752	-0.0000	0.163	-0.000
16155.23	0.0134	0.5752	-0.0000	0.163	-0.000
16602.45	0.0130	0.5752	-0.0000	0.163	-0.000
16955.33	0.0127	0.5752	-0.0000	0.163	-0.000
17306.72	0.0125	0.5752	-0.0000	0.163	-0.000
17653.93	0.0122	0.5752	-0.0000	0.163	-0.000
18054.52	0.0119	0.5752	-0.0000	0.163	-0.000
18404.79	0.0117	0.5752	-0.0000	0.163	-0.000
18751.45	0.0115	0.5752	-0.0000	0.163	-0.000
19149.37	0.0113	0.5752	-0.0000	0.163	-0.000
19756.40	0.0110	0.5752	-0.0000	0.163	-0.000
20260.36	0.0107	0.5752	-0.0000	0.163	-0.000
20769.51	0.0104	0.5752	-0.0000	0.163	-0.000
21173.36	0.0102	0.5752	-0.0000	0.163	-0.000
21626.21	0.0100	0.5752	-0.0000	0.163	-0.000
22029.35	0.0098	0.5752	-0.0000	0.163	-0.000
22632.30	0.0096	0.5752	-0.0000	0.163	-0.000
23184.10	0.0093	0.5752	-0.0000	0.163	-0.000
23736.05	0.0091	0.5752	-0.0000	0.163	-0.000
24086.63	0.0089	0.5752	-0.0000	0.163	-0.000
24637.72	0.0088	0.5752	-0.0000	0.163	-0.000
25038.36	0.0086	0.5752	-0.0000	0.163	-0.000
25439.16	0.0085	0.5752	-0.0000	0.163	-0.000
25889.64	0.0083	0.5752	-0.0000	0.163	-0.000
26440.39	0.0082	0.5752	-0.0000	0.163	-0.000
26940.83	0.0080	0.5752	-0.0000	0.163	-0.000
27391.33	0.0079	0.5752	-0.0000	0.163	-0.000
27791.18	0.0077	0.5752	-0.0000	0.163	-0.000
28242.32	0.0076	0.5752	-0.0000	0.163	-0.000
28991.96	0.0075	0.5752	-0.0000	0.163	-0.000

micromeritics

Micromeritics Instrument Corporation

Sample: 2AV(2000) 63-106 um
Operator: DL
Submitter: MICROMERITICS FOR SHEFFIELD UNIVERSITY
File: C:\DEMO9500\DATA\MCA\MCA-844.SMP

LP Analysis Time:	9/5/2003 10:28:26AM	Sample Weight:	0.3000 g
HP Analysis Time:	9/5/2003 11:45:44AM	Correction Type:	Blank
Report Time:	9/6/2003 9:35:50AM	Show Neg. Int:	No

Tabular Report

Pressure (psia)	Mean Diameter (μm)	Cumulative Pore Volume (mL/g)	Incremental Pore Volume (mL/g)	Cumulative Pore Area (m^2/g)	Incremental Pore Area (m^2/g)
29492.76	0.0073	0.5752	-0.0000	0.163	-0.000
29992.67	0.0072	0.5752	-0.0000	0.163	-0.000

micromeritics

Micromeritics Instrument Corporation

Sample: 2AV(2000) 63-106 um
Operator: DL
Submitter: MICROMERITICS FOR SHEFFIELD UNIVERSITY
File: C:\DEMO9500\DATA\MCA\MCA-844.SMP

LP Analysis Time:	9/5/2003 10:28:26AM	Sample Weight:	0.3000 g
HP Analysis Time:	9/5/2003 11:45:44AM	Correction Type:	Blank
Report Time:	9/6/2003 9:35:50AM	Show Neg. Int:	No

Cumulative Intrusion vs Pore size

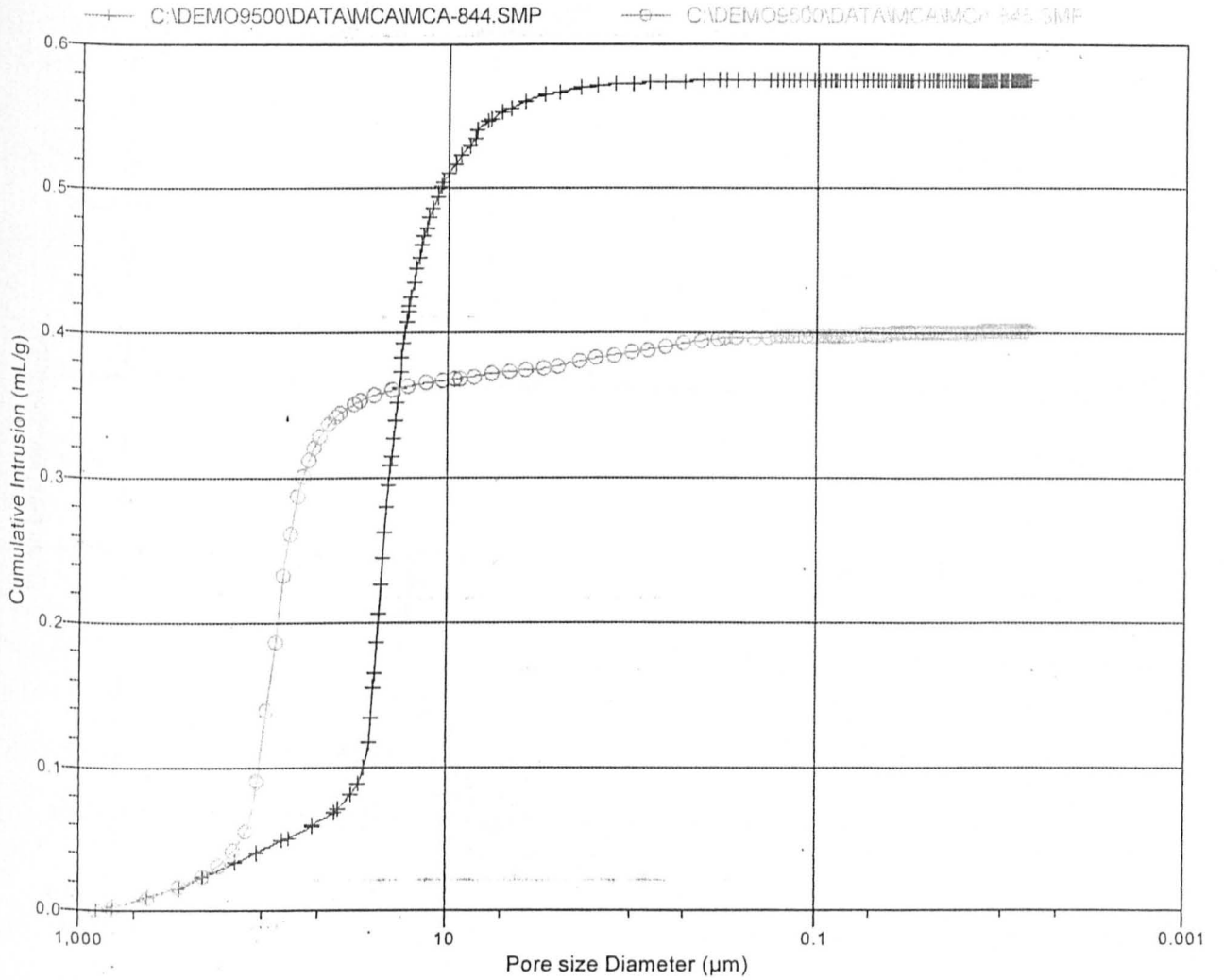

micromeritics

Micromeritics Instrument Corporation

Sample: 2AV(2000) 63-106 um
Operator: DL
Submitter: MICROMERITICS FOR SHEFFIELD UNIVERSITY
File: C:\DEMO9500\DATA\MCA\MCA-844.SMP

LP Analysis Time:	9/5/2003 10:28:26AM	Sample Weight:	0.3000 g
HP Analysis Time:	9/5/2003 11:45:44AM	Correction Type:	Blank
Report Time:	9/6/2003 9:35:50AM	Show Neg. Int:	No

Incremental Intrusion vs Pore size

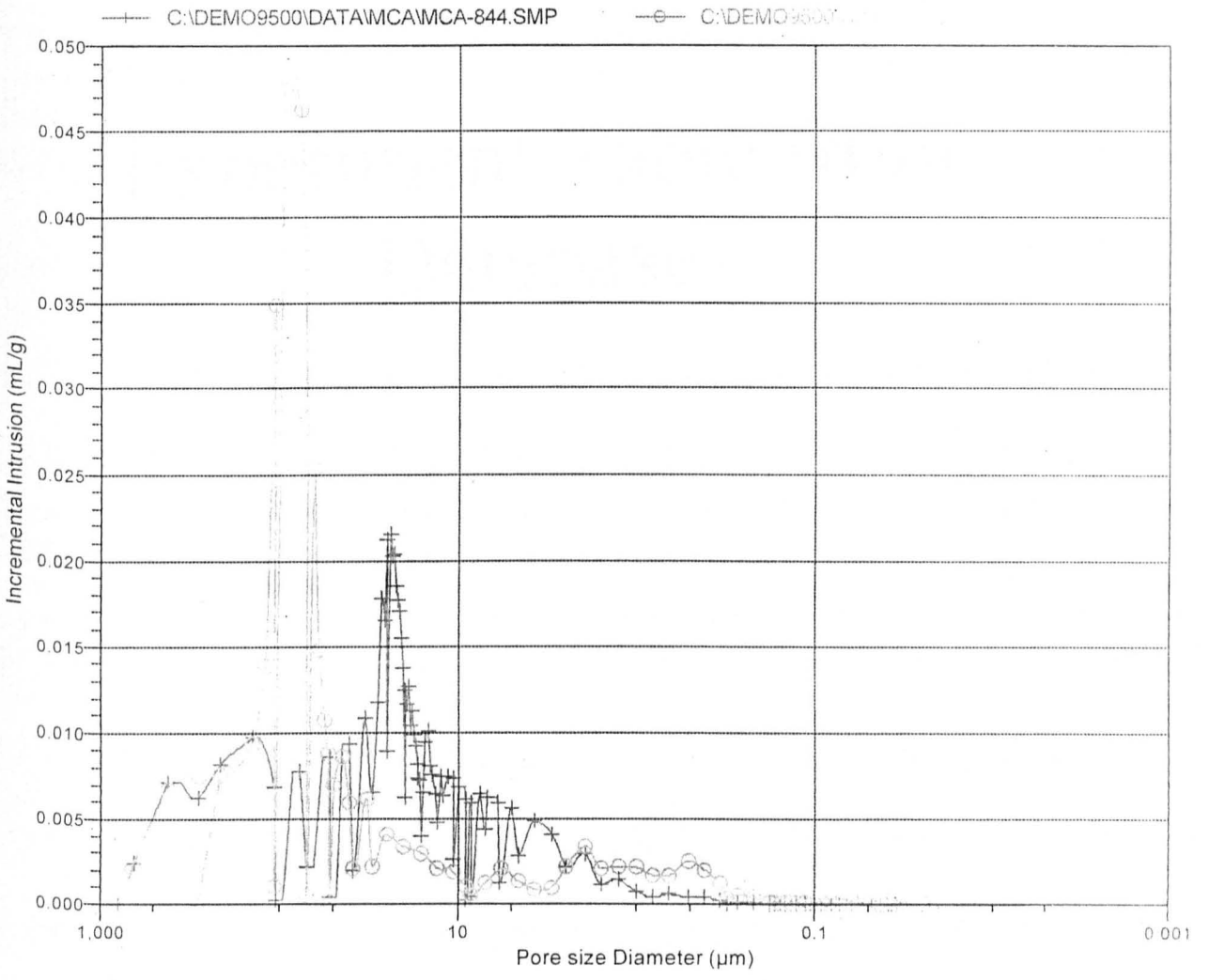

Appendix J

Experiment Table from Database

Experiment No	PP Type	Binder Type	Binder Ratio	Mass PP (g)	Mass Binder (g)	Addition Method	Impellor speed (rpm)	Chopper speed (rpm)	Temp. (°C)	Run Time
1	Omyacarb 2um	PEG 1500	15	2000	300	Spray	400	1400	60	30min
2	Zeolite	PEG 1500	15	2000	300	Spray	400	1400	60	30min
3	PacalH	PEG 1500	15	2000	300	Spray	400	1400	60	30min
4	Durcal 65	PEG 1500	15	2000	300	Spray	400	1400	60	30min
5	Omyacarb 2um	PEG 1000	15	2000	300	Spray	400	1400	60	30min
6	Omyacarb 2um	PEG 6000	15	2000	300	Spray	400	1400	60	30min
7	Omyacarb 2um	PVP	15	2000	300	Spray	400	1400	60	30min
8	Omyacarb 2um	PEG 1500	12	2000	240	Spray	400	1400	60	30min
9	Omyacarb 2um	PEG 1500	13.5	2000	270	Spray	400	1400	60	30min
10	Omyacarb 2um	PEG 1500	18	2000	360	Spray	400	1400	60	30min
11	Omyacarb 2um	PEG 1500	15	2000	300	pour-on	400	1400	60	30min
12	Omyacarb 2um	PEG 1500	15	2000	300	melt-in	400	1400	60	30min
13	Omyacarb 2um	PEG 1500	15	2000	300	spray	400	1400	40	30min
14	Omyacarb 2um	PEG 1500	15	2000	300	Spray	200	1400	60	30min
15	Omyacarb 2um	PEG 1500	15	2000	300	Spray	600	1400	60	30min
16	Omyacarb 2um	PEG 1500	15	2000	300	Spray	800	1400	60	30min
17	Omyacarb 2um	PEG 1500	15	2000	300	Spray	400	0	60	30min
18	Omyacarb 2um	PEG 1500	15	2000	300	Spray	400	700	60	30min
19	Omyacarb 2um	PEG 1500	15	2000	300	Spray	400	1400	60	20min
20	Omyacarb 2um	PEG 1500	15	2000	300	Spray	400	1400	60	1hr
21	Omyacarb 2um	PEG 1500	15	2000	300	Spray	400	1400	60	2hr
22	Durcal 65	PEG 1500	15	2000	300	Pour-on	400	1400	60	30min
23	Omyacarb 2um	PEG 400	15	2000	300	Pour-on	400	1400	60	30min
24	Omyacarb 2um	PEG 1500	13.5	2000	270	Pour-on	400	1400	60	2hr

Appendix K

Theoretical impact failure distribution of granules

Advanced Powder Technol., Vol. 14, No. 4, pp. 393–400 (2003)

Also available online - www.vsppub.com

Theoretical impact failure distribution of granules

R. E. MAXIM [1], A. D. SALMAN [1,*], M. PICKLES [2] and M. J. HOUNSLOW [1]

[1] *Particle Products Group, Department of Chemical and Process Engineering, University of Sheffield, Sheffield SI 3JD, UK*
[2] *Unilever R&D, Port Sunlight, UK*

Received 6 December 2002; accepted 17 February 2003

Abstract—A two-parameter Weibull distribution is presented that predicts the number of undamaged granules after impact with a rigid surface (platen) as a function of the impact velocity. The Weibull distribution is fitted, using experimental results from the breakage of fertilizer granules, to find the two parameters. The number of undamaged granules can be found using the velocity and angle of impact. A theoretical model derived by Maxim *et al.* is used to define a failure velocity as the criterion for failure. This model allows the theoretical prediction of the impact velocity required to induce 63.2% failure (c parameter in the Weibull distribution) from knowledge of measurable granule and platen material properties.

Keywords: Impact; breakage; agglomerate; granule; failure.

NOMENCLATURE

A	dimensionless area constant	
c	parameter in the Weibull distribution	
D	diameter of granule	(m)
E	Young's modulus of granule	(N/m^2)
E_1	Young's modulus of platen	(N/m^2)
F	force	(N)
F'	dimensionless force constant	
F_{cr}	critical load	(N)
H	parameter in equation (1)	
k	constant in the Laugier equation	
m	parameter in the Weibull distribution	

*To whom correspondence should be addressed. E-mail: a.d.salman@shef.ac.uk

N	number of undamaged granules per 100 fired	
r	radius of circle of contact	(m)
R	radius of granule	(m)
T	dimensionless time constant	
u	normal velocity	(m/s)
u_f	normal failure velocity	(m/s)
Y	yield strength of granule	(N/m^2)
z	elevation of the centroid of a granule above the platen	(m)

Greek

γ	Poissons ratio of granule	
γ_1	Poissons ratio of platen	
θ	angle of impact with platen (90° being perpendicular)	
v	velocity of granule	(m/s)
ρ	density	(kg/m^3)
σ	normal stress	(N/m^2)

1. INTRODUCTION

The transportation and processing of granular material is very important to many industries. Granules can impact upon each other and process equipment, which can lead to granule breakage. It is important to know the mechanisms of breakage and to have a way of predicting the breakage. Granule breakage upon impact with a rigid surface depends upon material properties, size, and velocity and angle of impact. There will be a spread of velocity required to induce failure for a given sample of granules due to the random nature of the number and position of flaws/pores and their arrangement within granules.

This spread of failure velocity can be seen when particles of identical size and material are fired at a rigid surface and the number of undamaged granules is counted, as shown by Salman *et al.* [1]. Figure 1 shows a typical set of data and the Weibull distribution curve fits for N, the number of undamaged granules per 100 fired as a function of velocity, v, and impact angle, θ.

If there was no random spread, there should be a single discreet velocity at which failure occurs and the results from Salman *et al.* [1] would be drastically different. This spread is seen for other materials such as aluminum oxide [2] and it is assumed to apply to most dense granular material. In real-life granule-processing industries it would be extremely useful if this failure distribution, as a function of velocity, could be known and adapted to a material's properties. A model is used in this paper that does just this; predicts the number of undamaged granules after impact using a two-parameter Weibull distribution, and knowledge of the impact angle and

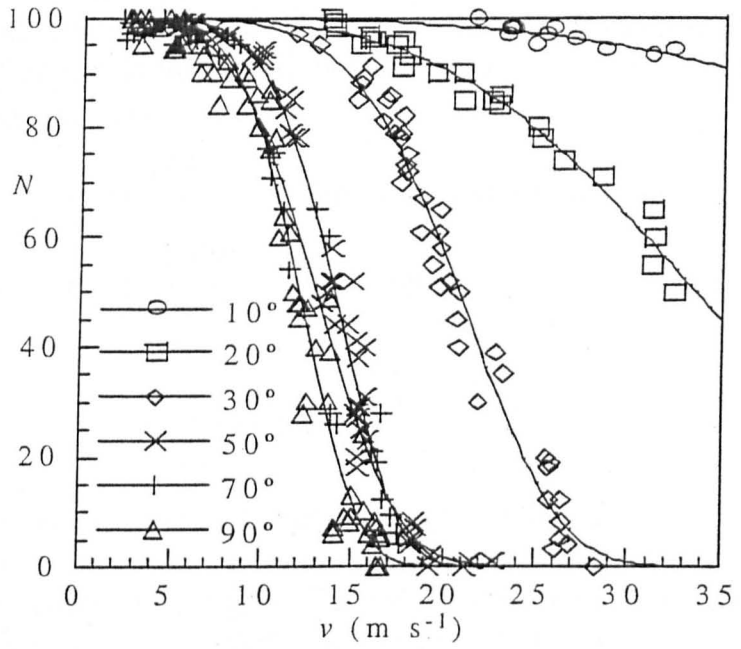

Figure 1. Number of undamaged fertilizer granules, N, per 100 fired as a function of impact velocity and angle.

velocity, granule size, and material properties of the granule and impact surface. The only material properties required are the static critical load, Young's modulus, Poissons ratio and density of the granule, and the Young's modulus and Poissons ratio of the impact surface.

It is well known that many granules fail by rupture of their interparticle bonds [3]. Thornton *et al.* [4] have used numerical solutions to analyze aspects of the impact failure of granules. Numerical simulations of systems of discrete particles as developed by Thornton *et al.* [4] are one approach to tackling this problem. Another approach, applicable to granules with low porosity, is to consider them as brittle elastic bodies. This is the approach adopted in this work, as the porosity of the granules is roughly 0.03%.

Most work on brittle particle failure assumes spherical particles and deals with elastic failure based on the original Hertzian theory developed by Hertz in 1886. Shipman and Hutchings [5] present a method to find the internal and surface stress fields in a sphere as a function of applied load and contact area. Observations for some brittle materials, known to have more surface flaws than internal flaws, indicate that failure occurs at internal stresses below the yield stress of the material and failure appears to propagate from the surface. Hutchings [6] argues that in these materials a surface failure stress exists that is lower than the internal failure stress and that the surface failure stress is exceeded before the internal stress is exceeded. For materials failing by internal stress, the maximum internal stress fields and yield stresses should be used to predict a load at failure. For materials failing by surface stress, the surface stress fields and surface failure stress should be used to predict the load at failure.

This paper deals with stresses based on Shipman and Hutchings's [5] estimates of peak stress and forces predicted by Laugier [7]. The predictions by Laugier deal with the force of impact in the platen, but this can be equated to the force acting on the sphere by Newton's law.

$$\sigma = \frac{HF}{\pi R^2}, \qquad \text{(Shipman and Hutchings)} \tag{1}$$

$$r^3 = \frac{4kFR}{3E}, \qquad \text{(Laugier)} \tag{2}$$

where:

$$k = \frac{9}{16}\left[(1-\gamma^2) + (1-\gamma_1^2)\frac{E}{E_1}\right]. \tag{3}$$

F is the applied load at a contact surface on a sphere of radius R. The radius of the circle of contact is r. E, E_1 and γ, γ_1 are the Young's modulus and Poisson's ratios of the sphere and platen, respectively. The value of the parameter H depends on the type of deformation. For plastic deformation $H \sim 0.4$ and for elastic deformation the value depends on the relative size of the contact area (e.g. $H = 1.24$ for $\gamma = 1/3$ and $r/R = 0.07$).

2. THE MODEL

A two-parameter Weibull distribution is used to relate the number of undamaged granules, N, to the impact velocity, v, as given below:

$$N = 100\exp\left[-\left(\frac{v}{c}\right)^m\right]. \tag{4}$$

The parameter, m, will be shown not to vary with impact angle and has a weighted average value of 4.50 ± 0.08.

Parameter c is interpreted as a measure of the impact velocity required to induce 63.2% failure, further related to the normal failure velocity, u_f by:

$$c = \frac{u_f}{\sin\theta}. \tag{5}$$

Maxim *et al.* [8] define the normal failure velocity, u_f, as a function of material properties and particle size. For granules undergoing elastic failure with no plastic deformation, the elastic failure theory defines u_f as a function of static critical load, density, Young's modulus of the granule and constant, k.

3. RESULTS/EXPERIMENTAL FITTING

Salman *et al.* [1], have characterized the failure of spherical granules of fertilizer, of diameter 5.3 mm, by firing them at a rigid platen at various velocities, v, and

incident angles, θ (90° being perpendicular). Figure 1 shows a typical set of data and curve fits of the form given by the cumulative Weibull distribution (4). Each point represents the number of undamaged granules, N, from 100 fired at the platen for that given velocity and angle.

For all angles used, the curve fit parameters obtained are shown in Table 1, and Figs 2 and 3. Values of m show no systematic variation with angle; the weighted average value is 4.50 ± 0.08.

Parameter c clearly declines as the incident angle approaches perpendicular. We interpret c as a measure of the impact velocity required to induce 63.2% failure; further related to normal failure velocity u_f by (5). Equation (5) implies that we should find parameter c is directly proportional to $1/\sin\theta$. Figure 4 shows that this is indeed the case.

According to Maxim *et al.* [8] the theory developed in the 'elastic failure model' defines u_f as a function of granule physical properties. It follows that it should be possible to represent all data for a fixed granule size using the Weibull distribution with N as a function of the normal velocity component only.

Table 1.
Curve fit parameters ($D = 5.3$ mm)

θ (deg)	c	m
90	12.94 ± 0.11	5.11 ± 0.29
70	14.18 ± 0.20	$4.03 \pm .0.29$
50	14.91 ± 0.08	5.49 ± 0.29
30	22.22 ± 0.15	5.19 ± 0.22
20	37.14 ± 0.56	3.66 ± 0.17
10	67.34 ± 12.03	3.54 ± 0.73

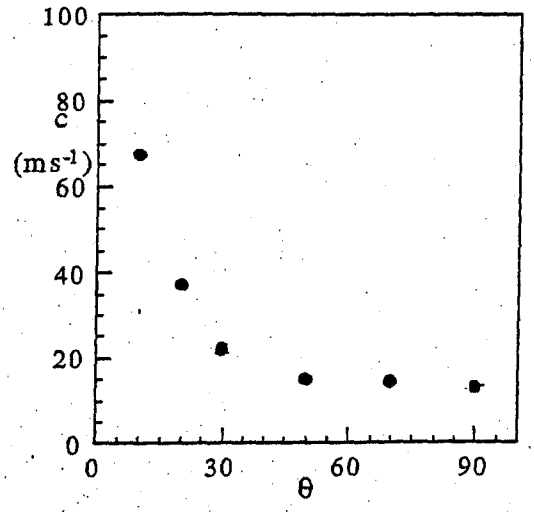

Figure 2. Curve fit values: c.

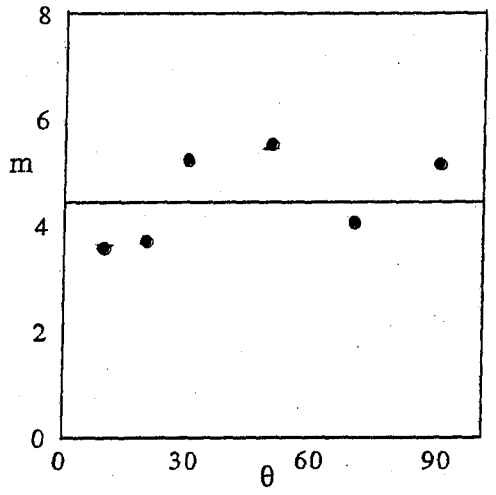

Figure 3. Curve fit values: m.

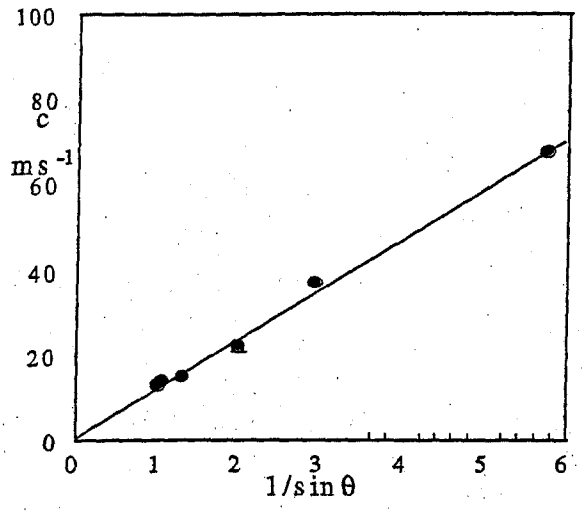

Figure 4. Parameter c as a function of $1/\sin\theta$.

4. THEORY: ELASTIC FAILURE MODEL

Maxim *et al.* [8] define the normal failure velocity for granules undergoing elastic failure with no plastic deformation as a function of critical static load, density, Young's modulus and Poisson ratio.

Consider a sphere approaching and colliding with a rigid planar surface (the platen) at a normal velocity u as shown in Fig. 5.

It is assumed that the force acting on the sphere is given by rearranging (2):

$$F = \frac{3}{4} r^3 \frac{E}{kR}. \tag{6}$$

Dimensionless force, area and time, respectively, are defined by the following non-dimensionalizing constants:

$$F' = 2R^2 \left(\frac{u^6 \rho^3 \pi E^2}{3k^2} \right)^{1/5}, \tag{7}$$

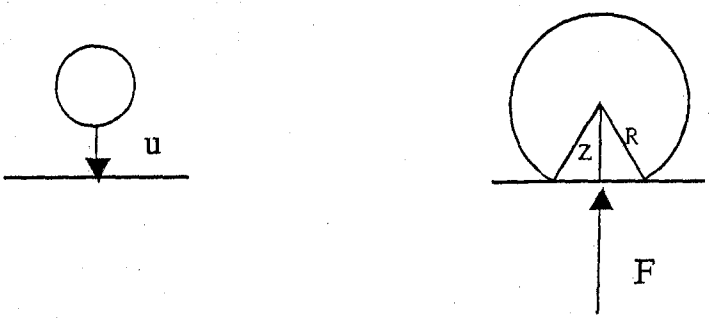

Figure 5. Schematic of collision.

$$A = 4R^2\left(\frac{u^2\rho\pi k}{9E}\right)^{2/5}, \tag{8}$$

$$T = 2R\left(\frac{\rho\pi k}{9\sqrt{u}E}\right)^{2/5}. \tag{9}$$

The maximum force (assuming no failure) is found to be:

$$2R^2\left(\frac{\pi\rho^3E^2u^6}{3k^2}\right)^{1/5}. \tag{10}$$

Substituting the static critical failure load for the theoretical maximum force in (10) implies a normal velocity for failure, u_f, for cases involving elastic failure. This is defined as:

$$u_f = \left[\frac{F_{cr}}{2R^2}\left(\frac{3k^2}{\pi E^2\rho^3}\right)^{1/5}\right]^{5/6}. \tag{11}$$

The theoretical normal failure velocity, u_f determined from (11) is interpreted as the normal impact velocity used in (5); used in conjunction with the angle of impact the c parameter is defined theoretically. The real impact velocity, v, then needs to be decided in order to use the Weibull distribution model to find the number of undamaged granules, N, at that velocity. Using (11) and (5) to find the c parameter theoretically removes the need to perform multiple impact experiments in order to find the c parameter graphically.

5. CONCLUSION

This paper presented a method for finding the number of undamaged granules involved in impact with a rigid surface. It was shown that a model using a two-parameter Weibull distribution could represent the failure distribution. It was further shown that the c parameter can be found by fitting experimental impact data or theoretically from static compression tests using the equations given by Maxim *et al.* [8]. To use a theoretically derived c parameter, it must be determined if the granule fails with or without plastic deformation taking place before failure.

If no plastic deformation takes place, then the 'elastic failure model' can be used — (11) is the important result.

REFERENCES

1. A. D. Salman, J. Fu, D. A. Gorham and M. J. Hounslow, Impact breakage of fertilizer granules, in: *Proc. 7th Int. Symp. on Agglomeration*, Vol. 1, pp. 451–461. European Federation of Chemical Engineering (2001).
2. A. D. Salman, C. A. Biggs, J. Fu, I. Angyal, M. Szabo and M. J. Hounslow, An experimental investigation of particle fragmentation using single particle impact studies, *Powder Technol.* **128**, 36–46 (2002).
3. J. Subero, Z. Ning, M. Ghadiri and C. Thornton, Effect of interface energy on the impact strength of agglomerates, *Powder Technol.* **105**, 66–73 (1999).
4. C. Thornton, K. K. Yin and M. J. Adams, Numerical simulation of the impact fracture and fragmentation of agglomerates, *J. Phys. D Appl. Phys.* **29**, 424–435 (1996).
5. P. H. Shipway and I. M. Hutchings, Fracture of brittle sphere under compression and impact loading 1. Elastic stress distributions, *Philos. Mag. A* **67** (6), 1389–1404 (1993).
6. I. M. Hutchings, Deformation and fracture of brittle solids, in: *Solid–Solid Interaction*, M. J. Adams, S. K. Biswas and B. J. Briscoe (Eds), pp 211–224. Imperial College Press, London (1996).
7. M. T. Laugier, Hertzian indentation of sintered Alumina, *J. Mater. Sci.* **19**, 254–258 (1984).
8. R. E. Maxim, A. D. Salman and M. J. Hounslow, Impact — failure criterion: elastic failure and approximate elastic-plastic failure, *Powder Technol.* (2003) (submitted).

Appendix L

Modelling effects of processing parameters on granule porosity in high-shear granulation

Granular Matter 6, 131–135 © Springer-Verlag 2004
DOI 10.1007/s10035-004-0173-y

Modelling effects of processing parameters on granule porosity in high-shear granulation

Robert Maxim, Jin Sheng Fu, Matthew Pickles, Agba Salman, Mike Hounslow

Abstract When trying to meet final product specifications for porosity of granules made using high-shear granulation there are many choices for the formulation recipe and processing conditions. This paper presents the concept of a Critical Packing State of the primary particles forming a granule and the associated Limiting Binder Ratio, which allows granule consolidation to be modelled.

The effect on consolidation of varying the following processing parameters is explained: Mixing intensity, mixing time and binder addition method. The effects of varying the following aspects of the formulation recipe are explained: Primary particle type, shape and size distribution, binder type and binder: solid ratio.

Keywords High-Shear Granulation, Consolidation, Particle Packing

Symbols

B_v	Interparticle space (m^3/m^3)
V_s	Volume of spheres in control volume (m^3)
V_c	Volume of control volume (m^3)
$\acute{d}$	Diameter of mono-size sphere (m)
$\acute{k}$	Packing factor used in mono-size sphere analysis
$\acute{a}$	Thickness of binder layer at maximum packing of mono-size spheres (m)
B_{lbr}	Limiting interparticle space (m^3/m^3)
V_b	Volume of binder (m^3)
V_p	Volume of primary particles (m^3)
d	Characteristic length of PPSD (Primary particle size distribution) (m)
k	Packing factor
a	Binder constant (m)
B_{va}	Asymptotic interparticle space (m^3/m^3)
ω	Agitation rate constant (s^{-1})
B_{v0}	Interparticle space at end of induction period (m^3/m^3)
t	Time defined by Eq. (5) (s)
t'	Critical start time (s)
t_{real}	Granulation run time (s)
a''	Modified binder constant (m)
B''_v	Internal granule interparticle space (m^3/m^3)
B^*_{va}	Granule interparticle space at start of internal granule consolidation (m^3/m^3)
t^*	Time defined by Eq. (8) (s)
t''	Time at onset of internal granule consolidation (s)
B_s	Volume of binder on granule surface (m^3/m^3)

Received: 26 August 2003

R. Maxim (✉), J. S. Fu, A. Salman, M. Hounslow
Particle Products Group,
Department of Chemical Engineering,
University of Sheffield,
Sheffield, S1 3JD, UK
e-mail: CPP01REM@sheffield.ac.uk
Tel.: 0114 2227543
Fax: 0114 2227501

M. Pickles
Unilever R&D Port Sunlight,
Bebington, CH63 3JW, UK
e-mail: Matthew.Pickles@unilever.com
Tel.: +44 (0)151 641 1547
Fax: +44 (0)151 641 1806

1 Introduction

Granule porosity is an important end product specification in many granulation processes as it affects the density and strength of the granule, Wikberg and Alderhorn [1], as well as the dispersal properties of active ingredients. There are a lot of experimental observations from a number of sources [2–5] giving the effect of varying processing conditions and formulation recipes on the granule porosity when using high-shear granulation.

This paper describes granule consolidation and how a surface wet granule can be thought of as having a granule core surrounded by excess binder. An analysis of the interparticle space between primary particles within a granule is given followed by the concept of a critical packing state, which is used to describe the interparticle space of the granule core. A model is then presented to predict granule consolidation. This is followed by a description of the effect on the model of varying processing parameters and the formulation recipe used. Similar work has been carried out by Iveson et al. [6] and the section on Granule Consolidation in the review by Iveson et al. [7] gives a good alternative interpretation of the processing parameter and formulation recipe effects.

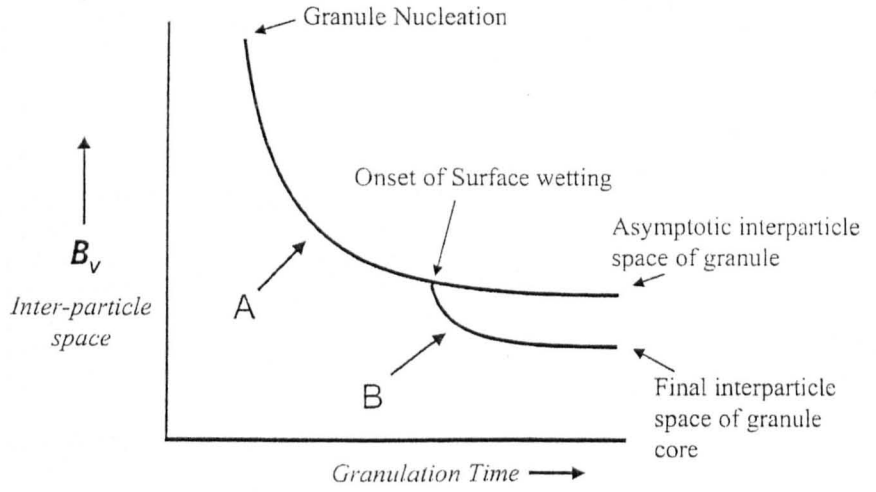

Fig. 1. Granule consolidation with time

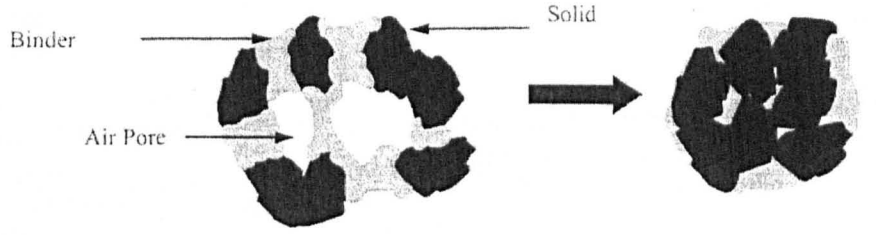

Fig. 2. Showing air, solid and binder components of a granule before and after consolidation of whole granule

2 Granule Consolidation

Granules are generally made up of three phases, solid primary particles, liquid binder and air. As the granules collide with other granules and the process equipment the primary particles pack closer together squeezing out the air and binder. The extent of granule consolidation affects the surface wetness and interparticle space of the granule product. The interparticle space is defined as the fraction of the granule occupied by binder and air. Fig. 1 shows how granule consolidation with time affects the interparticle space. Curve A represents the consolidation of the whole granule, shown in Fig. 2. Curve B starts at the onset of surface wetting and represents the continuing consolidation of the primary particles. This can be imagined to represent the granule core consolidating towards its limiting interparticle space, squeezing out binder and making the granule more surface wet; this is shown in Fig. 3.

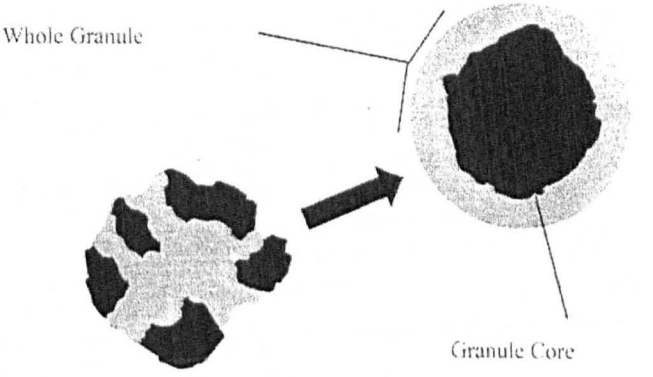

Fig. 3. Showing consolidation of the granule core

3 Analysis of interparticle space

An analysis of the binder content associated with two different packing structures (body-centred cubic and a tetrahedral control volume) of mono-disperse spheres was done, shown in Fig. 4. This yields a general equation, Eq. (2), for the interparticle space, available for binder and air, in terms of the packing structure, particle diameter and interparticle binder layer thickness. The inter-particle space, B_v, is defined as:

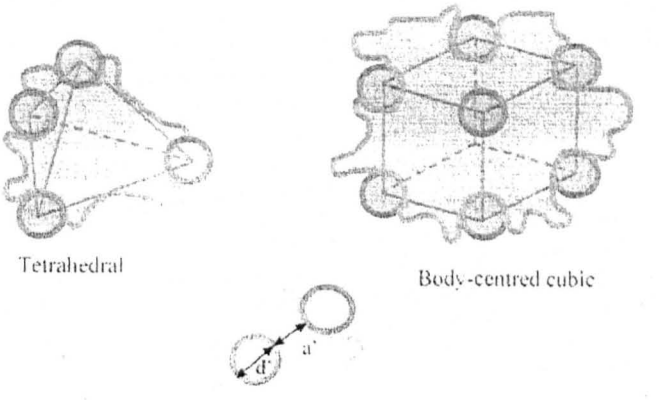

Fig. 4. Showing spherical particles and binder in the control volumes for the analysis of the interparticle space

$$B_v = 1 - \frac{V_s}{V_c} \tag{1}$$

where V_s is the total volume of the spheres within the control volume and V_c is the volume of the control volume. The control volume is found in terms of the diameter of the spheres, d', and the thickness of the binder layer, $\acute{a}$, at the minimum separation of the spheres. The general equation for the interparticle space of a packing structure is:

$$B_v = 1 - \frac{k' d'^3}{(d' + a')^3} \tag{2}$$

where k' is a factor dependent on the packing structure of the control volume; for body-centred cubic packing $k' = \pi\sqrt{3}/\,8$ and for a tetrahedral control volume $k' = \pi\sqrt{2}/\,5$.

4 Critical Packing State

The critical packing state is defined as the closest packing of solid particles forming a granule. For any primary particle size distribution (PPSD) there exists a theoretical state (critical packing state) in which the primary particles are packed as close as they will ever get. The critical packing state has an associated minimum interparticle space. When binder is added the existence of a minimum binder layer between particles will expand the structure increasing the theoretical interparticle space. For any given PPSD and binder combination there is a corresponding interparticle space at maximum compaction defined as the limiting interparticle space, B_{lbr}. If this space is completely filled with binder then the limiting binder ratio can be found from:

$$Limiting\ Binder\ ratio = \frac{V_b}{V_p} = \frac{B_{lbr}}{1 - B_{lbr}} \tag{3}$$

where, V_b, is the volume of binder and, V_p, is the volume of primary particles forming a granule.

It can be expected that Eq. (2) could be used to describe the limiting interparticle space such that:

$$B_{lbr} = 1 - \frac{kd^3}{(d + a)^3} \tag{4}$$

where, d, is a characteristic length of the PPSD, k, is a packing factor taking into account the shape of the particles and the spread of the PPSD and, a, is the binder constant equivalent to the minimum binder layer thickness. Surface roughness and solid-binder wetting properties are accounted for in the binder constant.

The limiting interparticle space can also be found by splitting the PPSD into segments, converting the segments into spheres and packing these into a 3D shape – the critical packing state, this is shown in Fig. 5. The limiting interparticle space is the fraction of the total volume that is not spheres. The effect of the minimum binder layer thickness is accounted for by increasing the diameter of each sphere before packing.

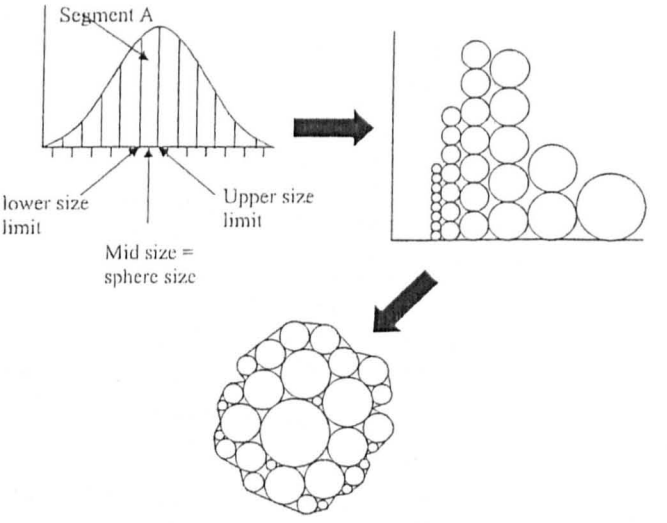

Fig. 5. Showing a PPSD cut into segments. The segments are converted into equivalent spheres. The spheres are then packed to find the limiting interparticle space

5 Predicting Granule Consolidation

Fu et al. [3] and Knight et al. [4] show that granule porosity decreases to an asymptotic value as a batch granulation progresses. The interparticle space decreases to an asymptotic value as shown in Fig. 1., as the granule nears this value the granule becomes more surface wet as the granule core continues consolidating. The concept of the critical packing state and the analysis of the interparticle space allow the prediction of the limiting interparticle space of the granule core, B_{lbr}. This is an imaginary end point that the granule is trying to reach, squeezing out the air to reduce the porosity then squeezing out excess binder to form surface wet granules. In reality it is not possible for the primary particles to reach the critical packing state because the random way that particles move in the consolidation process means they do not all orientate exactly as required.

Iveson et al. [6] give an exponential decay model for predicting the effect of granule consolidation on porosity based on a consolidation rate constant and the number of drum revolutions. A similar general rate equation is defined here for the interparticle space, B_v, of the whole granule representing consolidation along curve A with time.

$$B_v = (B_{v0} - B_{va})\, e^{-\omega t} + B_{va} \tag{5}$$

where, B_{va}, is the asymptotic interparticle space, ω, is the agitation intensity rate constant and, B_{v0}, is the interparticle space at the end of the formation period, defining the critical start time, t', such that:

$$t = t_{real} - \acute{t}. \tag{6}$$

where, t_{real}, is the granulation run time.

By comparing the limiting binder ratio to the binder ratio of the start system we can modify the binder constant in Eq. (4) to a modified binder constant, a'', accounting for the extra thickness between primary particles. This gives an expression for the asymptotic interparticle space:

$$B_{va} = 1 - \frac{kd^3}{(d + a'')^3} \tag{7}$$

Once the granule has reached the asymptotic interparticle space then further agitation will result in the primary particles getting squeezed closer together in an attempt to reach the maximum packing state, this can be thought of as the primary particles forming an internal granule with its own associated interparticle space, B_v''. This results in excess binder being squeezed out and producing a surface binder layer. This phase of granule consolidation can be modelled by an adapted version of Eq. (5) such that:

$$B_v'' = (B_{va}^* - B_{lbr})\, e^{-\omega t^*} + B_{lbr} \tag{8}$$

where B_{va}^* is the point considered to be the start of internal granule consolidation resulting in surface wetness occurring at time, t'', thus t^* is defined by:

$$t^* = t_{real} - t'' \tag{9}$$

The amount of binder on the surface, B_s, is equivalent to the difference between the asymptotic interparticle space and the consolidated internal granule interparticle space:

$$B_s = B_{va} - B_v'' \tag{10}$$

Fig. 6 shows Eq. (5) as line A and Eq. (8) as line B with the important associated times and interparticle spaces marked out.

6 Qualitative effects of processing parameters and formulation

In high-shear granulation formulation parameters and processing parameters can be varied in an attempt to alter the interparticle space of final granules. Many of these parameters act interdependently, for example the binder type and temperature act together to determine the viscosity and surface tension of the binder, this in turn combines with the primary particle material to give the wetting characteristics of the binder.

6.1 Primary Particle Type

The primary particle type dictates the material, the shape and the size distribution of the primary particles. If particles are very spherical in shape then the orientation during packing will not affect the final interparticle space. Flat plate-like particles or needles will have a much greater dependency on the orientation of the particles. If they align parallel to each other then the final interparticle space will be very low and the value of, k, will be high. If they align perpendicular or at angles then the final interparticle space will increase and the value of, B_{va}, will increase. The size distribution will affect the final interparticle space. It is thought that a wide size distribution will increase the value of, k, due to the smaller particles fitting into the spaces between large particles. The particle material dictates the chemistry of its surface and importantly the surface free energy, when this is combined with the chemistry of the binder it determines the wettability of liquid binder on the solid. Iveson et al. [4] report that a non-wetting liquid will not spread or form a film, but stay as discrete bridges. This will have the effect of increasing the value of the binder constant, a, in the general packing equation, which in turn will increase the value of B_{va}.

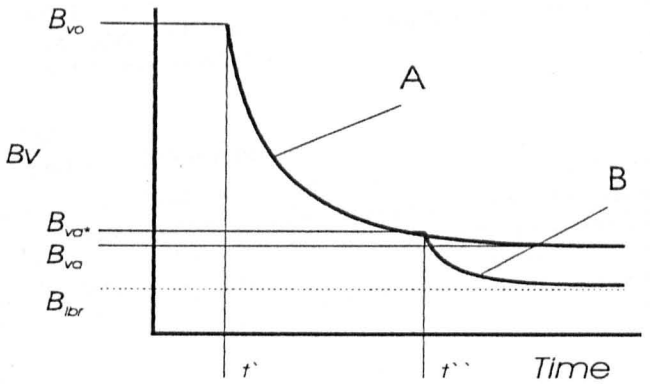

Fig. 6. Consolidation curves with important parameters marked on. A - general rate Eq. (5), B - consolidation rate Eq. (8)

6.2 Binder Type

The binder type has several important properties, viscosity, surface tension and wettability. The wettability depends on the chemistry of the binder and primary particle material as already described. Changing the viscosity of the system will change the magnitude of the agitation rate constant, ω. The viscosity varies as a function of temperature and shearing forces. Generally the viscosity will decrease with temperature. For Newtonian binders reducing the viscosity will reduce the consolidating effects of any agitation and reduce, ω. For shear-thinning binders the effect is compounded with agitation intensity; increasing agitation intensity will increase the value of, ω, but will also decrease the viscosity further increasing the magnitude of, ω. For shear-thickening binders the effect is confounded. It is assumed that binder type also affects the thickness of the minimum binder layer between particles at their maximum compaction, this is reflected in the value of the binder constant, a. It can be visualised that this is dependent on the molecular arrangement of the binder when squeezed into very thin films between two surfaces. It is assumed that surface tension will affect the stability of air pockets within the granule and the net force felt by binder bridges (as oppose to continuum) during compaction, increasing the surface tension would reduce the net force and reduce the value of the agitation intensity rate constant, ω.

6.3 Binder Ratio

We define binder ratio as volume of binder per unit volume of primary particles. For any given PPSD and binder type there is a binder ratio at maximum packing defined as the limiting binder ratio. If the initial feed binder ratio is the same as the limiting binder ratio then theoretically all the granules could consolidate to their maximum compaction and there would be no air phase within the granules. In reality this does not happen, if the initial binder ratio is less then either granulation will not occur or a

portion of the internal space must be occupied by air. If the initial binder ratio is greater than the limiting binder ratio then the value of, a'', will increase and if it is assumed that no air is present at the onset of internal granule compaction, when $t = t^*$, then, a'', scales as:

$$a'' = d^3 \sqrt{k \left(\frac{V_b}{V_p} + 1 \right)} - d \tag{11}$$

If air is present then the asymptotic interparticle space must be increased appropriately. When the binder ratio is greater than the limiting binder ratio then as the granule consolidates it will squeeze binder out to the surface and produce surface wet granules. The extent of surface wetting is modelled by Eq.'s (8), (9) and (10). When a granule is surface wet it will attract more fines and grow by layering, thus changing the volume of primary particles and the granule binder ratio—this will continue until the binder ratio has reached a stable value and the surface is no longer wet. Growth and stabilisation can also occur by coalescence with other surface dry granules, but coalescence of 2 surface wet granules will lead to a less stable state.

6.4 Run Time

The effect of granulation run time is accounted for by Eq.'s (5) and (8), increasing the run time increases the extent of agitation and thus the extent of consolidation and production of surface wet granules. It is important to note that this model predicts a region before, t', when granules will be highly porous. When high binder ratios are used long run times will lead to formation of large surface wet granules.

6.5 Agitation intensity

Increasing the mixer speed will increase the agitation intensity and increase the value of the agitation rate constant, ω, leading to faster consolidation. However it must be noted that there is a limit to this effect, at elevated intensities breakage of granules occurs limiting the size of granule growth. When surface wet granules collide with other granules such that the combined size is greater than the stable size it is thought the surface binder will be stripped away by the impacting granule rather than absorbed by the coalescence.

6.6 Binder Addition method

Work by Knight et al. [4] suggests that granule porosity is independent of addition method at extended mixing times, it is proposed that individual granule interparticle space is independent of addition method after time t''. The addition method will affect time, t', the modified binder constant, a'', and the initial interparticle space, B_{v0}, of individual granules. Spray addition will have a large spread of, t', values compared to say pour-on addition, but might have a narrower spread of values for, a'', and, B_{v0}.

7 Conclusion

A model has been proposed to represent firstly the reduction in porosity of a granule with time and secondly the subsequent consolidation and squeezing out of binder to form surface wet granules. The model allows the theoretical prediction of the amount of binder on surface wet granules as a function of time, Eq. (10). This model allows qualitative predictions of how changes in the granulation process and formulation will affect the consolidation rate and final surface wetness. The practical value of the model for quantitative predictions is currently limited by the determination of appropriate values in Eq. (4) and by the absence of a computer code for the algorithm converting a PPSD into a critical packing state. Experimental verification will be difficult due to the heterogeneous nature of any granulation system, realised in the model by the spread of values for, B_{v0}, t'', and a'', as a result of the addition method. Further work combining this models prediction of surface wetness with existing growth and breakage rate models should make experimental verification possible.

References

1. M. Wikberg & G Alderhorn, Pore size distributions, assessed by mercury penetration of compacts of two lactose granulations with different fragmentation propensities, International Journal of Pharmaceutics 84 (1992), p. 191–195
2. A. C. Scott, Heterogeneity in high-shear granulation, PhD Dissertation Clare College—Cambridge, 2000
3. J. S. Fu, G. K. Reynolds, Y. S. Cheong, M. J. Adams, A. D. Salman & M. J. Hounslow, Feasibility of improving granule quality (working title), Powder Technology (to be submitted), 2003
4. P. C. Knight, T. Instone, J. M. K. Pearson & M. J. Hounslow, An investigation into the kinetics of liquid distribution and growth in high shear mixer agglomeration, Powder Technol. 97 (1998), p. 246–257
5. P. Holm, O. Jungersen, T. Schaefer & H. G. Kristensen, Granulation in High Speed Mixers Part 1: Effects of process variables during kneading, Pharm. Ind. 45 (1983), 806–811
6. S. M. Iveson, J. D. Litster & B. J. Ennis, Fundamental studies of granule consolidation: Part 1. Effects of binder viscosity and binder content, Powder Technol. 88 (1996), 15–20
7. S. M. Iveson, J. D. Litster, K. Hapgood & B. J. Ennis, Nucleation, growth and breakage phenomena in agitated wet granulation processes: a review, Powder Technol. 117 (2001), 3–39

Acknowledgements

This thesis would not have been possible without the support and encouragement of my friend and supervisor Dr. Agba Salman, without his support I would probably have abandoned this work long before the end.

Thanks go to Unilever for the financial support of this research and specifically to Matthew Pickles for his ideas and guidance in the early stages of the work and for arranging the initial placement using the specialist equipment at the Unilever Port Sunlight research facilities.

I would also like to thank all my friends and family who encouraged me and kept me sane during my research and the writing up period.

I would specifically like to thank Jin Sheng Fu for passing on his knowledge in the early parts of my research and enabling me to get off to a flying start.

Special thanks has to go to Bob Sochon, Sellasi Dorvlo and Seth Ong. The help with conducting experiments that these three gave me in the summer of 2004 enabled me to produce enough meaningful results on which to base my work.

Chris Turner and Stuart the technicians deserve thanks for their patience and work they did on making and maintaining the experimental rigs.

Thanks go to Dr. Rob Dwyer-Joyce from the Mechanical Engineering department for his helpful advice on tribology and the pleasant manner of our meetings.

Finally I would like to thank all those people who are too numerous to name personally who I have worked with and offered tit-bits of advice and kept the personal and social side of my research fun and exciting.